NASA Contractor Report 3065

Analysis of a Theoretically Optimized Transonic Airfoil

M. E. Lores, K. P. Burdges,
and G. D. Shrewsbury

CONTRACT NAS2-8697
NOVEMBER 1978

NASA

NASA Contractor Report 3065

Analysis of a Theoretically Optimized Transonic Airfoil

M. E. Lores, K. P. Burdges,
and G. D. Shrewsbury
Lockheed-Georgia Company
Marietta, Georgia

Prepared for
Ames Research Center
under Contract NAS2-8697

National Aeronautics
and Space Administration

**Scientific and Technical
Information Office**

1978

SUMMARY

Numerical optimization was used in conjunction with an inviscid, full potential equation, transonic flow analysis computer code to design an upper surface contour for a conventional airfoil to improve its supercritical performance. The modified airfoil was tested in the Lockheed-Georgia Compressible Flow Wind Tunnel. The majority of the test was done at eleven million Reynolds number and a four percent tunnel top and bottom wall porosity. A limited amount of testing was done to obtain data at other Reynolds numbers and wall porosities.

The modified airfoil's performance was evaluated by comparison with test data for the baseline airfoil and for an airfoil developed by optimization of only the baseline airfoil's leading edge. While the leading edge modification performed as expected, the upper surface re-design did not produce all of the expected performance improvements. Although the drag divergence Mach number was increased, the modified airfoil exhibited more drag creep than for the baseline section. This larger drag creep is attributable to the early formulation (at approximately $M_\infty = .68$) of a relatively strong leading edge shock wave.

Theoretical solutions computed using a viscous, full potential equation transonic airfoil code were compared to experimental data for the baseline airfoil and the upper surface modification. These correlations showed that the theory predicted the baseline airfoil's aerodynamics fairly well, but failed to accurately compute results for the upper surface modification. This failure is shown to be attributable to the inability of the theory to properly treat the thick trailing edge boundary layer associated with the upper surface modification.

Numerical optimization is concluded to offer the means for efficiently designing advanced airfoils. However, until a completely reliable viscous airfoil analysis technique is developed, optimization can be used with confidence only when the character of the viscous flow is not significantly altered during the optimization process.

TABLE OF CONTENTS

INTRODUCTION

Efficient transonic performance continues to be an important design requirement for many new aircraft. Specialized airfoils whose contours are dependent upon design conditions are needed to achieve the desired transonic performance. To design these airfoils rapidly and effectively, aerodynamicists must have available accurate and easy-to-use theoretical design methods. The nonlinearity of the partial differential equations that describe transonic flows has hampered the development of such theoretical design methods. However, advances in computational fluid dynamics, together with the availability of large and fast computers, have resulted in the recent availability of a number of transonic design techniques.

Airfoil design methods can be categorized as either inverse or direct procedures. Inverse methods involve the specification of a desired pressure distribution and the calculation of the corresponding airfoil. The need to specify a priori a pressure distribution that will result in a physically realistic optimized airfoil is a disadvantage of inverse procedures. Inverse methods have been formulated either by using hodograph equations or by solving the problem in the physical plane (e.g., refs. 1 and 2, respectively). Since hodograph formulations are applicable only to shock-free flows, they are of limited usefulness in transonic design. Also, considerable user expertise is required to employ hodograph design methods. Physical-plane solutions suffer computational difficulties in the leading edge region which are usually avoided by specifying the airfoil geometry near the leading edge. Since proper leading edge design is needed to design optimized transonic airfoils, this approach limits the usefulness of physical plane inverse solutions in transonic design work.

The above-mentioned difficulties are avoided in direct design methods. In this design approach, a numerical optimization algorithm is coupled with a suitable aerodynamic analysis method to design airfoils that are in some sense optimized for specific flight conditions. For example, an airfoil contour can be determined which minimizes drag at a specific lift coefficient with the pitching-moment coefficient constrained to be within acceptable

limits. Perhaps the most promising direct design method is under development at NASA-Ames by Hicks and his associates. The method is described and example designs are discussed in references 3 and 4. Briefly, the method involves coupling a numerical optimization scheme developed by Vanderplaats (ref. 5) with proven airfoil analysis methods. The ability to use any theoretical analysis method and any numerical optimization algorithm makes the technique very versatile.

Currently, the transonic full potential code developed by Jameson (ref. 6) is being used to provide the needed aerodynamic data. Viscous effects, known to be important in transonic flow calculations, are neglected in Jameson's analysis method. An inviscid aerodynamic module is used because currently available viscous transonic airfoil analysis programs are not completely reliable, and they require more computation time than inviscid techniques. Experience with applying the procedure to design subsonic airfoils has indicated that aerodynamic performance predicted by inviscid methods will be manifested when a viscous analysis of the resulting airfoil is performed. There is, nevertheless, a need to experimentally verify the performance of transonic airfoils designed using the inviscid procedure.

Because of its versatility, Hicks' method should be useful both in transonic design projects in which performance improvements in existing aircraft are sought by airfoil modification, and in projects in which new airfoils for advanced aircraft are required. The first application is being investigated in a project being conducted by Lockheed. With the aid of Hicks, Lockheed researchers recently applied the procedure to the redesign of the forward 12% of the C-141 airfoil leading edge. This application was selected because that airfoil exhibits a large drag creep which might be reduced by a limited modification of the leading edge. This work was successful in that the predicted drag creep was reduced to the same level obtained by a trial and correction process in which analysis methods were used to evaluate many candidate leading-edge modifications, but in a fraction of the time.

The airfoil leading-edge design using Hicks' method was obtained by modifying only the C-141 airfoil upper surface. In contrast, the airfoils designed using the trial-and-correction procedure involved simultaneous upper

and lower surface modifications. Consequently, Hicks' modification may be easier to incorporate as an aircraft change. Further, because it has a larger leading-edge radius, Hicks' airfoil may provide better low-speed stall characteristics than either the basic C-141 section or the other proposed airfoil modifications.

The Hicks' modification to the C-141 airfoil leading-edge, as well as the basic C-141 section, have been tested in the Lockheed Compressible Flow Wind-Tunnel (CFWT) at transonic speeds under an internal Lockheed research program. Airfoil surface pressure distributions and the attendant forces and moments were obtained for an extensive range of Mach numbers and lift coefficients. These data substantiated the theoretically predicted performance improvements resulting from numerical optimization. The wind tunnel test data showed that a 7% improvement in (ML/D) may have resulted from the modification of the upper surface of the forward 12% of the airfoil. In addition to producing an efficient airfoil modification, numerical optimization required about half the computation time and resulted in a 25% reduction in engineering hours when compared to a conventional trail-and-correction approach.

The purpose of the work reported herein was to determine the applicability of numerical optimization in an extensive redesign of a conventional airfoil to improve its supercritical performance. The problem selected was the re-contouring of the entire upper surface of the baseline C-141A wing airfoil section. This problem was selected because the availability of the work already done on the C-141 airfoil upper surface leading-edge modification premitted an efficient comparison of the use of numerical optimization for limited and extensive airfoil modification.

In this report, the aerodynamic design of the upper surface modification using numerical optimization is discussed, the wind tunnel model design and test are described, the redesigned airfoil performance is compared with that of the baseline and modified leading-edge airfoils, and the design procedure is evaluated.

For reasons which will become apparent, the upper surface modified airfoil will be referred to as C141H7472. The baseline airfoil and the optimized

Error

An error occurred while processing this page. See the system log for more details.

V	optimization design variables
Z	coordinate normal to airfoil chord line, cm (in.)
α	geometric angle of airfoil chord line, degrees
γ	ratio of specific heats
τ	wind tunnel wall porosity, %

Subscripts:

t.e.	trailing edge
T	transition strip location
o	zero normal force
1	tunnel station one chord length downstream of model
∞	denotes freestream conditions

Abbreviations:

CFWT	Lockheed Compressible Flow Wind Tunnel
l, l.s.	lower surface
u, u.s.	upper surface
L.E.	leading edge

AIRFOIL DESIGN

Problem Definition

The design objective of this study was to minimize the cruise drag of the baseline C-141 airfoil, and to increase the drag divergence Mach number at cruise lift. The section Mach number and lift coefficient corresponding to airplane cruise conditions are .72 and .57, respectively. In order to have a direct comparison with the leading-edge upper surface modification of the baseline airfoil designed by Lockheed and Ames, the airfoil modification was restricted to the upper surface. Geometric constraints imposed on the airfoil modification were that the thickness-to-chord ratio not be reduced and that

the airfoil leading-edge retain at least the same degree of bluntness. The latter condition was imposed to avoid potentially poor airfoil stall characteristics.

Numerical Optimization

The airfoil upper surface contour needed to attain the design objective was determined using the previously discussed NASA-Ames aerodynamic numerical optimization scheme.

Design point definition. - Since the optimization scheme used an inviscid transonic method to provide aerodynamic data required during the optimization process, the first step in the design study was to determine an inviscid design condition. The underlying hypothesis in this inviscid optimization is that improvements made at the inviscid design conditions will be realized in a viscous flow.

The inviscid design condition was determined by first computing a viscous solution using the NYU transonic flow analysis routine (ref. 1) for the baseline airfoil (C141-1) at cruise conditions. Since the evaluation of the optimized airfoil would be done using wind tunnel data, the solutions were computed at the tunnel Reynolds number. Thus, the following conditions were specified in performing the viscous calculations:

$$C_n = .57$$
$$M_\infty = .72$$
$$R_N = 11 \times 10^6$$
$$X/C = .10$$

The results of these calculations are shown in figure 1 where they are compared with experimental data. The agreement between theory and experiment shown here is fair, with the major discrepancy being the slightly more aft theoretical shock location. Since recent work by Blackwell, et al., reported in reference 7 shows the strong dependence of shock location to wall porosity

and since the theoretical calcualtions are done with free-air boundary conditions, no attempt was made to seek better theory-to-experiment agreement.

The viscous solution indicated that the airfoil angle of attack to achieve the above conditions was approximately two degrees. The assumption was made that the lift loss due to viscosity for the optimized airfoil would be about the same as for the baseline airfoil. The inviscid design point was thus defined to be:

$$M_\infty = .72$$
$$\alpha = 2^\circ$$

Design objective. - The design objective (i.e., the parameter to be minimized at the design point) for this study was wave drag minimization at the design point. In an attempt to increase M_{DD}, and at the same time avoid a point optimization which would be reflected in a local bucket in the C_d variation with Mach number, a secondary design objective was to reduce C_{d_w} at .74 Mach number. This second design objective was introduced as a constraint in the optimization scheme, and its imposition is discussed in the following section. Consequently, the objective function in the minimization scheme was:

$$OBJ = C_{d_w}(\alpha = 2^\circ, M_\infty = .72)$$

Design constraints. - Four constraints were imposed during the optimization scheme:

(1) Z upper /C (X/C = .5) > .074
(2) Z upper /C (X/C = .005) > .01
(3) $C_n > .85$
(4) C_{d_w} ($\alpha = 2^\circ$, $M_\infty = .74$) > .0020

The first constraint was imposed to ensure that the optimized airfoil was at least as thick as the baseline section. An arbitrary nose bluntness was forced by the second constraint. The third constraint was required in an attempt to ensure that when viscous effects were taken into account, the airfoil would

produce at least the desired cruise lift. The final constraint enforces the secondary design objective by requiring C_{d_w} at $M_\infty = .74$ be less than 20 counts. The 20-count level was selected to be compatible with the drag at $M_\infty = .72$ to produce a flat C_{d_w} versus M_∞ curve at $C_n = .57$.

Design variables. - Proper selection of design variables is imperative if the design objective is to be efficiently attained in numerical optimization. In the leading-edge modification study a single polynomial representation of the forward 12% of the upper surface was used. In that case, the design variables (i.e., the parameters perturbed during the optimization scheme) were the coefficients of the polynomial and/or the exponents on the polynomial terms. This approach proved to be successful because only a few terms were required to achieve sufficient design flexibility and hence computation times were small.

However, numerous polynomials would be required to provide an entire upper surface parameterization with adequate design flexibility with each polynomial maintaing ordinate and at least first derivative continuity at the match points. Such an approach would not only be complex, it would also be computationally expensive. Therefore, an alternative airfoil parameterization scheme was used in this study. The scheme was developed by Ames researchers and it involves the use of perturbation shape functions to distort the upper surface contour of the baseline airfoil. The shape functions used in this work are shown in figure 2 with their defining equations. In this case, the design variables are the pre-multiplying coefficients which determine the magnitude of the individual shape functions. These pre-multiplying (or participation) coefficients are adjusted by the optimization scheme until the design objective is met without violating the constraints. Thus, twelve (12) geometric design variables were used in this study. An additional design variable, the angle of attack (α), was tried and found to be unnecessary.

Airfoil nomencalture. - Since the upper surface modification was developed with the objective of reducing the drag of the baseline C-141 airfoil at .72 and .74 Mach numbers, and since perturbation shape functions were developed by Hicks at NASA-Ames, the resulting airfoil will be referred to as C141H7472. For the purposes of this report, the baseline section will be called C141-1.

Since the optimized leading edge was the sixth in a series of leading edges designed for the baseline section, this airfoil is called C141-6.

Optimization results. - The numerical optimization was done by starting with the baseline airfoil at $\alpha = 2^\circ$ and computing solutions for $M_\infty = .72$ and $M_\infty = .74$ for the perturbations of the design variables until the design objective and the four constraints were met. The initial and final inviscid pressure distributions for $M_\infty = 0.72$ and $M_\infty = .74$ for the C141-1 and the C141H7472 airfoils are shown in figure 3. The amelioration of the inviscid flow field and the attendant reduction in wave drag resulting from numerical optimization is evident in these data.

The C141-1 and C141H7472 airfoil geometries are shown in figure 4 and the coordinates of the C141H7472 airfoil are listed in table I. Evident in this figure is the attempt by the optimization code to use aft-camber to achieve the design objective. Since the lower surface was fixed, the only way to incorporate aft-camber was to "hump" the upper surface at about 75% chord.

The aft hump leads to a strong adverse pressure gradient on the upper surface near the trailing edge which conceivably could have a catastrophic effect on the boundary layer. This possibility was examined by computing the viscous flow about both airfoils using the NYU 2-D transonic airfoil program. The results of these calculations are shown in figure 5 where inviscid and viscous results for the airfoils at $\alpha = 2^\circ$ and $M_\infty = .72$ and $M_\infty = .74$ are shown. The separation point predicted by the Nash-Macdonald (ref. 1) criteria used in the NYU program are flagged in the pressure distributions. Separation is predicted to occur on both airfoils, with the separation point being further forward on the C141H7472 airfoil. The default procedure of the NYU program for treating trailing-edge separations was used in these calculations. (The procedure is described in detail in reference 1.) Using the default procedure, the program predicts that both airfoils will have about the same drag, despite the apparent shock-free flow associated with the modified airfoil.

The lift loss due to viscosity is also evident in the results shown in figure 5, and it is larger than estimated. Consequently, the airfoils have to operate at an angle of attack greater than 2° to achieve a $C_n = .57$.

The decision was made at this point to test the C141H7472 airfoil despite the predictions of flow separation and the uncertainty in the actual viscous design condition. This decision was made because of the belief that test data were needed to provide guidance for future applications of numerical optimization. The model design and wind tunnel test are discussed in the next section of this report.

EXPERIMENTAL TESTS

Apparatus and Test Procedures

Model. - A two-dimensional model of the C141H7472 airfoil was fabricated from 17-4PH stainless steel in accordance with the coordinates given in table I. The model has a chord of 17.78 cm (7.00 in.) and a span of 50.80 cm (20.00 in.). The model completely spans the two-dimensional test section and is supported from the side walls by means of tangs. A photograph of the model installed in the Lockheed Compressible Flow Wind-Tunnel is shown in figure 6.

The model was instrumented with fifty-three (53) static-pressure measuring orifices: 27 on the upper surface and 26 on the lower surface. The orifices were located near the mid-span of the model and were mounted flush and normal to the local contour. The measured orifice locations are listed in table II.

The model contour was checked dimensionally using a template and feeler gage. Discrepancies from the design contour were mostly within ±.025 mm (.001 in.) with some areas reaching deviations of ±.050 mm (.002 in.). The airfoil surface was polished to conventional transonic model surface finish of less than .4 microns (15 microinches). Spanwise twist and warp of the model were found to be nil.

Test facility. - The model was tested in the Lockheed CFWT. Reference 8 contains a complete description of this facility. The tunnel is of the blow-down type, exhausting directly to the atmosphere. The air storage capability is 368 m^3 (13,000 ft^3) at 4.13×10^6 N/m^2 (600 psia). A sleeve-type control

valve accurately maintains the settling chamber stagnation pressure at selected pressure less than or equal to the 1.72×10^6 N/m^2 (250 psia) maximum and at mass flow rates less than 1089 kg/sec. (2400 lb/sec.).

The test section is 50.8 cm (20.0 in.) wide by 71.2 cm (28.0 in.) high by 183 cm (72.0 in.) long and is enclosed in a 3.7 m (12.0 ft.) diameter plenum chamber. For the model tested, the tunnel height to model chord ratio is 4.0 and the tunnel span to model chord ratio is 2.9. Model blockage was 3 percent of the test section cross sectional area. The top and bottom walls of the two-dimensional test section have variable porosity capability (from 0 to 10%), obtained by sliding two parallel plates with .635 cm (.250 in.) diameter holes slanted 60 degrees from the vertical. The 2-D test section side walls are not porous.

Wake survey rake. - The fixed wake-survey rake used for section drag measurements is described in figure 7 and shown installed in the tunnel in figure 6. The wake rake was mounted at the tunnel centerline one chord length behind the airfoil model. The rake has a total of 90 total head measurement tubes and four static pressure tubes. The tubes are .15 cm (.06 in.) in diameter. The wake rake has been calibrated in the tunnel without a model present.

Data have been obtained in previous CFWT airfoil tests similar to that conducted herein with the wake rake installed and removed to determine its influence on the flow over the airfoil. These unpublished data indicated the wake rake had negligible effects on the normal-force coefficient, the pitching-moment coefficient, and the airfoil pressure distribution.

Instrumentation. - Measurements of the static pressures on the airfoil surfaces and the wake rake pressure were made using electronically actuated pressure scanning valves. The full-scale range of the quarter-percent accuracy for the wind tunnel conditions tested: wake rake — ±8.6 dynes/cm^2 (±12.5 psi); and airfoil pressures ±34.4 dynes/cm^2 (±50.0 psi). CEC force balance pressure transducers were used in conjunction with CEC servo amplifiers to provide a precise measurement of the atmospheric pressure, stagnation pressure, and test section static pressure to .025% of the transducer capability: 6.89×10^5 N/m^2 (100.0 psi) for the test section static and 1.38×10^6 N/m^2 (200.0 psi)

for stagnation pressure. These transducers allow determination of the test section Mach number to a accuracy of ±.001 at the higherst stagnation pressure.

Angle of attack was measured with a calibrated potentiometer operated by the angle of attack drive mechanism.

Raw pressure data were recorded on magnetic tape utilizing the CFWT high speed data acquisition system.

Test and Methods

Test conditions. - The aerodynamic characteristics of the C141H7472 airfoil were investigated over a wide range of test conditions. The angle of attack of the airfoil was varied from 0 to 5 degrees and the Mach number range investigated was from 0.45 to 0.78. Tests were conducted at nominal Reynolds numbers based on airfoil chord of 4 and 11 million. The majority of the tests was conducted for a wind-tunnel porosity of 4%. Limited data were obtained over a wall porosity range of 2 to 6% to ascertain the sensitivity of the new airfoil to this parameter. These results are included in Appendix A.

Data reduction. - The static pressure measurements at the airfoil surface were reduced to standard pressure coefficients and then machine integrated to obtain section normal-force and section pitching-moment coefficients about the quarter chord using the following equations:

$$C_n = \int_0^1 (C_{P_\ell} - C_{P_u})\, d(X/C)$$

$$C_m = \int_0^1 (C_{P_\ell} - C_{P_u})\, (0.25 - X/C)\, d(X/C)$$

Section profile drag measurements were computed from the wake survey rake measurements by the method of reference 9 utilizing the following equations:

$$C_d = \int_{wake} C'_d\, d\left(\frac{Z}{C}\right) + \Delta C_d$$

and

$$C'_d = 2\left(\frac{H_1}{H_\infty}\right)^{\frac{\gamma-1}{\gamma}} \left(\frac{P_1}{P_\infty}\right)^{\frac{1}{\gamma}} \left\{\frac{1 - \left(\frac{P_1}{H_1}\right)^{\frac{\gamma-1}{\gamma}}}{1 - \left(\frac{P_\infty}{H_\infty}\right)^{\frac{\gamma-1}{\gamma}}}\right\}^{\frac{1}{2}} \left\{1 - \left[\frac{1 - \left(\frac{P_\infty}{H_1}\right)^{\frac{\gamma-1}{\gamma}}}{1 - \left(\frac{P_\infty}{H_\infty}\right)^{\frac{\gamma-1}{\gamma}}}\right]^{\frac{1}{2}}\right\}$$

The ΔC_d is a correction for the wake rake total head tube displacement effect when in a transverse velocity gradient. This correction is discussed in reference 9 and is given by

$$\Delta C_d = 0.36 \frac{d}{C} C'_{d_m} .$$

Transition. - For the Reynolds number tests of 4 million, boundary layer transition was fixed. The airfoil was investigated with roughness particles located on both surfaces at 0.05 C. The roughness height was 0.00039 C and was selected according to the criteria of reference 10. The roughness strips were 0.13 cm (0.05 in.) wide and consisted of Ballotini glass beads set in a plastic adhesive.

For the Reynolds number tests of 11 million no transition strips were utilized.

Tunnel wall effects. - The effect of the tunnel walls on the two dimensionality of the flow is considered to be small. This statement is supported by measurements reported in reference 11 on the baseline C-141 airfoil with a similar test arrangement. These results indicated very little variation of the pressure coefficient across the model span for various flow conditions. The conclusion was further substantiated by observation of oil flow patterns at the airfoil-wall intersction. Disturbances in this juncture were confined to a very small regions.

Standard subcritical wind-tunnel boundary corrections (normal-force interference and blockage) have been calculated for this test using the method of reference 12. Recent studies (ref. 7) have shown, however, this method to be

generally inadequate at transonic speeds. As a result, these corrections have not be applied to the data presented herein.

RESULTS AND DISCUSSION

A complete set of basic aerodynamic force and moment data as well as surface pressure distributions for the C141H7472 airfoil at a Reynolds number of 11 million and wind-tunnel wall porosity of 4% is contained in Appendix A. These data will form the basis for assessing the modified airfoil performance to be discussed below, and unless stated otherwise all data will be for these conditions. Appendix A also contains limited data for a Reynolds number of 4 million, wind-tunnel wall porosity data from 2 to 6%.

The evaluation of the performance of the C141H7472 airfoil will be made by comparing test data for this airfoil with data obtained in a recent test of the C141-1 and C141-6 airfoils. Following this airfoil performance evaluation, the efficacy of the design procedure will be examined.

C141H7472 Airfoil Aerodynamics

The experimental data obtained from the C141H7472 airfoil model in the Lockheed-Georgia CFWT are discussed in this section. This discussion is followed by a review of the aerodynamic forces resulting from the surface pressures.

Airfoil pressures. - The variation with free stream Mach number of the surface pressure distributions at the design normal force coefficient of 0.57 can be seen in the data shown in figure 8. A number of conclusions can be drawn from these results. First, the airfoil does not have the aft-loading associated with the cusped region of a modern supercritical airfoil. In fact, there is a small negative lift region covering the last ten percent chord. This lack of aft loading is attributable to the modification of only the upper surface. Since the lower surface could not deform, the amount of aft camber that could be designed into the airfoil was limited by geometric constraints.

The only way to induce any aft-loading was thus to "hump" the rear upper surface; a design change which was done by the optimization design code.

The airfoil has a substantial suction peak which becomes supersonic at about 0.6 Mach number. The supersonic region increases in size with increasing Mach number, and is terminated by a fairly strong shock wave for Mach numbers greater than about 0.64. The maximum shock strength prior to drag divergence is reached at a free stream Mach number of 0.68. In this case, the local Mach number ahead of the shock is 1.26, and the shock induces a localized separation bubble at the foot of the shock.

The variations with free stream Mach number of shock strength and location are summarized in figure 9. The shock movement is orderly, with the shock first forming at $M_\infty = 0.60$ at about 2% chord, and moving aft to approximately 55% chord at $M_\infty = 0.78$. The rapid increase in shock strength at about 0.68 Mach is evident in this figure. This early formation of a strong shock wave can be expected to have detrimental effect on airfoil drag characteristics.

Airfoil forces. - The airfoil drag coefficient variation with Mach number for $C_n = 0.57$ is shown in figure 10. These data exhibit a substantial drag increase in range of $M_\infty = 0.60$ to 0.72. This rapid and undesirable drag increase is no doubt caused by the formation of the relatively strong leading edge shock discussed in the preceeding section. From $M_\infty = 0.72$ to $M_\infty = 0.76$ the airfoil drag remains fairly constant. This result is interesting since a "flat" C_d vs M_∞ curve in this Mach range was one of the airfoil design goals. For Mach numbers greater than 0.76, the airfoil experiences the onset of rapid drag rise associated with the increasing strength of the shock wave.

Comparison of Airfoils

Airfoil C141H7472 was designed at an inviscid condition which was expected to produce a minimum wave drag airfoil at a normal-force coefficient of 0.57. In this section, the performance of this airfoil at its design point relative to both the C141-1 and C141-6 airfoils is evaluated. The variation of measured drag with Mach number for the three airfoils at $C_n = 0.57$ is shown in figure 11. The following observations can be made form these data:

1. Airfoil C141H7472 has a higher drag divergence Mach number than either of the other two sections.

2. For Mach numbers less than M_{DD} for the C141-1 airfoil, the C141H7472 airfoil has substantially more drag.

3. The leading-edge modification to the baseline airfoil (C141-6) reduces the supercritical drag and increases M_{DD} relative to the baseline airfoil (C141-1).

The reasons for these results can be deduced from the chordwise pressure distributions shown in figure 12. For $M_\infty = 0.55$, the flows are subcritical, and in the absence of any indications of flow separation, the higher drag of the modified airfoil is probably attributable to its blunt trailing edge. The rapid drag increase of the airfoil C141H7472 at approximately $M_\infty = 0.68$ can be seen to be due to the formation of a strong leading-edge shock wave which does not appear on either of the other two airfoils. The Mach number upstream of the shock wave is approximately 1.26 at $M_\infty = 0.68$ and $C_n = 0.56$.

As M_∞ increases and the design Mach numbers are approached, the pressure distributions show that the shock on airfoil C141H7472 moves downstream, and decreases in strength. At the same time, a shock wave forms on the other two airfoils, and increases rapidly in strength. This behavior results in the increased M_{DD} associated with the C141H7472 airfoil.

Not directly an outcome of this study, but nevertheless of interest, is the performance of the airfoil with the leading-edge modification (C141-6) near its design point. When compared with the baseline airfoil (C141-1), the leading-edge modification produces significantly more leading-edge suction (fig. 12). Also, the suction peak is followed by a nearly isotropic re-compression. This behavior results in the avoidance of the premature shock formation which occurred when the entire upper surface was modified. An interesting question, and one which remains to be definitely answered, is the failure of the optimization scheme to find a leading-edge geometry which would produce a similar isentropic compression when the entire upper surface was

modified. Perhaps the different results are attributable to the use of differing shape functions in the optimization scheme.

The airfoil C141H7472 did not perform as expected at $C_n = 0.57$. The preliminary theoretical analysis discussed in the airfoil design section indicated that the normal-force loss due to viscosity might have been underestimated in establishing the inviscid design point. Consequently, the airfoil C141H7472 might be expected to perform better at a reduced normal-force coefficient. However, the drag variations with Mach number for the three airfoils at $C_n = 0.50$ exhibit the same general characteristics as they did at $C_n = 0.57$, as evidenced by the data on figure 13.

Design Method Evaluation

The experimental data comparisons discussed above show that the upper surface modification increased M_∞ at the expense of more drag creep, and that in fact the C141H7472 airfoil's drag at the $M_\infty = 0.72$ and $M_\infty = 0.74$ design points was larger than that of the baseline airfoil. This less than satisfactory airfoil performance was not a result of the failure of numerical optimization, because the optimization did reduce the design objective, inviscid C_{d_w}. This fact is evidenced by figure 3 where the inviscid pressure distributions for both airfoils at the design conditions were shown.

The lack of performance by the C141H7472 airfoil, then, must be due to adverse viscous effects which were not taken into account. The effects of viscosity on airfoil performance were examined by computing solutions using the viscous NYU program (ref. 1) for both the baseline and the modified airfoils and comparing the solutions with experimental data. The solutions were computed using the non-conservative option in the NYU code, and employing the program in more-or-less "cook book" form. However, the boundary layer displacement effects had to be drastically under-relaxed, and two inviscid iterations were done between boundary layer calculations to permit a more stable convergence process.

The agreement between theoretical drag predictions and experimental results is in general poor for both the baseline and the modified airfoil as

demonstrated by the data shown in figure 14. The following observations can be made from these data:

1. M_{DD} is predicted to within .004 Mach number for both airfoils.
2. The shape of the drag curve for the baseline airfoil is fairly well predicted, but is underestimated by approximately 10 counts.
3. Both the level and the shape of the C141H7472 airfoil's drag curve are mispredicted by theory. In particular, the early drag rise occurring at $M_\infty \simeq 0.68$ is missed in the theoretical calculations.

The reasons for the failure of the NYU viscous transonic code can be deduced by comparing theoretical and experimental pressure distributions at the same Mach number and lift coefficient. These data are shown for the C141-1 and C141H7472 airfoils in figures 15 and 16, respectively.

The results shown in figure 15 indicate that the C141-1 airfoil pressure distributions are fairly well predicted by theory, with the major discrepancies being the shock location, trailing edge pressure recovery, and the lower surface pressure level. The failure to properly compute the trailing edge pressure recovery is probably due to the large (approximately 20 degrees) trailing-edge included angle which produces a thick boundary layer. The NYU code uses a conventional (albeit adjusted) boundary layer method which is not applicable to thick boundary layers. The improper calculation of the trailing edge flow causes erroneous results elsewhere, as manifested by the incorrect shock wave and lower surface pressures.

Dispite the fact that the theoretical shock wave is stronger than the experimental shock, the NYU program predicts a lower drag level than recorded in the test. Drag prediction using this code, then, is probably too uncertain for use in numerical optimization, even when the general character of the airfoil pressure distribution is fairly well predicted.

The theoretical pressures for the C141H7472 airfoil bear little resemblance to their experimental counterparts, as evidenced by the results shown in figure 16. At $M_\infty = 0.72$, the entire character of the leading edge shock is missed, while at $M_\infty = 0.74$, a dual shock is predicted when only one shock

occurred. In both cases, the trailing edge pressure recovery is over-predicted; even more so than for the baseline airfoil. Also, the lower surface pressures are under-predicted, but not quite to the same degree which they were missed for the C141-1 airfoil.

Solutions for the C141H7472 airfoil were also computed at off-design conditions, and results for $M_\infty = 0.45$ and $M_\infty = 0.78$ are shown in figures 17 and 18, respectively (both solutions are for $C_n = 0.57$). For the subcritical $M_\infty = 0.45$ condition, agreement between theory and experiment is good, except for the aforementioned trailing edge pressure recovery. At $M_\infty = 0.78$, the shock wave has moved aft to approximately 55% chord, and the supersonic re-expansion which occurred in the $M_\infty = 0.72$ and 0.74 solutions is not predicted. Although agreement here is better than at the design conditions, it is not sufficiently accurate for airfoil optimization. In fact, drag predictions are relatively accurate only for subcritical flows for the C141H7472 airfoil.

All of the discrepancies are probably attributable in the main to improper modeling of the viscous trailing edge flow. This failure is accentuated for the C141H7472 airfoil because the "hump" in the upper surface produces a strong adverse pressure gradient near the trailing edge. The resulting gradient produces a thicker boundary layer than can be predicted by simple boundary layer theory. This thick boundary layer produces a reduced trailing edge pressure recovery when compared to the baseline airfoil; a result which is not predicted by theory.

Experiences both at Lockheed and elsewhere have shown the NYU code to yield reliable transonic results for other airfoils. Consequently, alternate reasons for the failure to predict the C141H7472 airfoil's aerodynamics were explored.

One possibility examined was wind tunnel wall interference. Previous tests in the CFWT (including the baseline airfoil tests) indicate that 4% porosity best simulates free-air conditions. Was it possible, however, that good agreement could be attained between theory and experiment for the C141H7274 airfoil using a different wall porosity? This question was answered by using the limited variable porosity data taken in this test, and comparing them with

theoretical solutions at the same lift coefficients. The result of this side-study was that good agreement could not be found for any porosity (2% to 6%) investigated.

A second possibility for the disagreement might be the failure of the inviscid flow region nonconservative formulation. This possibility was explored by computing some solutions using the quasi-conservative differencing scheme option included in the NYU code. This study was done because a conservative problem formulation is known to be correct for flows with shock waves. Consequently there was a need to determine if the use of such a formulation would improve the data correlations for the modified airfoil. The results of this study are summarized in figure 19 where nonconservative and quasi-conservative solutions are compared with experimental data for the modified airfoil at the design points. As these comparisons show, the theoretical solutions are similar, and neither agrees well with test data. The fundamental problem of the failure to accurately compute the trailing edge flow is evident in both solution techniques.

An attempt was made to force a match between theory and experiment by varying the theoretical angle of attack and/or free stream Mach number. The comparisons were made for experimental $C_n = 0.57$ and $M_\infty = 0.72$, 0.74, and 0.78. Theoretical solutions were computed using both conservative and nonconservative differencing. The results of that investigation are summarized in figure 20. The improved correlation is evident in these data; however, the improvement was obtained for substantially different theoretical lift coefficients and free stream Mach numbers. Of interest is the close agreement between theoretical and experimental angle of attack. This result implies that the good correlation on shock strength and position was probably obtained because the airfoil was at the same effective attitude in both the theoretical calculations and experiment. The trailing edge flow is still not correctly predicted, and the erroneous drag predictions remain.

This attainment of the better theory/experiment correlation required, of course, a priori knowledge of the experimental results. Such a requirement obviously cannot be placed on an airfoil design methodology. Hence, the observation can be made that an improved transonic viscous airfoil method is

required to make airfoil design practical and reliable. The most needed improvement seems to be a better trailing edge flow formulation.

CONCLUDING COMMENTS

An upper surface for a conventional airfoil section has been designed using numerical optimization to improve the airfoil's supercritical performance. The modified airfoil (C141H7472) was tested in the Lockheed-Georgia Compressible Flow Wind Tunnel. The performance of the modified airfoil was evaluated by comparisons with test data for both the baseline conventional section (C141-1) and an airfoil development by modification of only the baseline airfoil's leading-edge (C141-6). An evaluation of the design procedure was then made by comparing theoretically predicted airfoil aerodynamics with experimental results. The salient results of the study are summarized below:

1. The airfoil with modified upper surface (C141H7472) increased M_{DD} relative to the baseline airfoil (C141-1) at the expense of larger drag creep which is attributable to the premature formation of a relatively strong shock wave.

2. Numerical optimization did produce an airfoil with reduced inviscid wave drag. However, viscous analysis failed to predict either the premature shock formation or the airfoil's drag level.

3. The failure of the viscous airfoil analysis method in this application is probably due to the inability of the method to compute the thick boundary layer resulting from the strong adverse pressure gradient occurring over the trailing-edge region of airfoil C141H7472.

4. The use of a quasi-conservative formulation in lieu of the standard non-conservative scheme did not have a significant effect on the useability of the theoretical results.

5. The concept of numerical optimization offers an efficient and versatile method for aerodynamic design. However, inviscid optimization should be restricted to limited modifications which do not significantly affect the

viscous flow (e.g., the leading-edge re-design study briefly discussed herein), or to airfoil designs for which viscous effects are well-understood.

6. Research should be devoted to developing an improved two-dimensional transonic viscous flow method. If such a method were available, its use with numerical optimization would provide a means for the efficient design of advanced transonic airfoils.

REFERENCES

1. Bauer, F.; Garabedian, P.; Korn, D; and Jameson, A.: Supercritical Wing Sections II. *Lecture Notes in Economics and Mathematical Systems*, Vol. 108, Springer-Verlag, New York, 1975.
2. Carlson, L. A.: Transonic Airfoil Design Using Cartesian Coordinates. NASA CR-2578, December 1975.
3. Hicks, R. M. and Vanderplaats, G. N.: Design of Low-Speed Airfoils by Numerical Optimization. SAE Business Aircraft Meeting, Wichita, April 1975. SAE Paper 750524.
4. Hicks, R. M.; Mendoza, J. P.; and Bandettini, A.: Effects of Forward Contour Modification on the Aerodynamic Characteristics of the NACA 64_{i}-212 Airfoil Section. NASA TM X-3293, Sept. 1975.
5. Vanderplaats, G. N.: CONMIN-A Fortran Program for Constrained Function Minimization — User's Manual. NASA TM X-62282, Aug. 1973.
6. Jameson, A.: Iterative Solution of Transonic Flows Over Airfoils and Wings. Comm. *Pure Applied Mach*, Vol. 27, 1974.
7. Blackwell, J. A., Jr.; Pounds, G. A.: Wind-Tunnel Wall Interference Effects on a Supercritical Airfoil at Transonic Speeds. *Journal of Aircraft*, Vol. 14, No. 10, pp. 939-935, October 1977.
8. Pounds, G. A. and Stanewsky, E.: The Research Compressible Flow Facility, Part 1: Design. Lockheed Engineering Report ER-9219-1, October 1967.
9. Pankhurst, R. C. and Holder, E. W.: *Wind-Tunnel Technique*. Sir Isaac Pitman and Sons, Ltd., London, p. 276, 1965.
10. Braslow, Albert L. and Knox, Eugene C.: Simplified Method for Determining of Critical Height of Distributed Roughness Particles for Boundary Layer Transition at Mach Numbers from 0 to 5. NACA TN 4363, 1958.

11. Pounds, G. A.: An Initial Two-Dimensional Wall Interference Investigation in a Transonic Wind Tunnel with Variable Porosity Test Section Walls. AIAA Paper No. 72-1011, September 1972.
12. Garner, H. C.; Rogers, E. W. E.; Acum, W. E. A.; and Maskell, E. C.: Subsonic Wind-Tunnel Wall Corrections. AGARDograph 109, October 1966.

TABLE 1. - DESIGN ORDINATES FOR C141H7472 AIRFOIL

UPPER SURFACE

X/C	Z/C	X/C	Z/C
.00000	.00000	.35000	.07070
.00020	.00489	.37500	.07185
.00040	.00625	.40000	.07277
.00060	.00724	.42500	.07347
.00080	.00804	.45000	.07395
.00100	.00874	.47500	.07421
.00200	.01133	.50000	.07426
.00300	.01320	.52500	.07410
.00400	.01471	.55000	.07374
.01000	.02069	.57500	.07318
.02000	.02653	.60000	.07239
.03000	.03059	.62500	.07135
.04000	.03385	.65000	.07002
.05000	.03664	.67500	.06834
.06000	.03911	.70000	.06624
.07000	.04133	.72500	.06366
.08000	.04337	.75000	.06051
.10000	.04698	.77500	.05672
.12500	.05083	.80000	.05222
.15000	.05414	.82500	.04698
.17500	.05704	.85000	.04108
.20000	.05963	.87500	.03476
.22500	.06197	.90000	.02840
.25000	.06410	.92500	.02240
.27500	.06604	.95000	.01673
.30000	.06779	.96000	.01446
.32500	.06934	.97000	.01214
		.98000	.00978
		1.00000	.00500

LOWER SURFACE

X/C	Z/C
.00000	.00000
.00241	.00781
.00961	.01527
.02153	.02192
.03806	.02735
.05904	.03228
.08427	.03664
.11349	.04016
.14645	.04287
.18280	.04516
.22221	.04697
.26430	.04820
.30866	.04895
.35486	.04928
.40245	.04891
.45099	.04784
.50000	.04619
.54901	.04398
.59755	.04093
.64514	.03717
.69134	.03314
.73570	.02927
.77779	.02524
.81720	.02140
.85355	.01769
.88651	.01410
.91573	.01072
.94096	.00765
.96194	.00498
.97847	.00278
.99039	.00122
.99759	.00030
1.00000	.00000

TABLE II. - AIRFOIL C141H7472 PRESSURE ORIFICE LOCATIONS

UPPER SURFACE

TUBE NO.	X/C
1	0.0
2	.0145
3	.0294
4	.0446
5	.0629
6	.0750
7	.1000
8	.1500
9	.2001
10	.2497
11	.3000
12	.3506
13	.4000
14	.4493
15	.5001
16	.5493
17	.5997
18	.6500
19	.6991
20	.7506
21	.7994
22	.8497
23	.8994
24	.9500
25	.9643
26	.9794
27	.9956

LOWER SURFACE

TUBE NO.	X/C
28	.0144
29	.0289
30	.0447
31	.0597
32	.0751
33	.0994
34	.1497
35	.1996
36	.2494
37	.3000
38	.3497
39	.3993
40	.4487
41	.4986
42	.5491
43	.5996
44	.6495
45	.6986
46	.7491
47	.7991
48	.8483
49	.8996
50	.9490
51	.9639
52	.9799
53	.9940

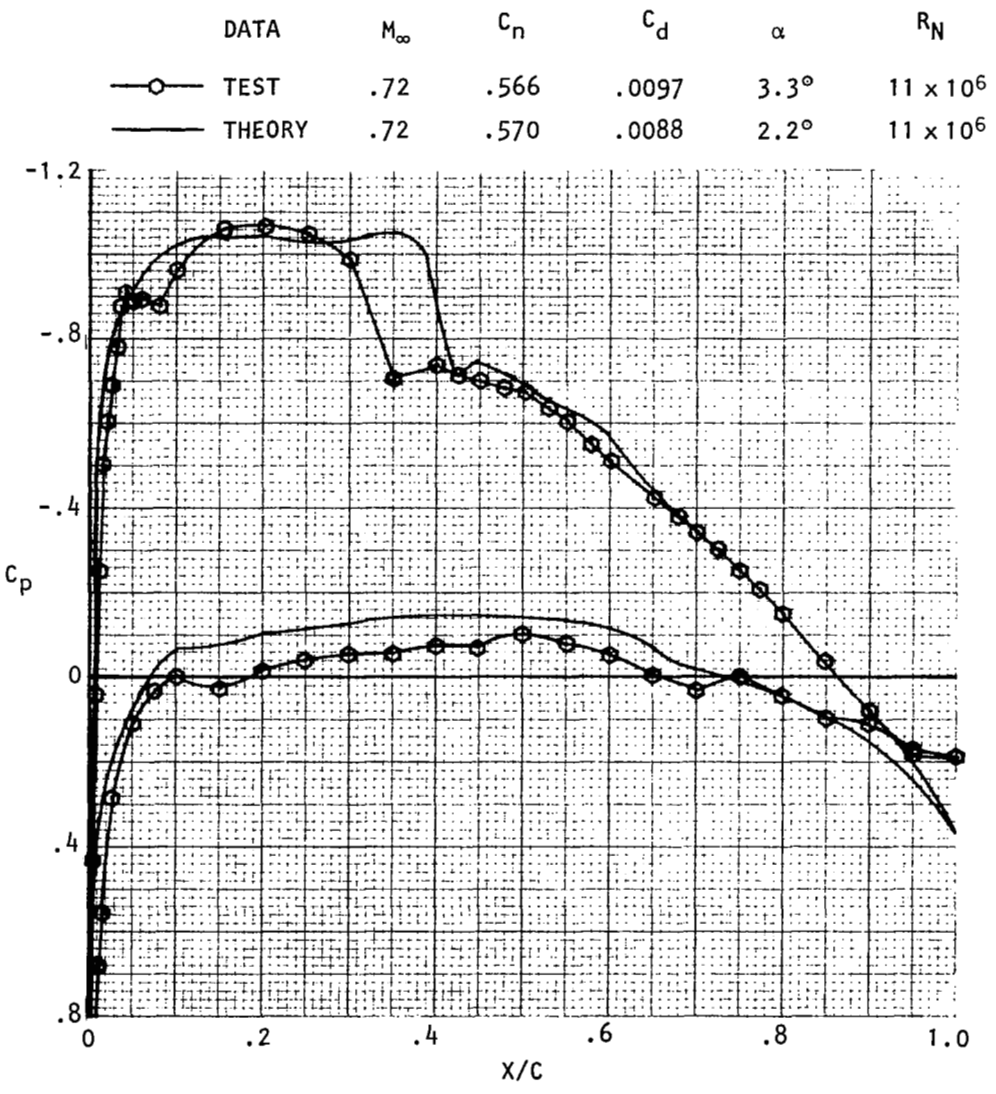

Figure 1. Design point theoretical and experimental pressures for the baseline airfoil (C141-1).

TERM	EQUATION
P(1)	$10(1-X)X^{V(12)}/e^{20X}$
P(2)	$10(1-X)X^{V(12)}/e^{40X}$
P(3)	$\sqrt{X}(1-X)/e^{3X}$
P(J), J=4, 10	$\sin^5(X^{n_j})$
P(11)	X^{10}

WHERE X IS INTERPRETED AS X/C

EXPONENT TABLE	
j	n
4	.5757166
5	.7564708
6	1.
7	1.356915
8	1.943358
9	3.106283
10	6.578813

$$Z/C = \sum_{N=1}^{11} V(N)\, P(N)$$

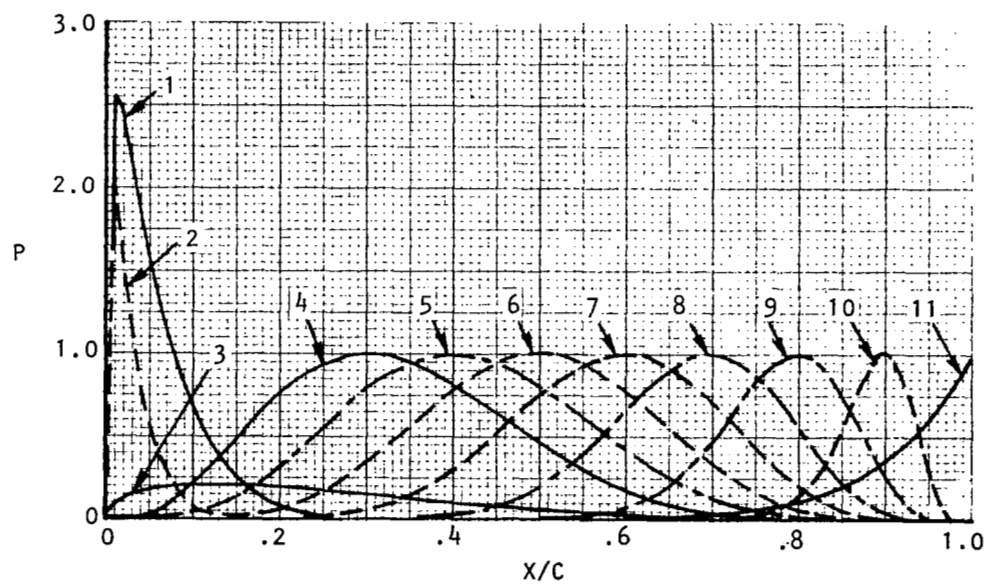

Figure 2. Upper surface modification airfoil parameterization.

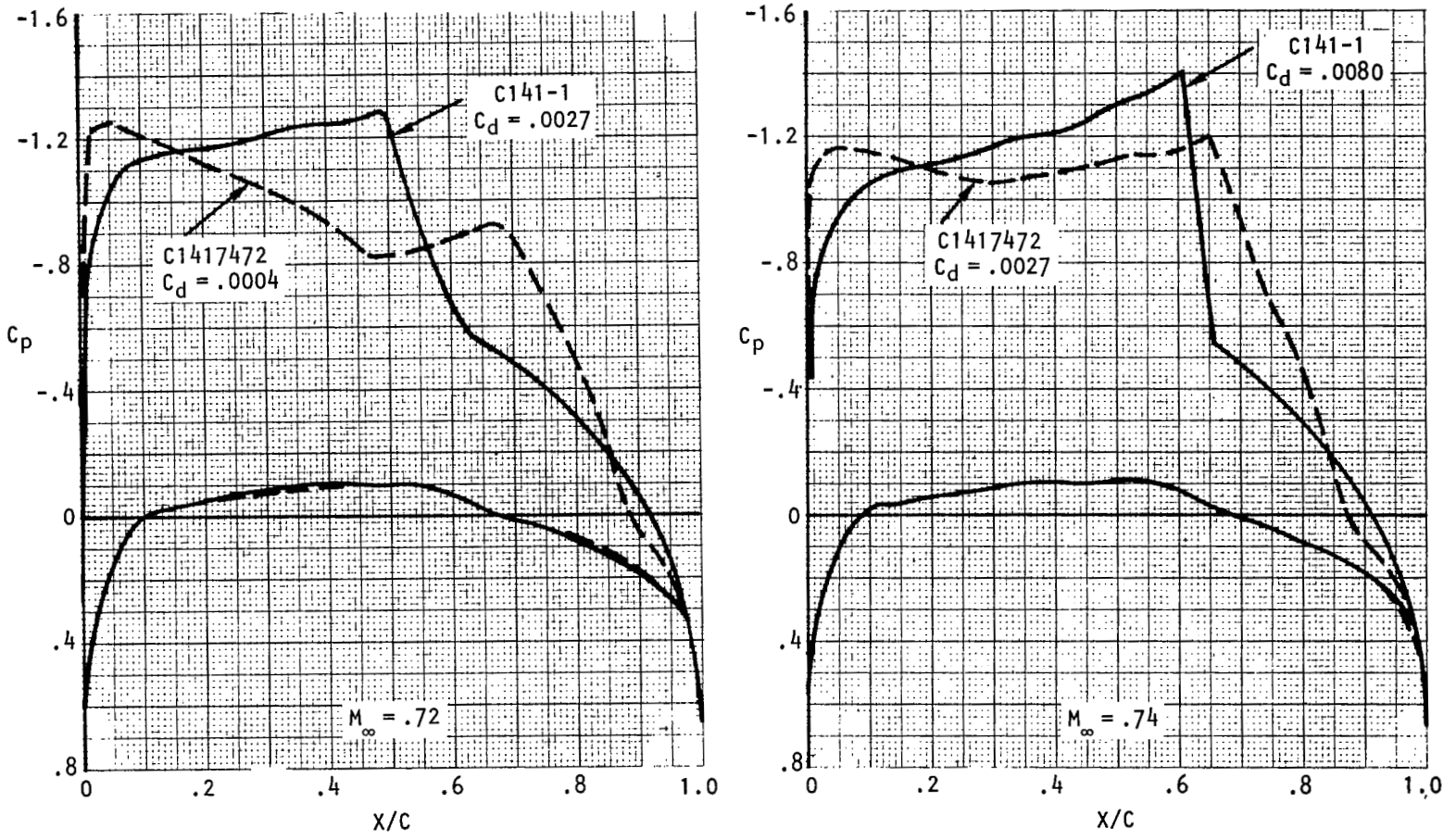

Figure 3. Airfoil C141H7472 inviscid design pressures ($\alpha = 2°$).

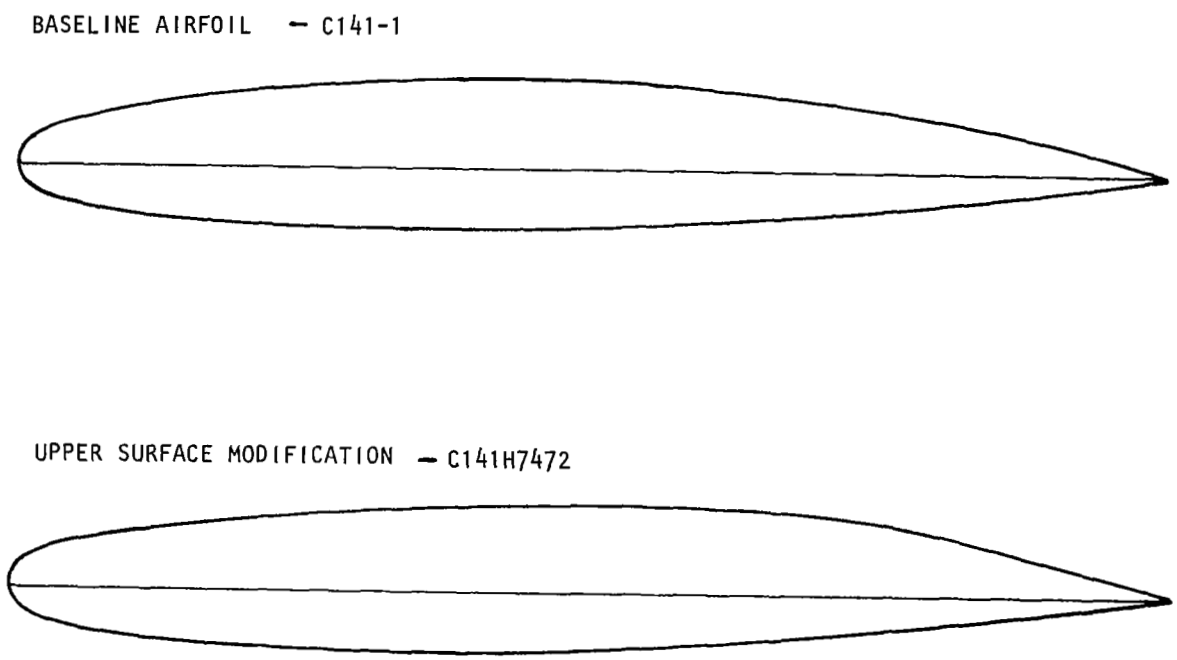

Figure 4. Comparison of airfoil geometries.

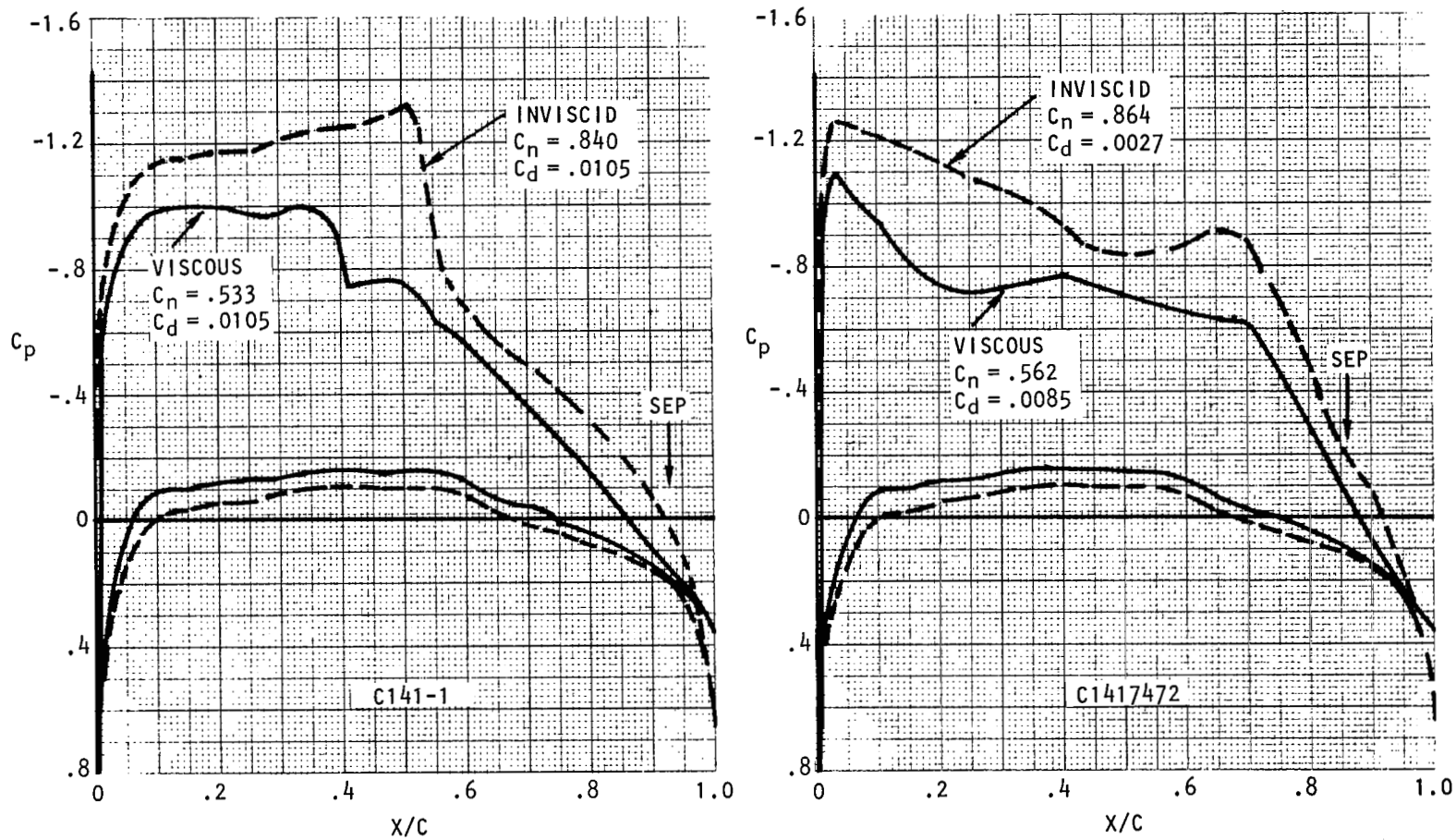

CONDITIONS: $M_\infty = 0.72$, $R_N = 11 \times 10^6$

Figure 5. Inviscid and viscous pressures on the baseline and modified airfoils at $\alpha = 2^\circ$ (Continued).

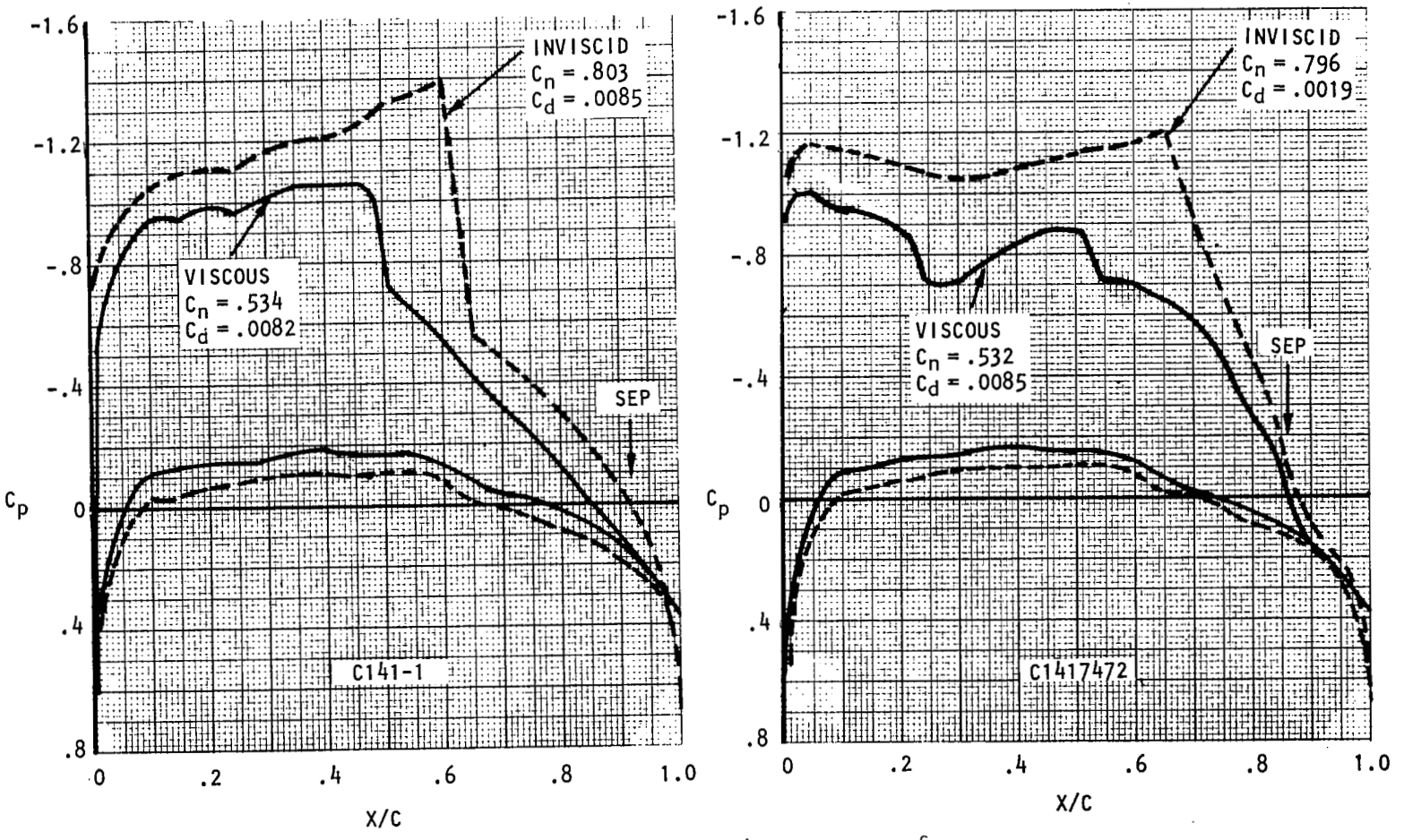

CONDITIONS: $M_\infty = .74$, $R_N = 11 \times 10^6$

Figure 5. Concluded.

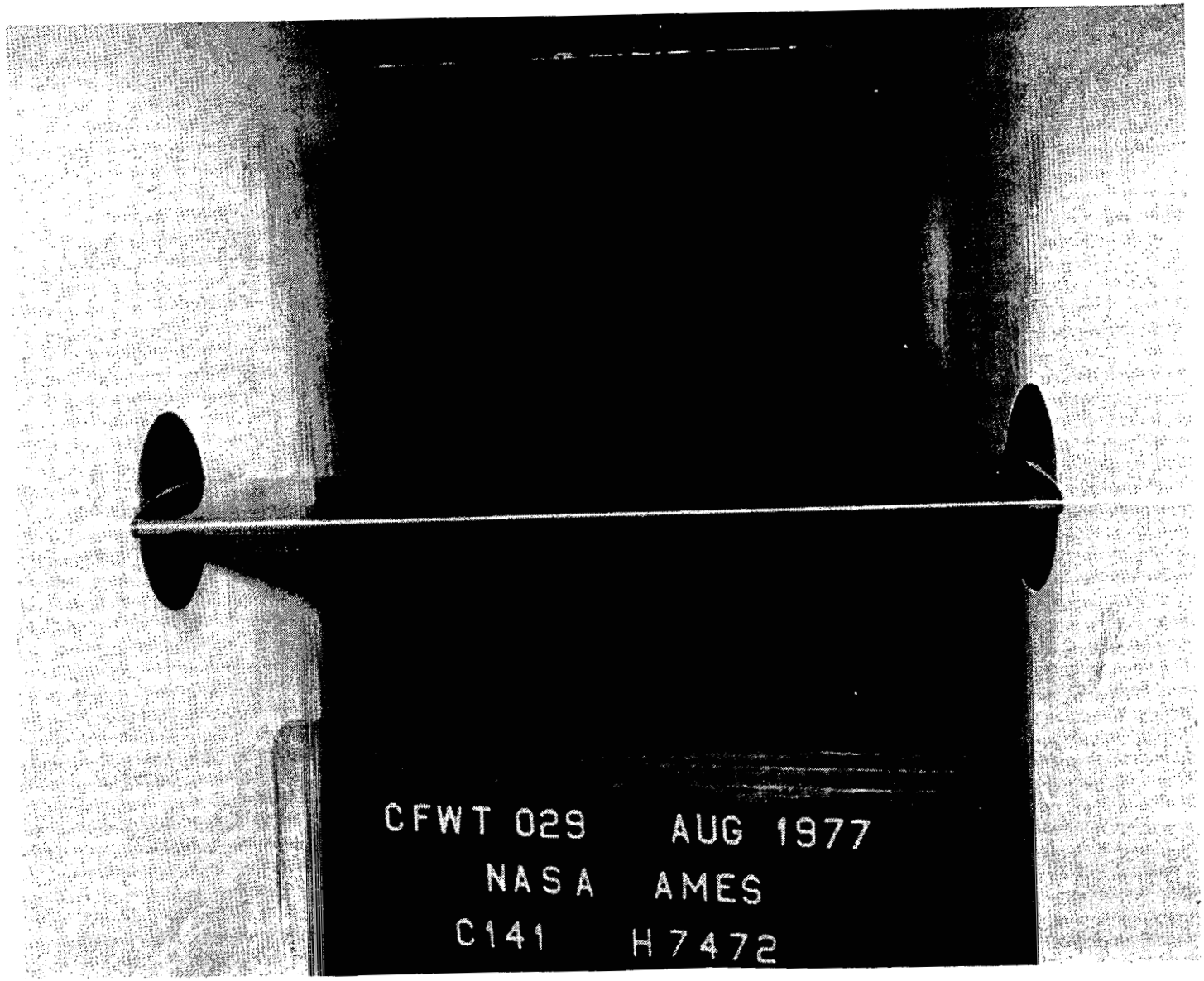

Figure 6. Wind tunnel model installation.

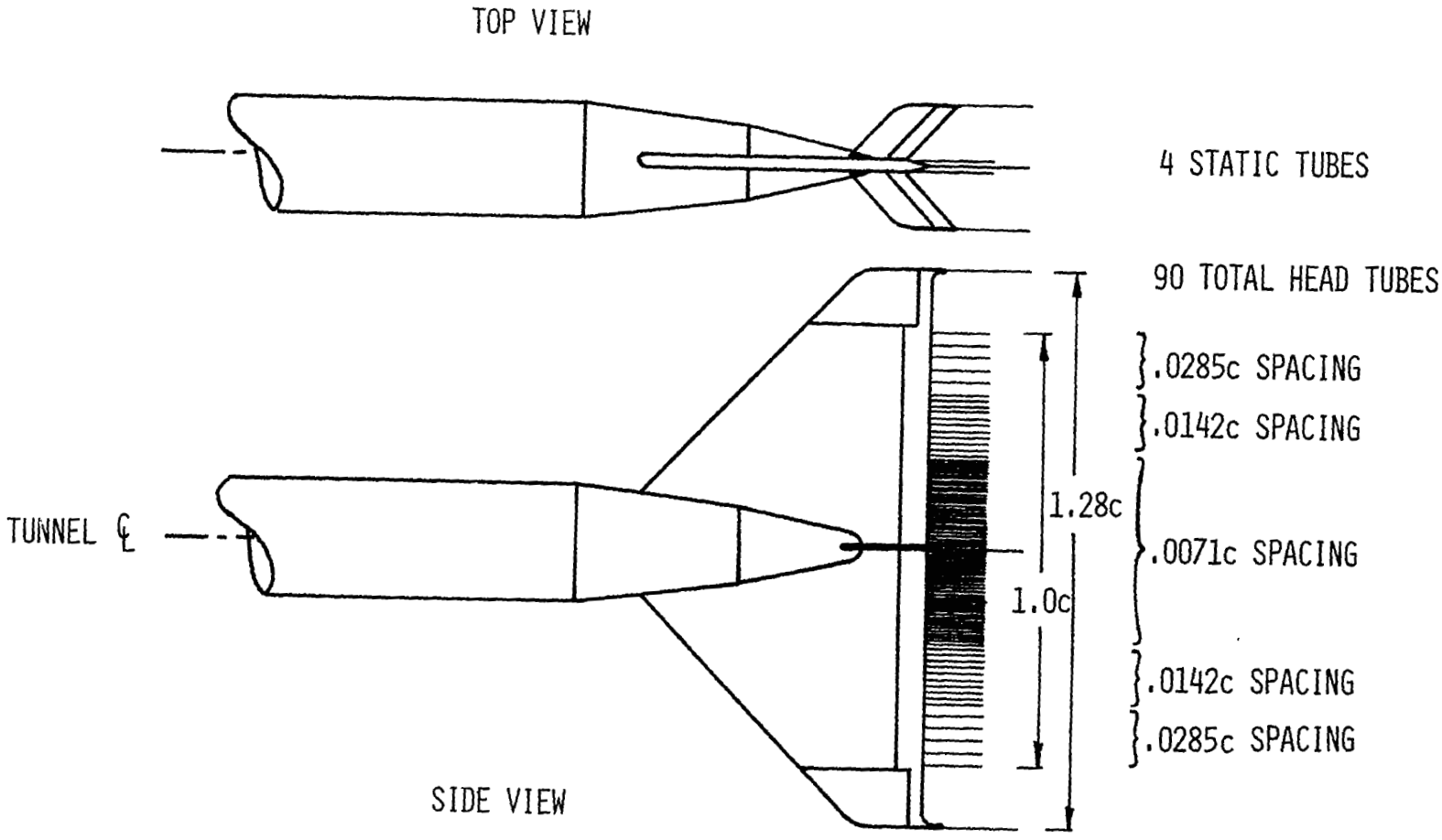

Figure 7. Compressible flow wind tunnel wake rake.

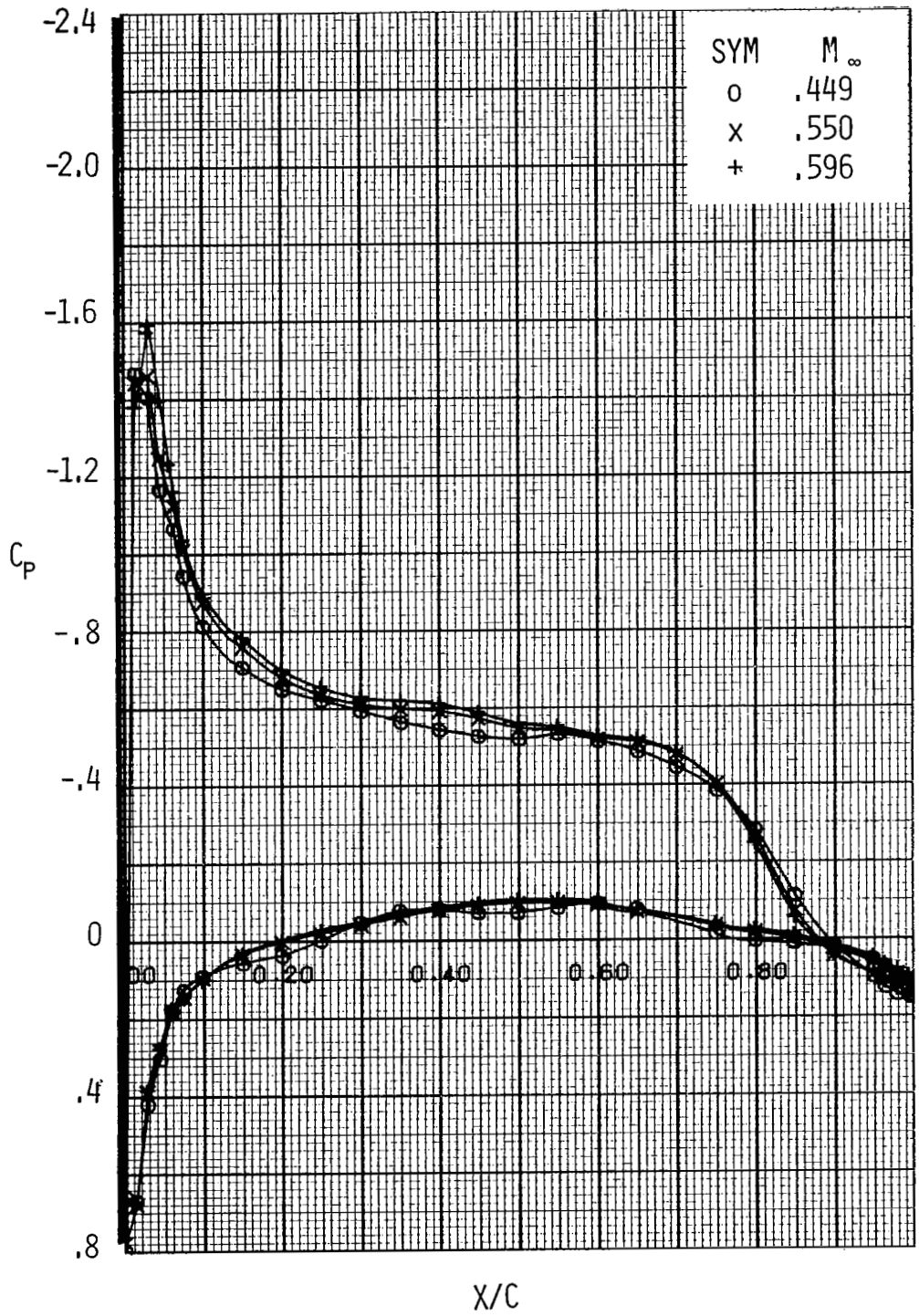

Figure 8. - Airfoil pressure distribution, $C_n = .57$, $R_N = 11 \times 10^6$, X/C_T = free.

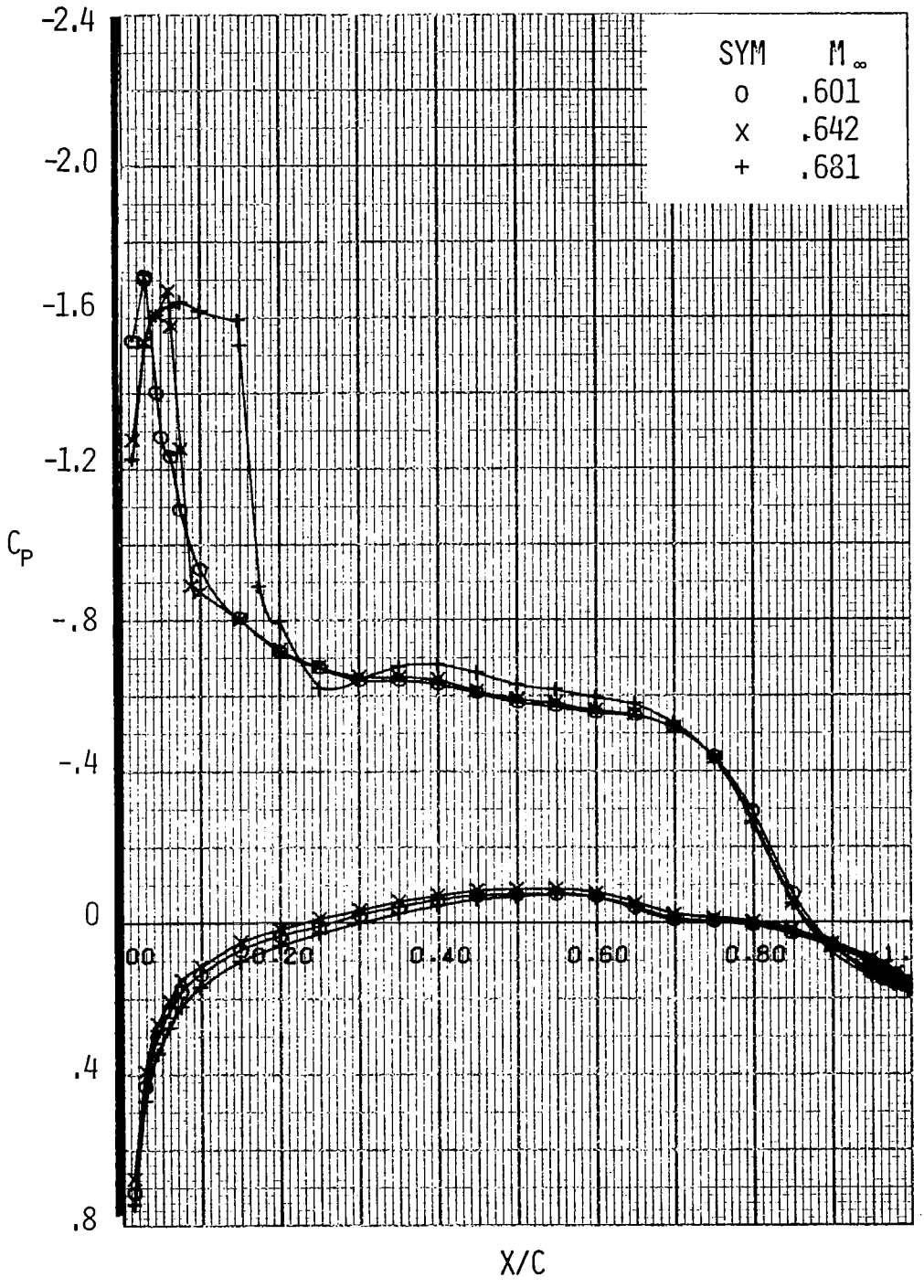

Figure 8. Continued.

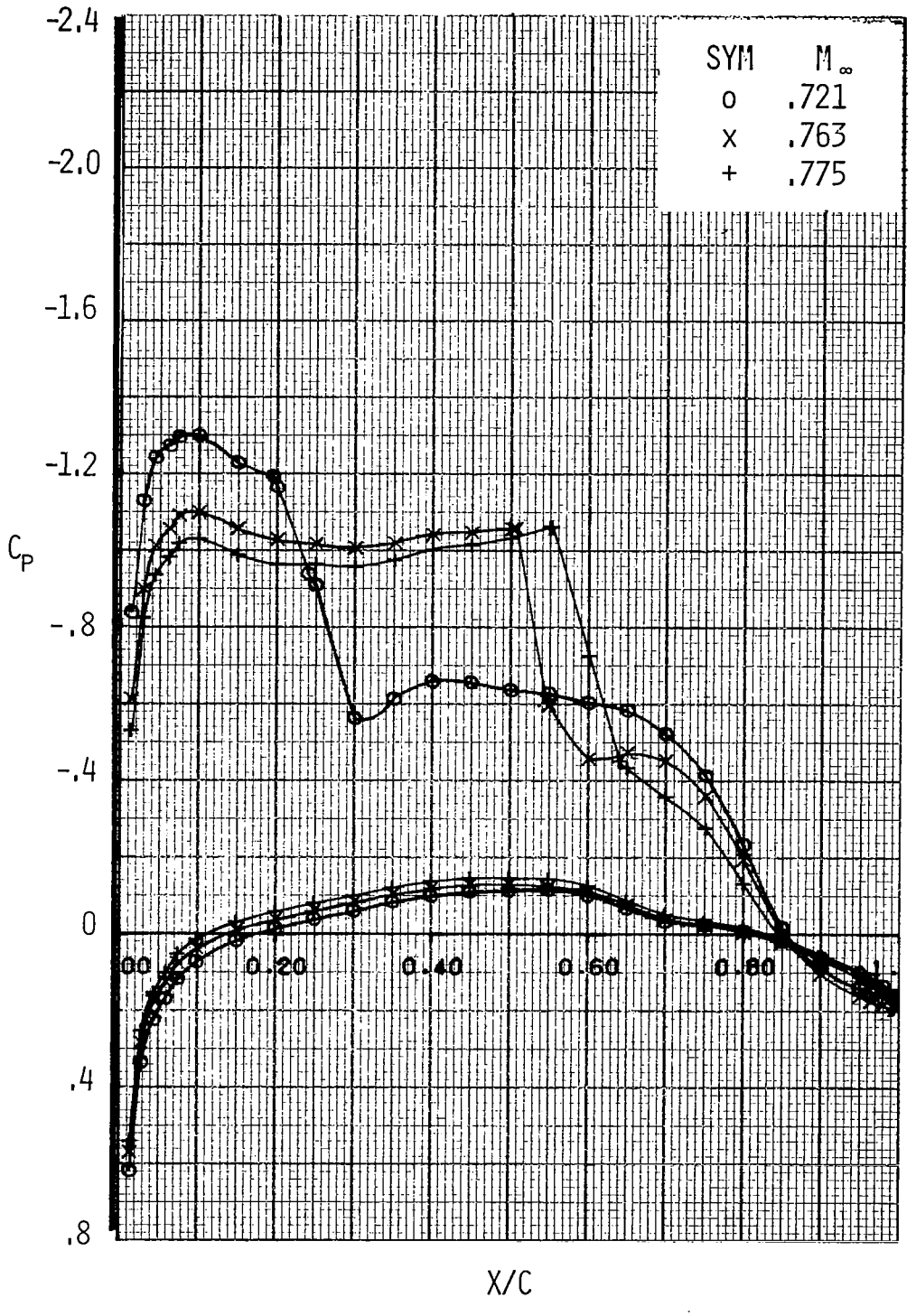

Figure 8. Continued.

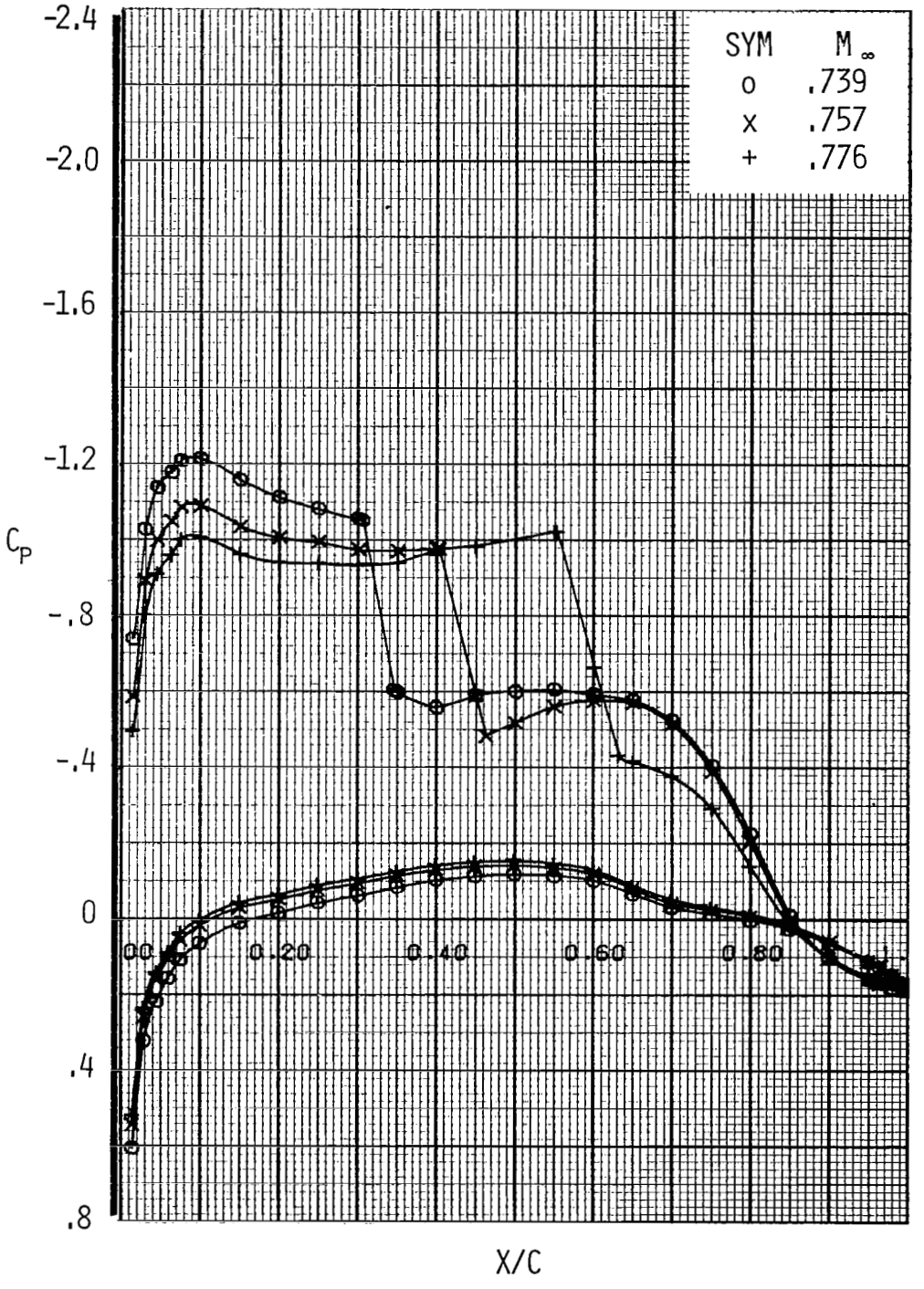

Figure 8 Concluded.

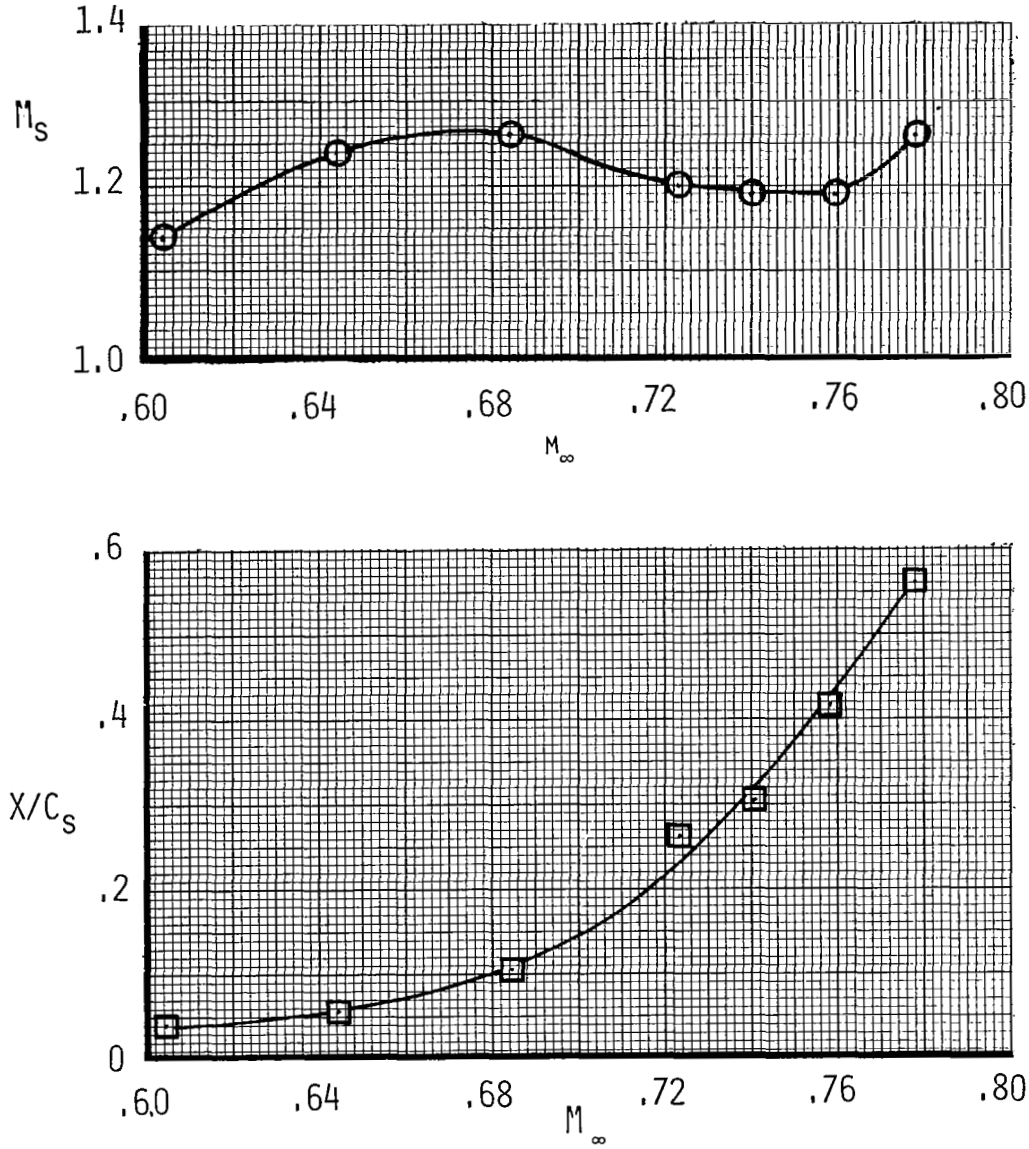

Figure 9. - Effect of Mach number on airfoil shock characteristics at $C_n = .57$, $R_N = 11 \times 10^6$, X/C_T = free.

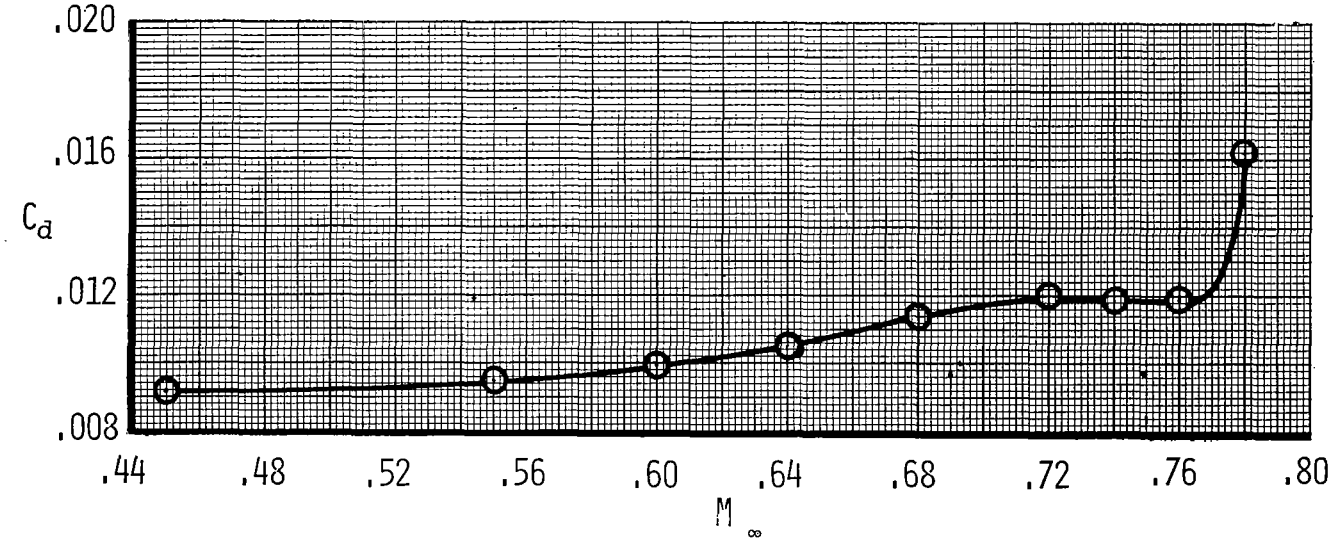

Figure 10. - Effect of Mach number on drag coefficient, $C_n = .57$, $R_N = 11 \times 10^6$, X/C_T = free.

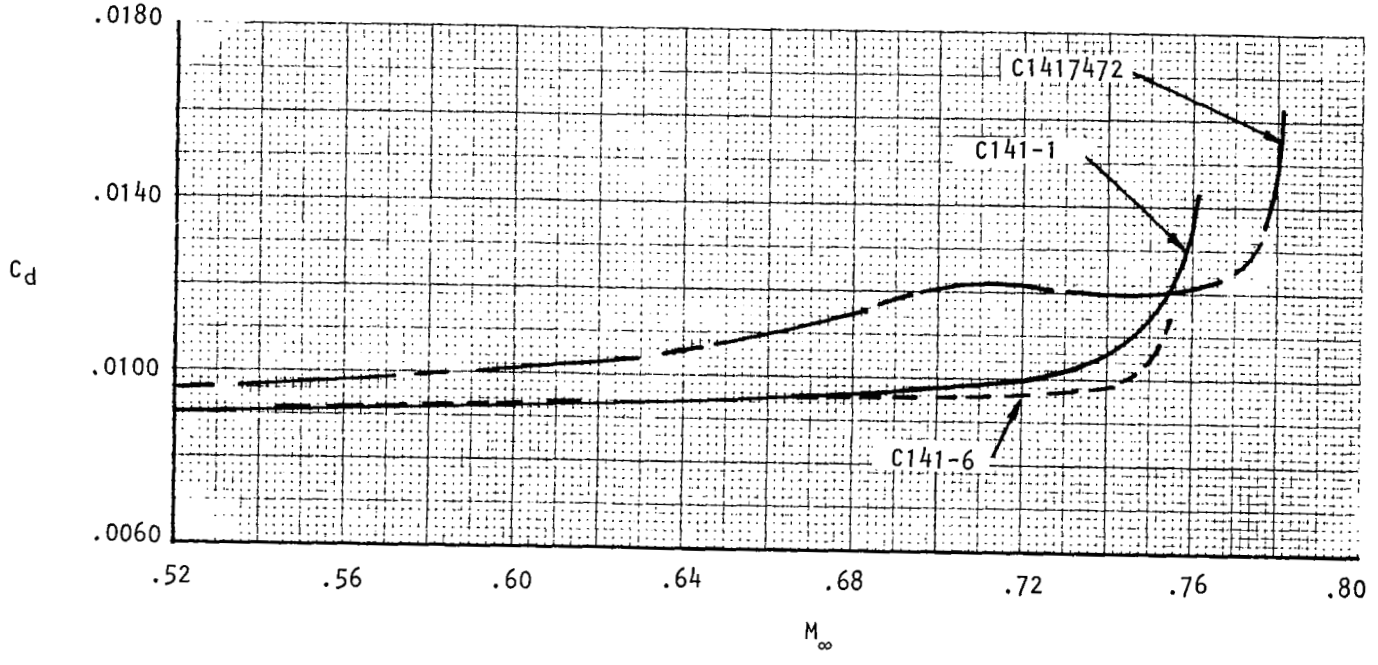

Figure 11. Comparison of measured airfoil performances at $C_n = 0.57$, $R_N = 11 \times 10^6$.

SYMBOL	AIRFOIL	C_n	C_d	C_m
△	C141-1	.567	.0092	-.0433
⬡	C141-6	.531	.0090	-.0406
⊡	C1417472	.569	.0096	-.0417

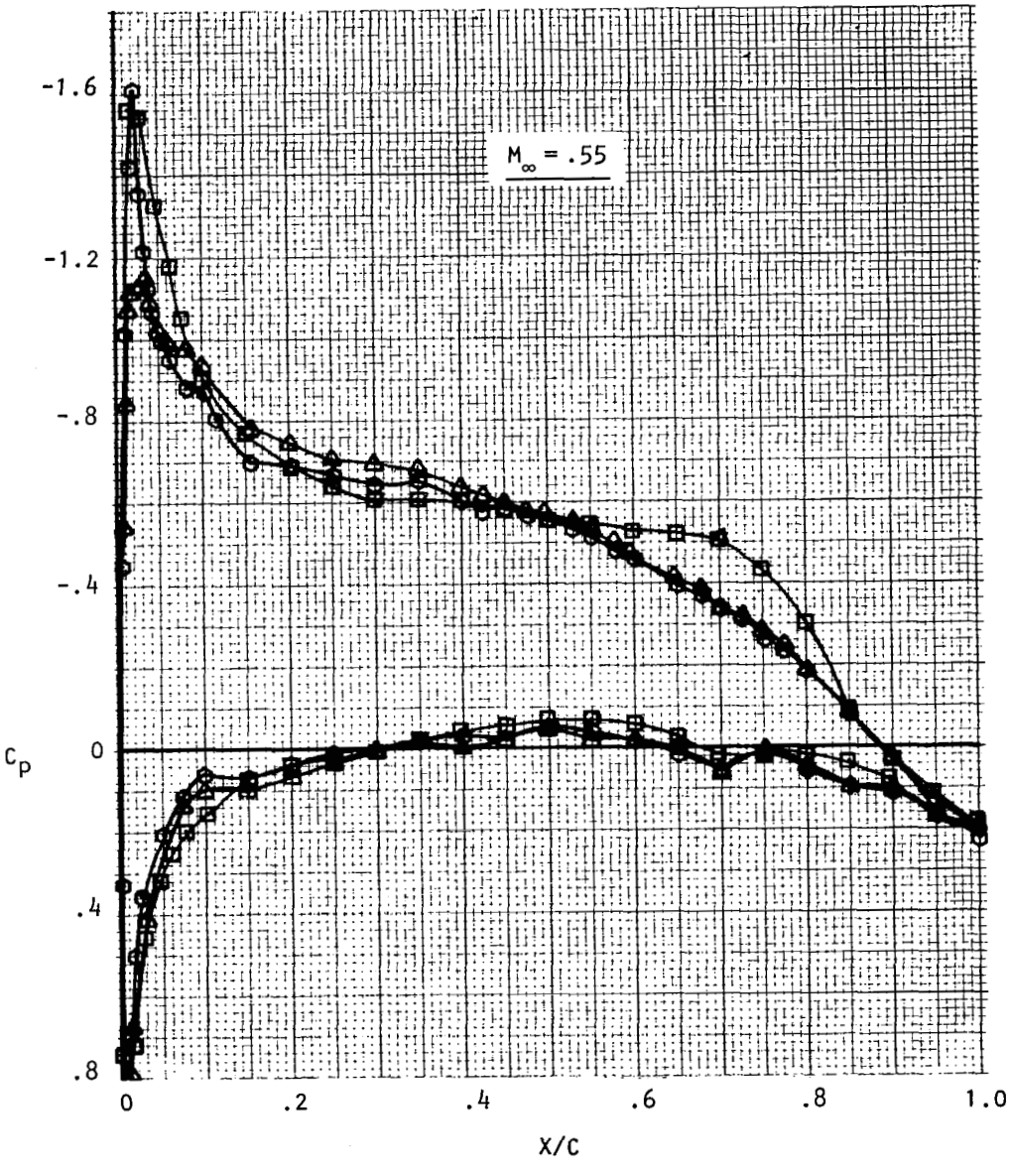

Figure 12. Comparison of measured airfoil pressures, $R_N = 11 \times 10^6$.

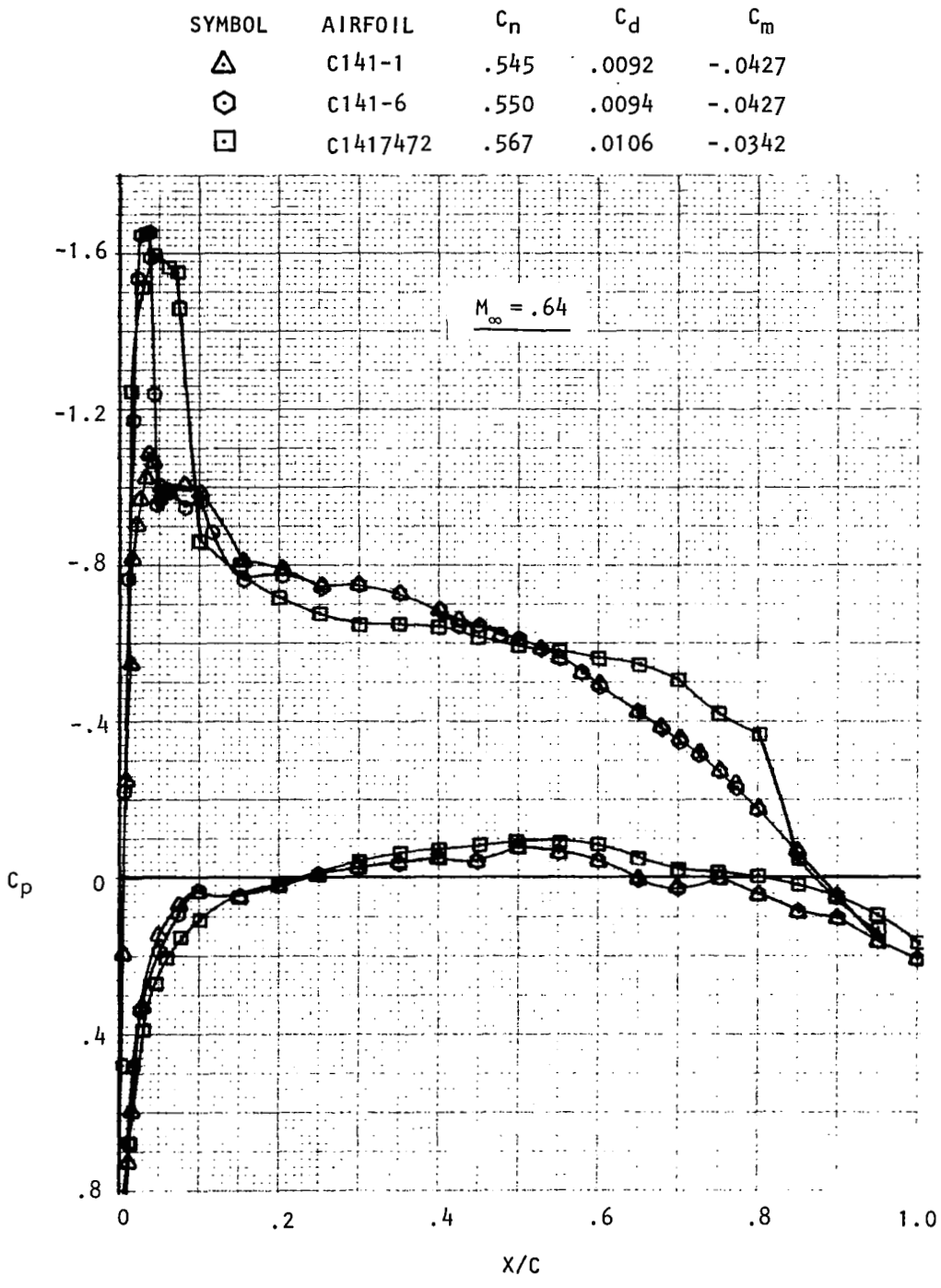

Figure 12. Continued.

SYMBOL	AIRFOIL	C_n	C_d	C_m
△	C141-1	.562	.0097	-.0431
⬡	C141-6	.579	.0095	-.0373
⊡	C1417472	.558	.0116	-.0333

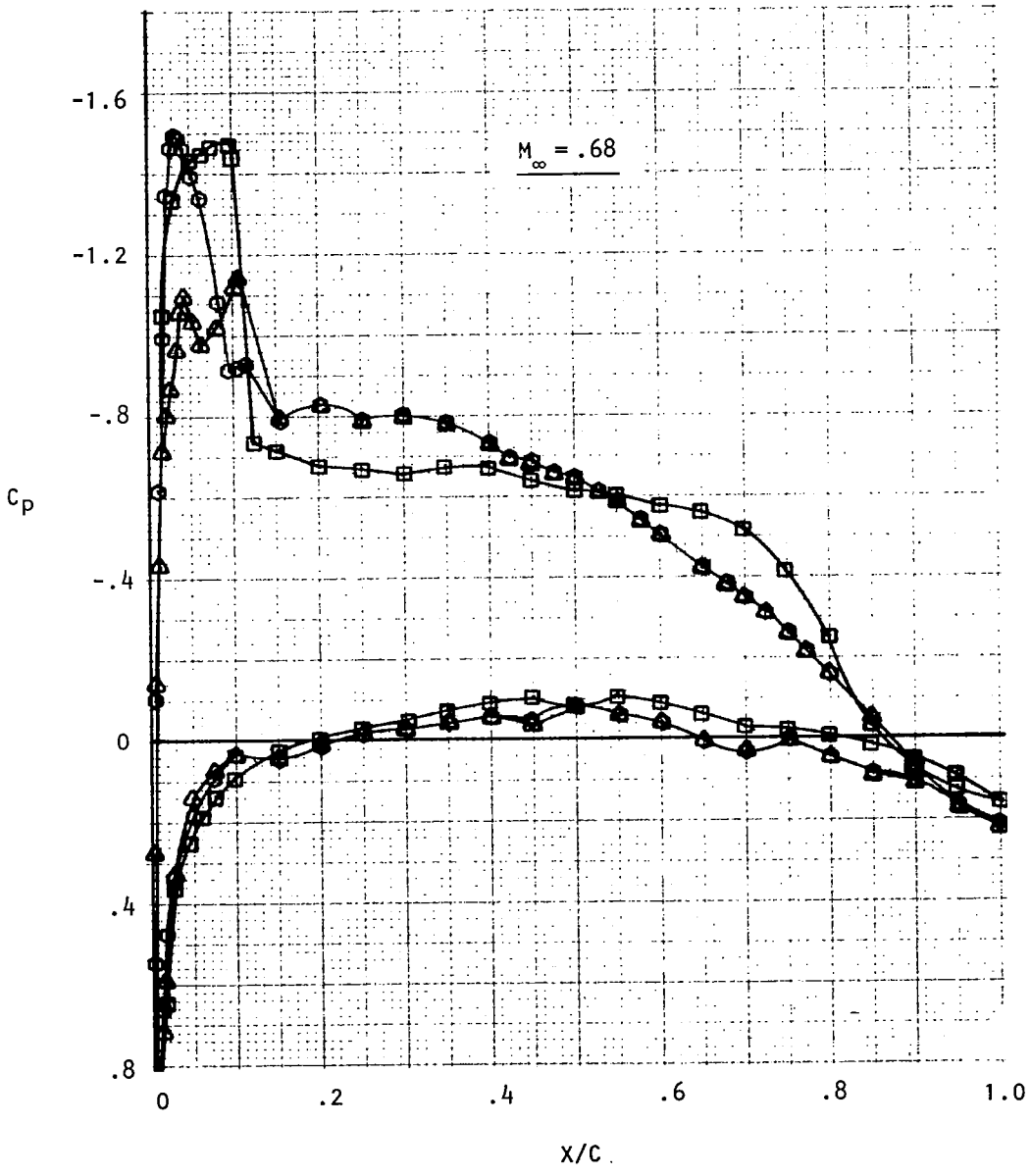

Figure 12. Continued.

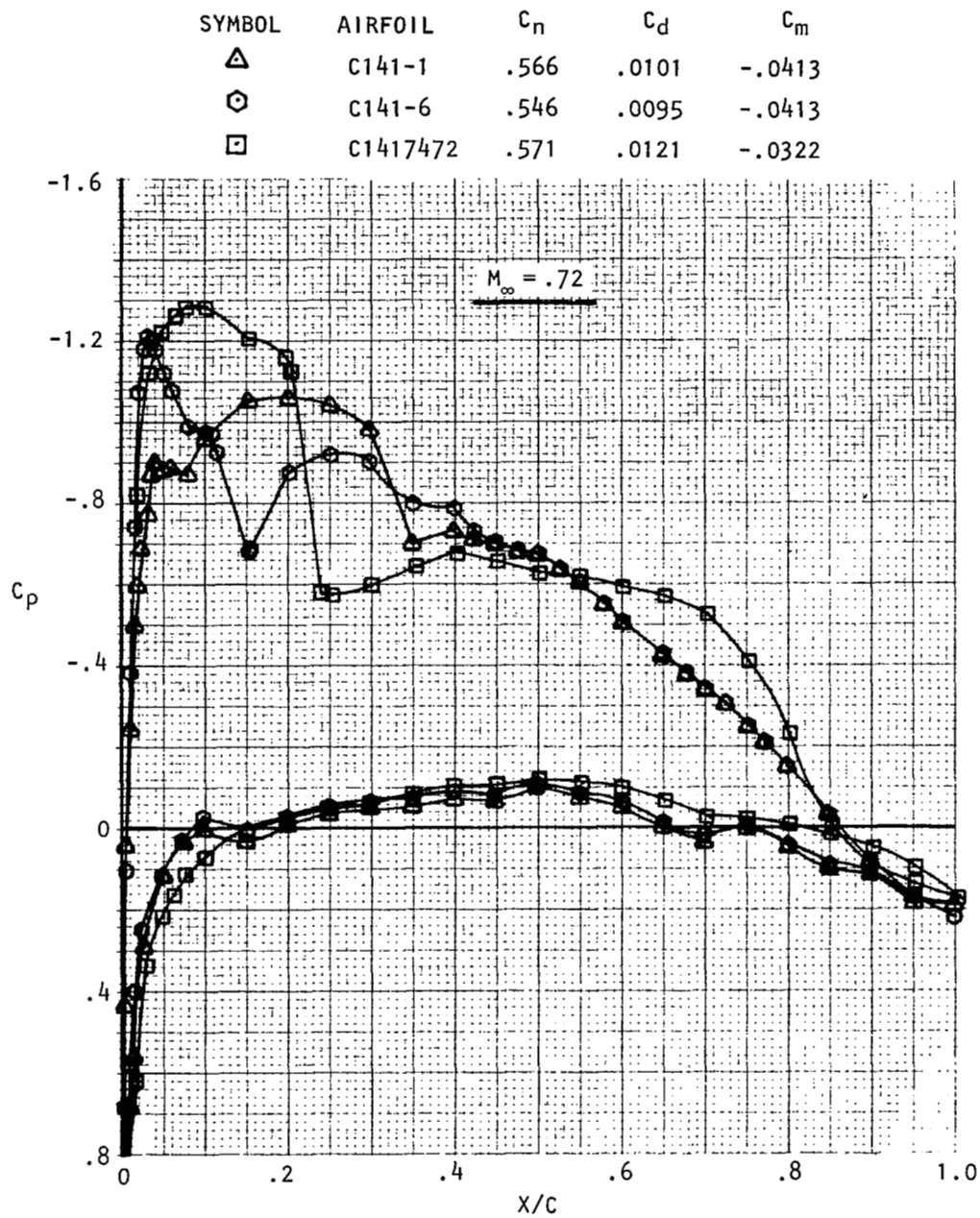

Figure 12. Continued.

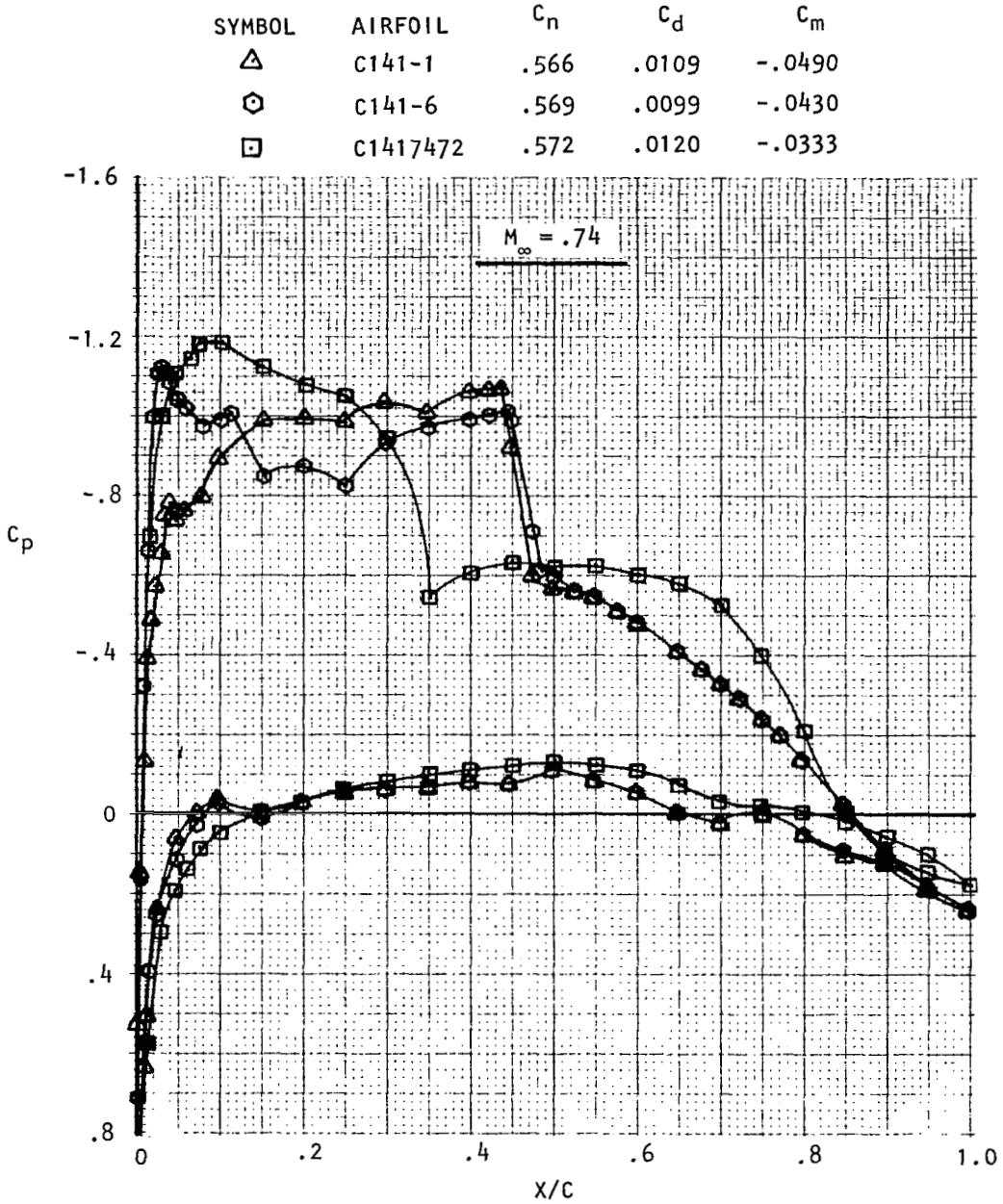

Figure 12. Continued.

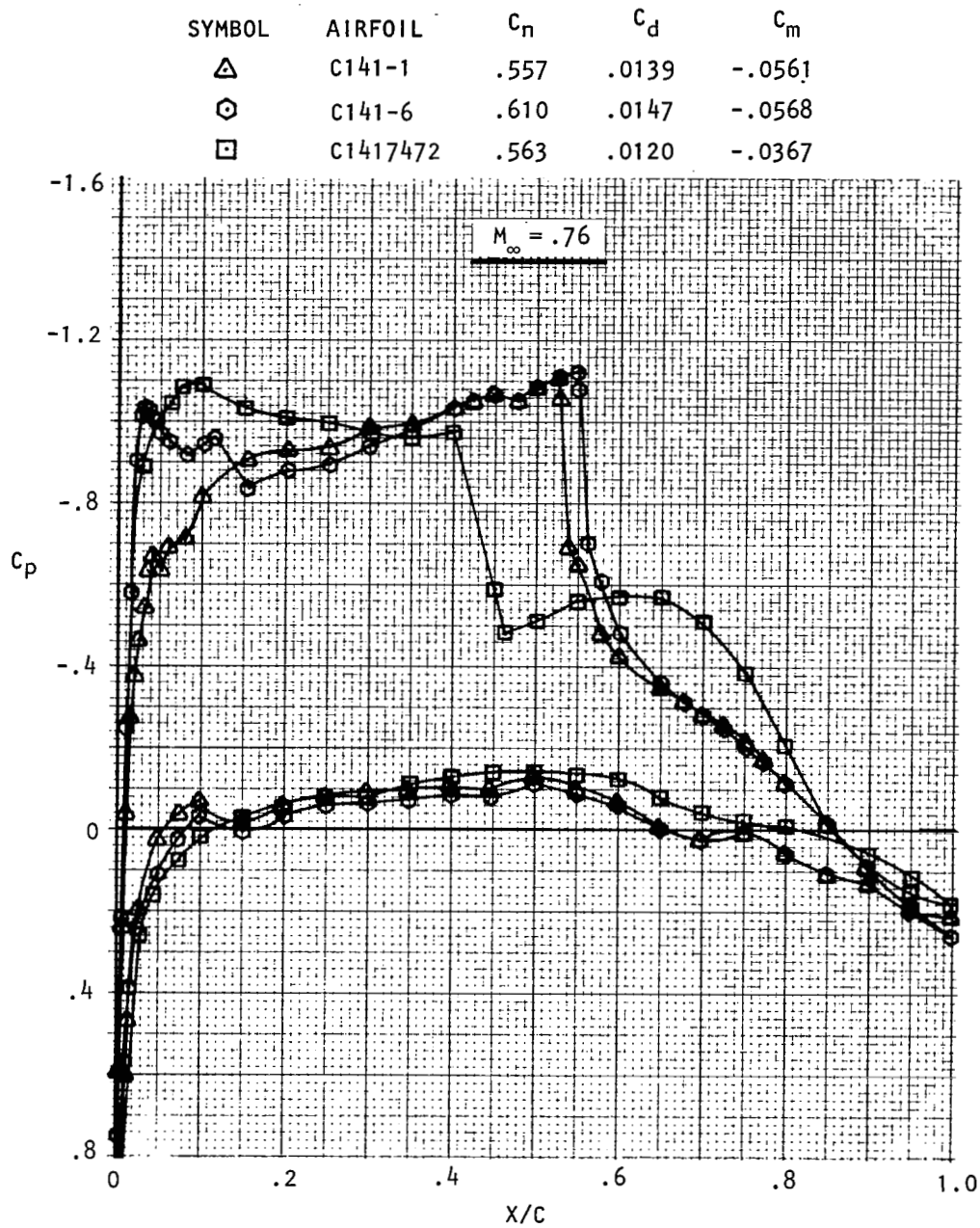

Figure 12. Continued.

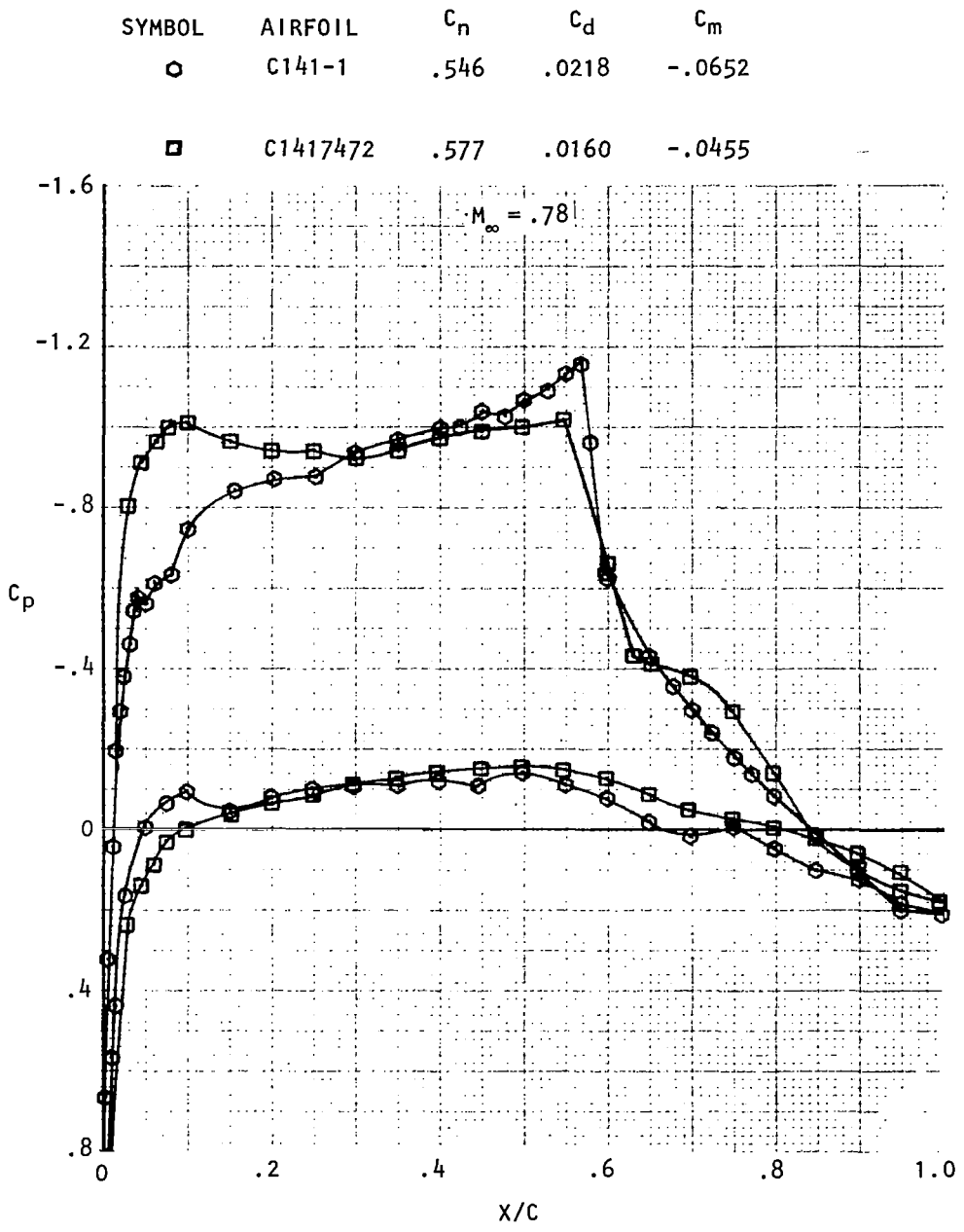

Figure 12. Concluded.

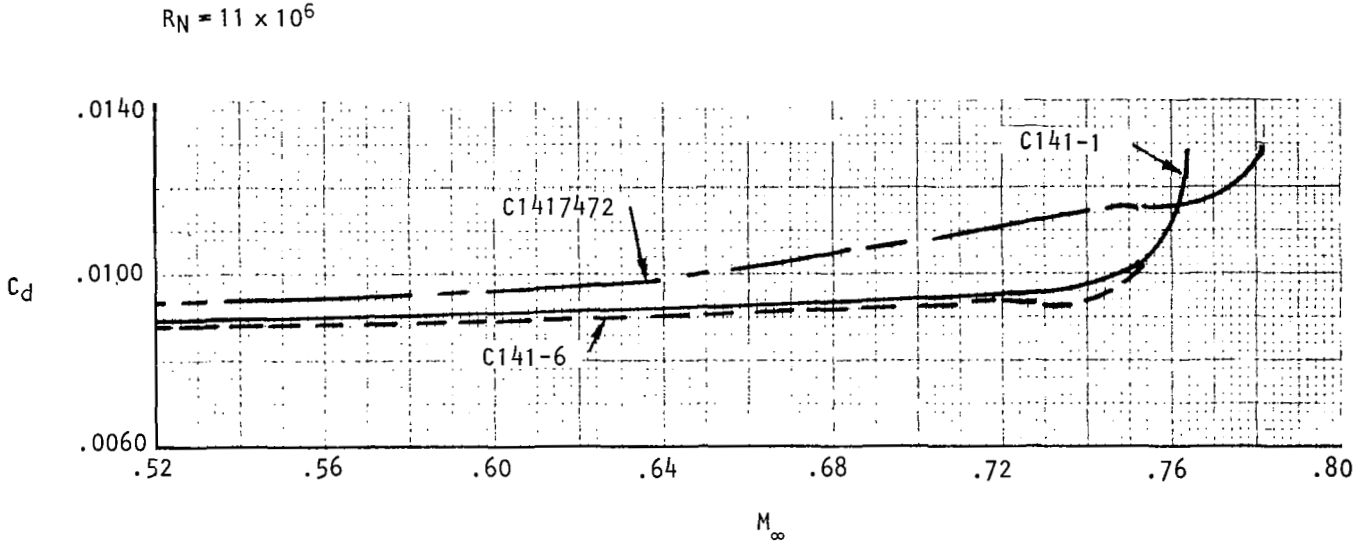

Figure 13. Measured airfoil performance at $C_n = 0.50$.

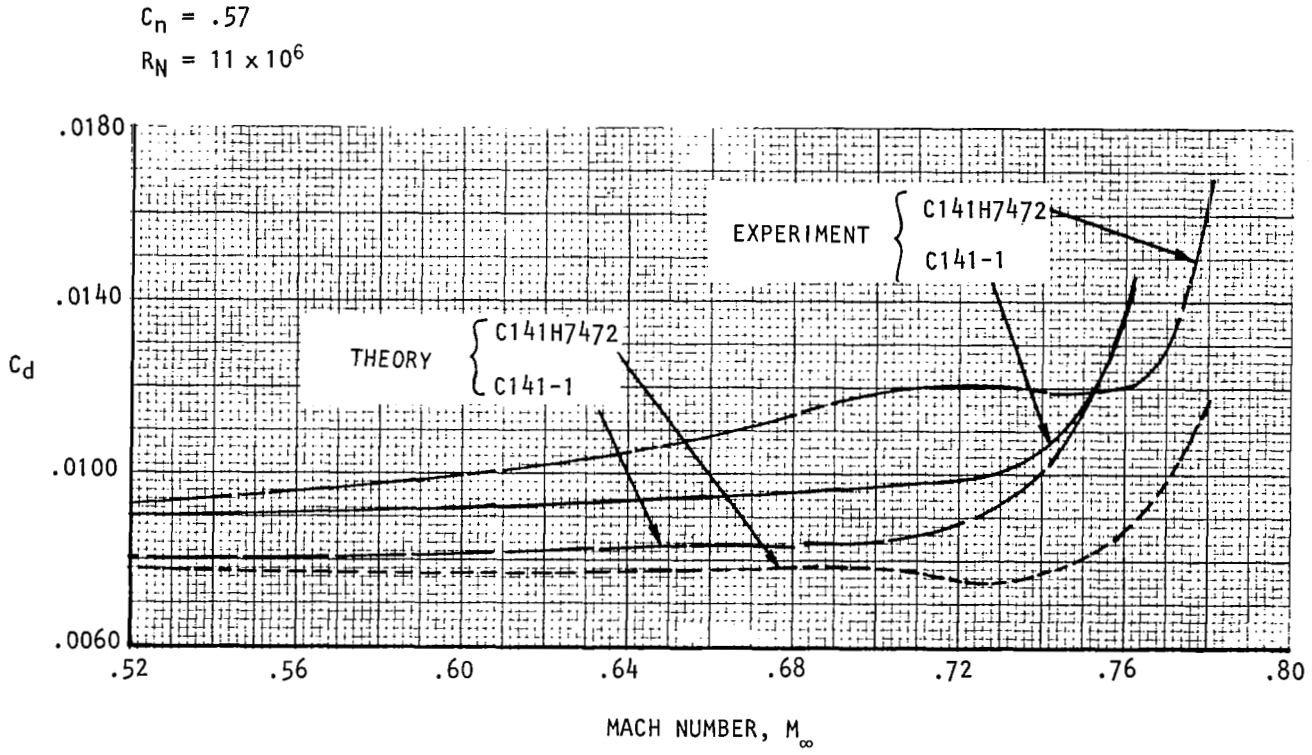

Figure 14. Theoretical and experimental drag for the baseline and upper surface modification.

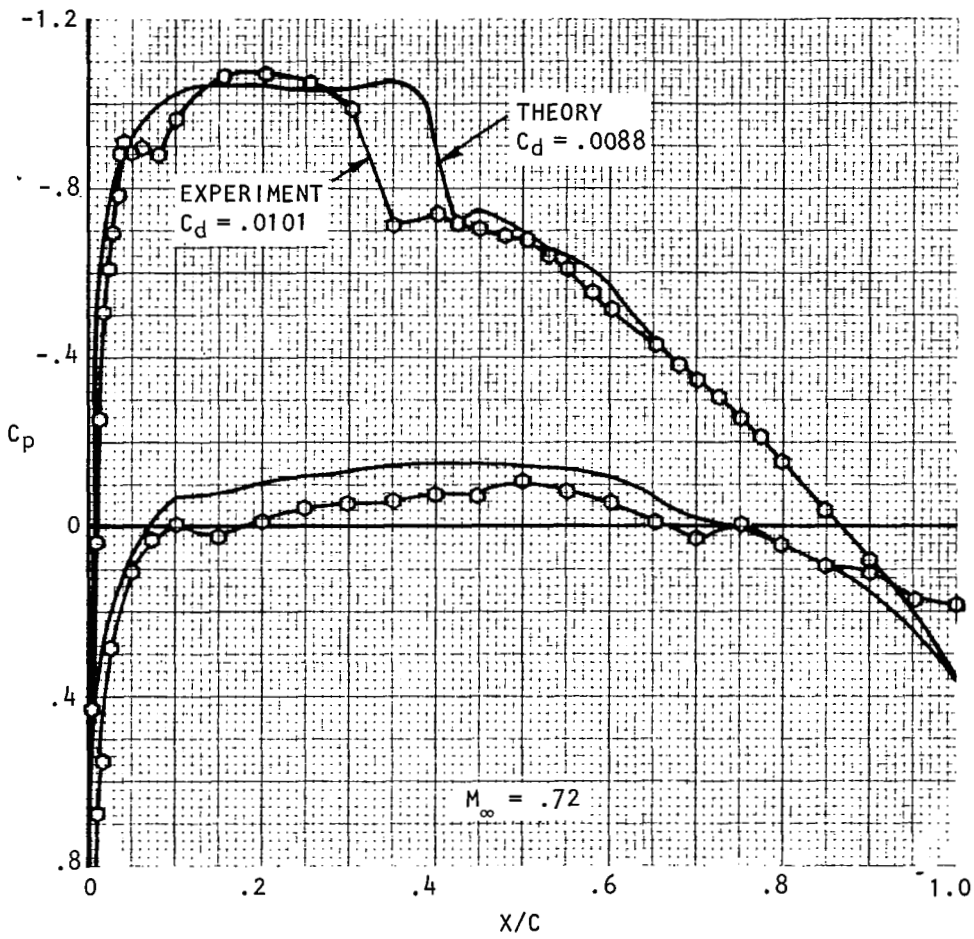

Figure 15. Baseline airfoil theoretical and experimental pressures at $C_n = 0.57$.

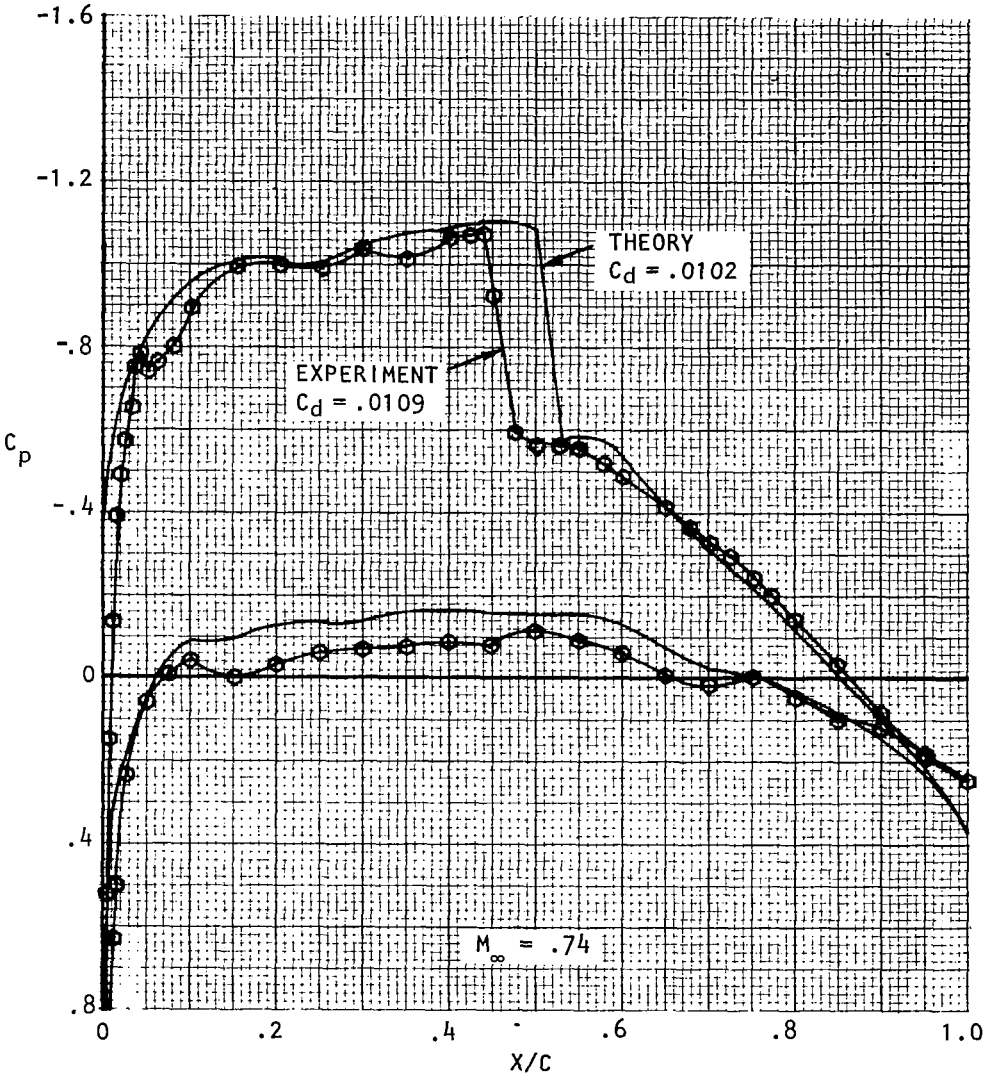

Figure 15. Concluded.

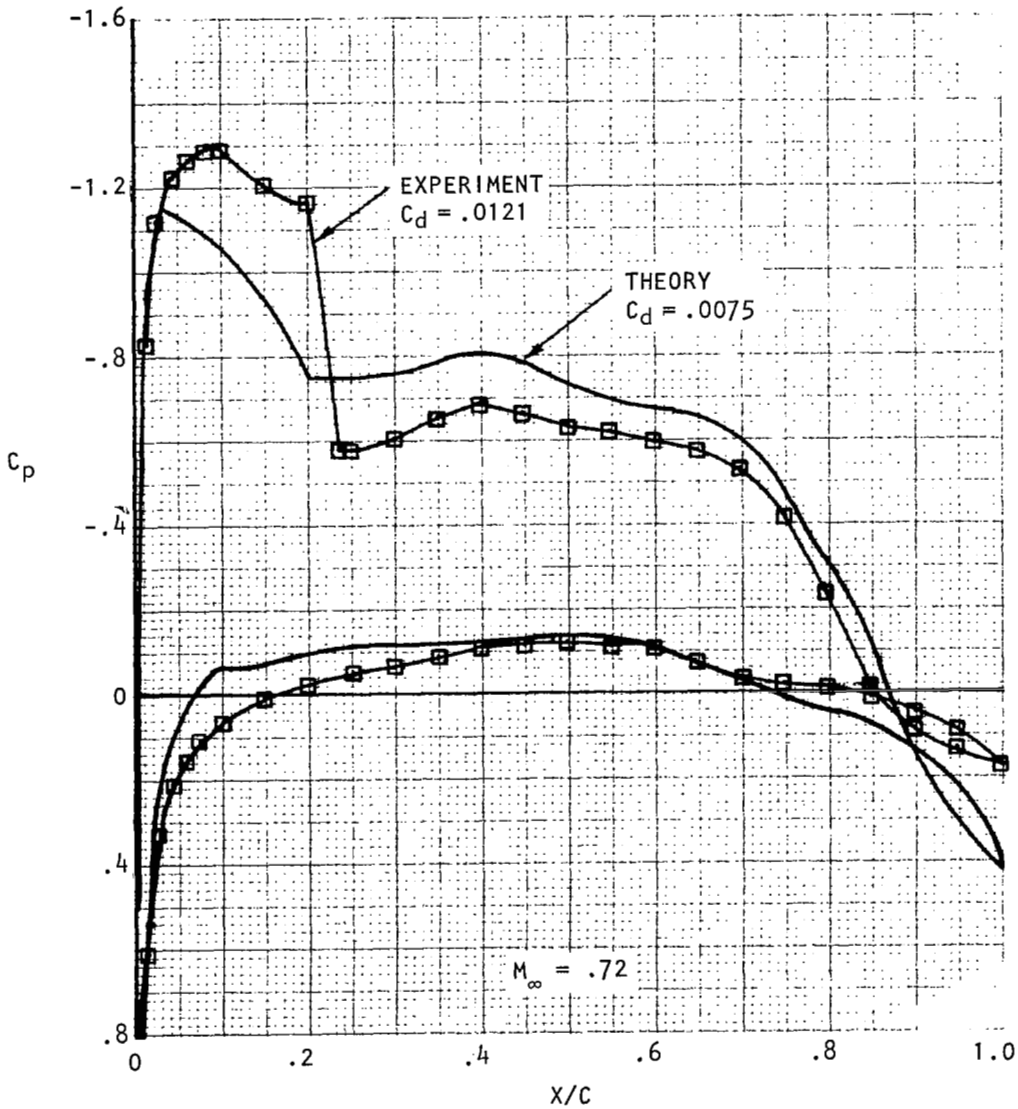

Figure 16. Airfoil C141H7472 theoretical and experimental pressures at C_n = 0.57.

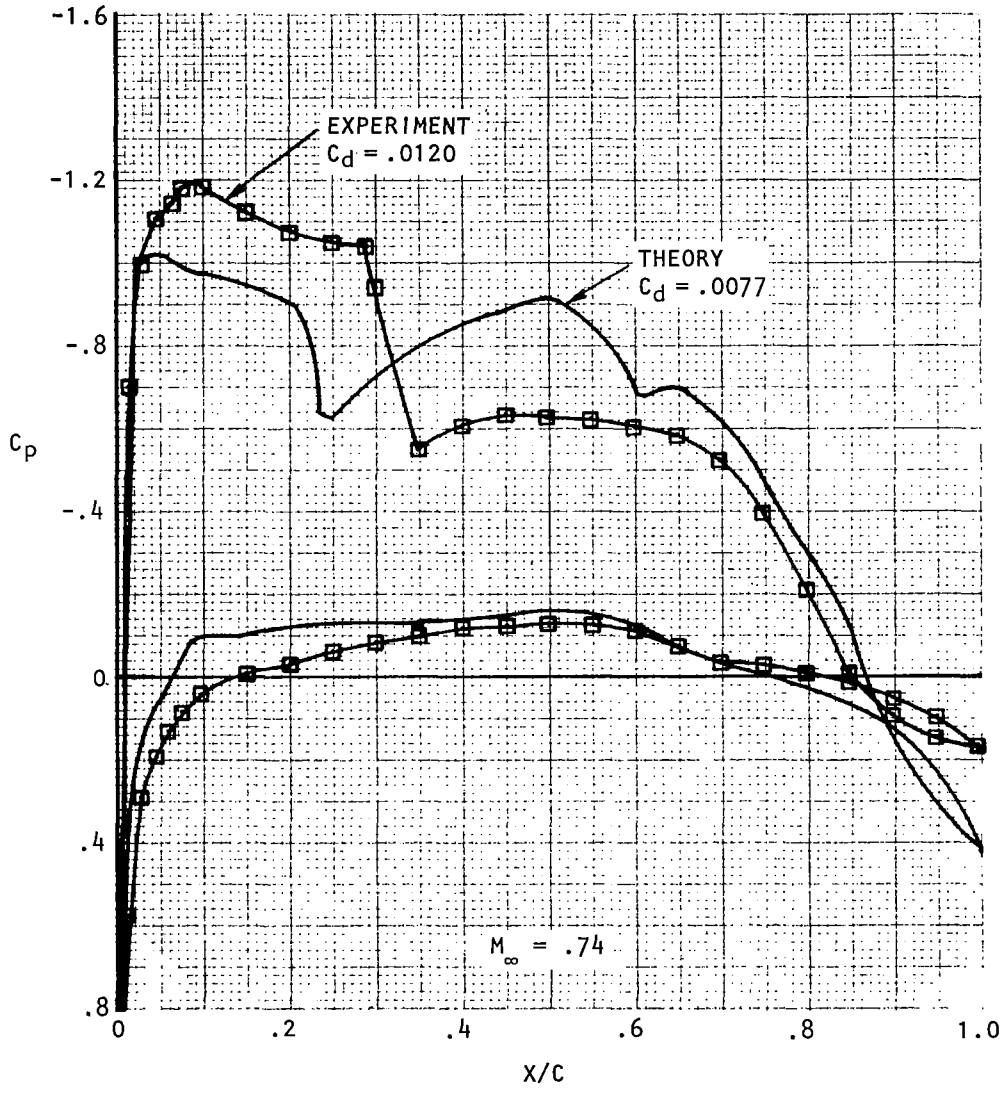

Figure 16. Concluded.

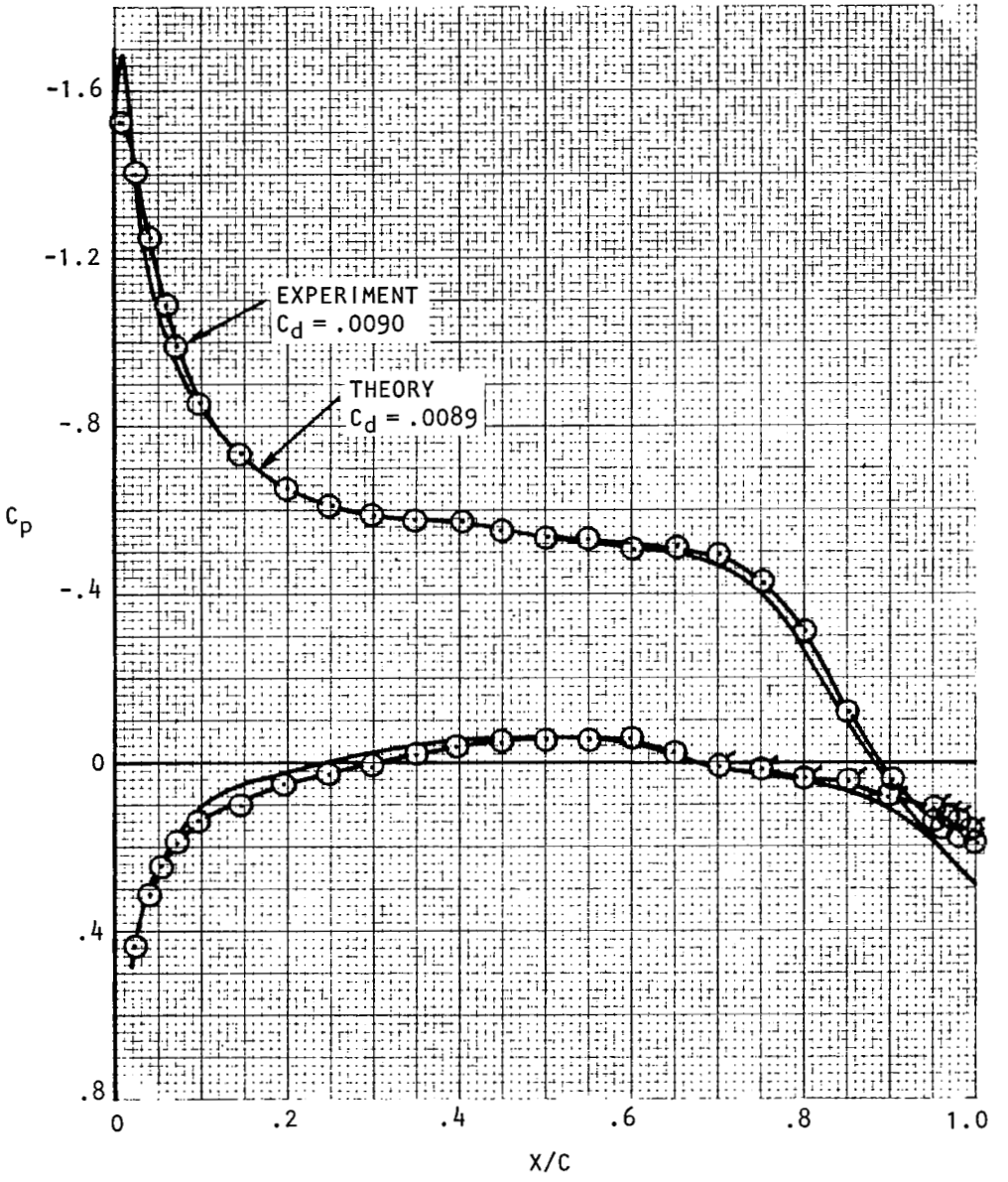

Figure 17. Comparison of airfoil C141H7472 pressures at subcritical conditions (C_n = .57, M_∞ = .45)

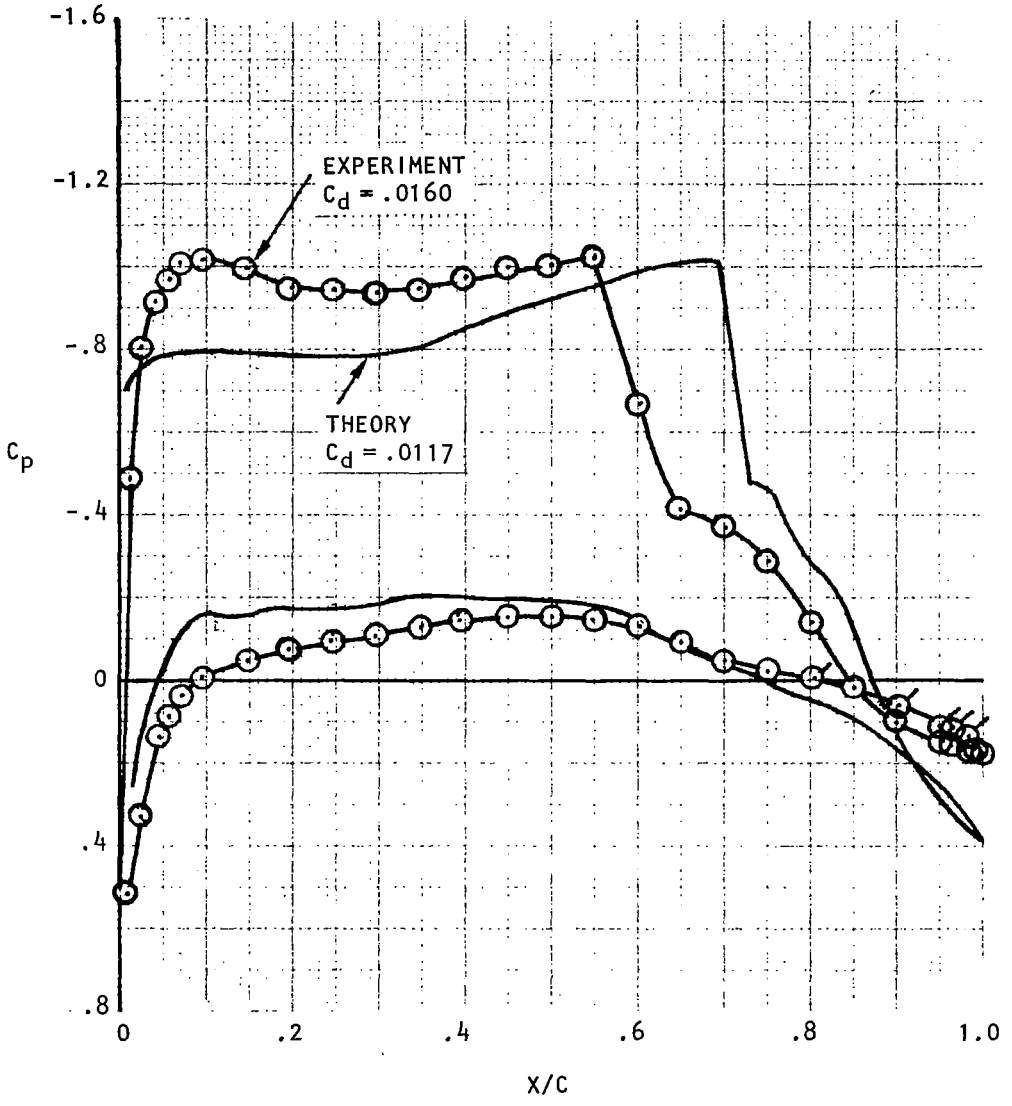

Figure 18. Comparison of airfoil C141H7472 pressures near drag divergence (C_n = .57, M_∞ = .78)

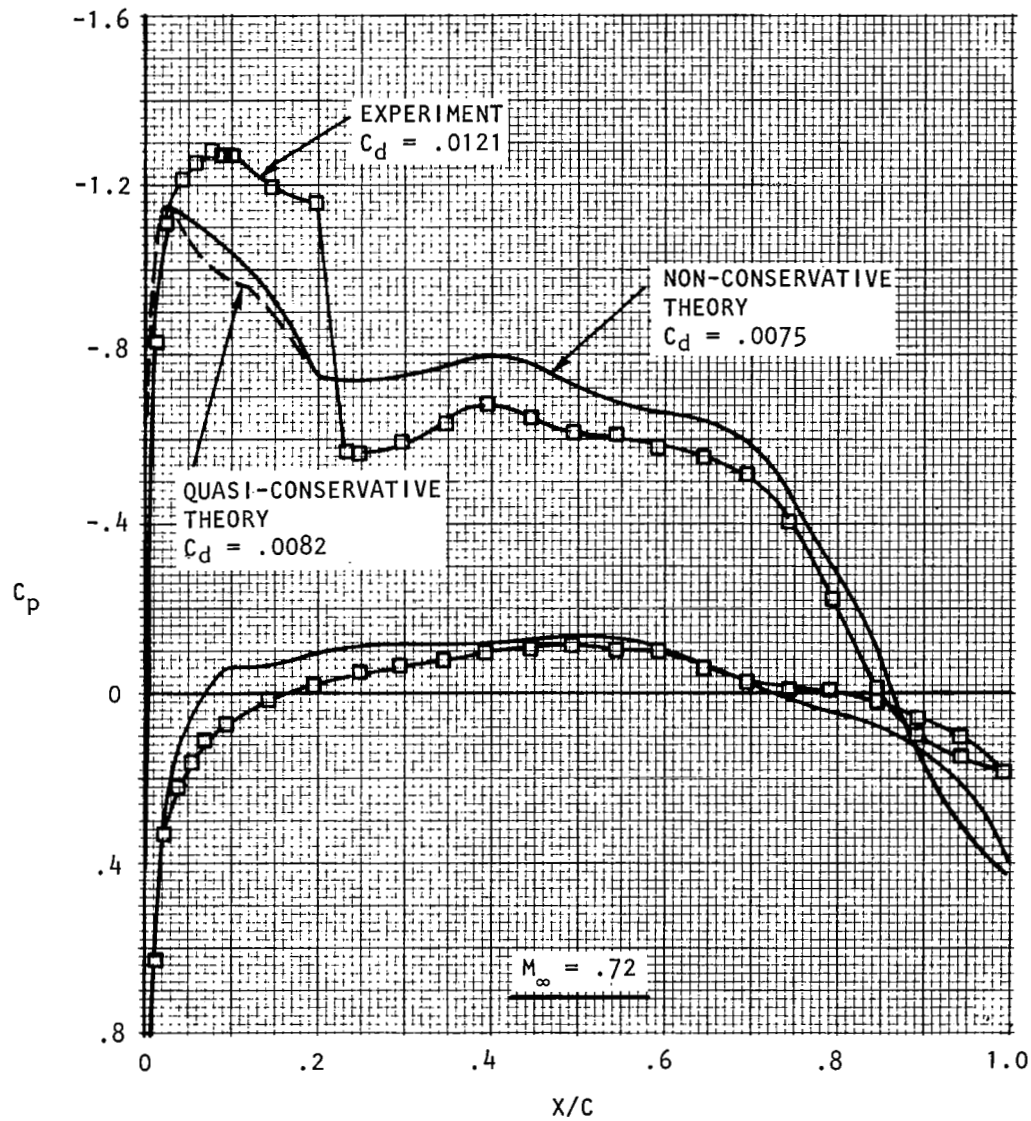

Figure 19. Comparison of theoretical solutions with experimental data for airfoil C141H7472 at C_n = 0.57

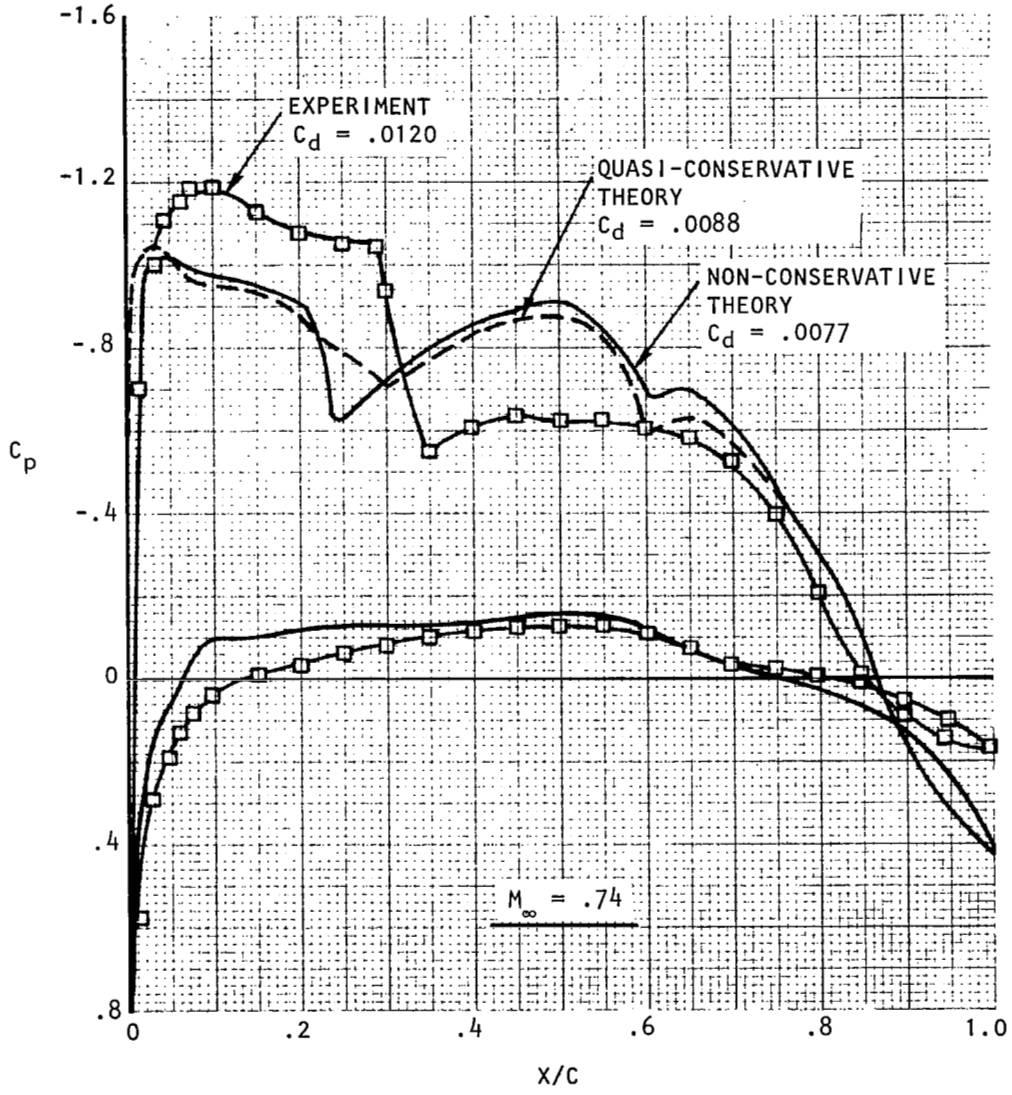

Figure 19. Concluded.

SYMBOL	DATA	MACH	α	C_n	C_d
O	EXP.	.72	3.0	0.57	.0121
———	NON-CONS.	.72	3.0	0.69	.0096
— — —	QUASI-CONS.	.71	3.0	0.65	.0080

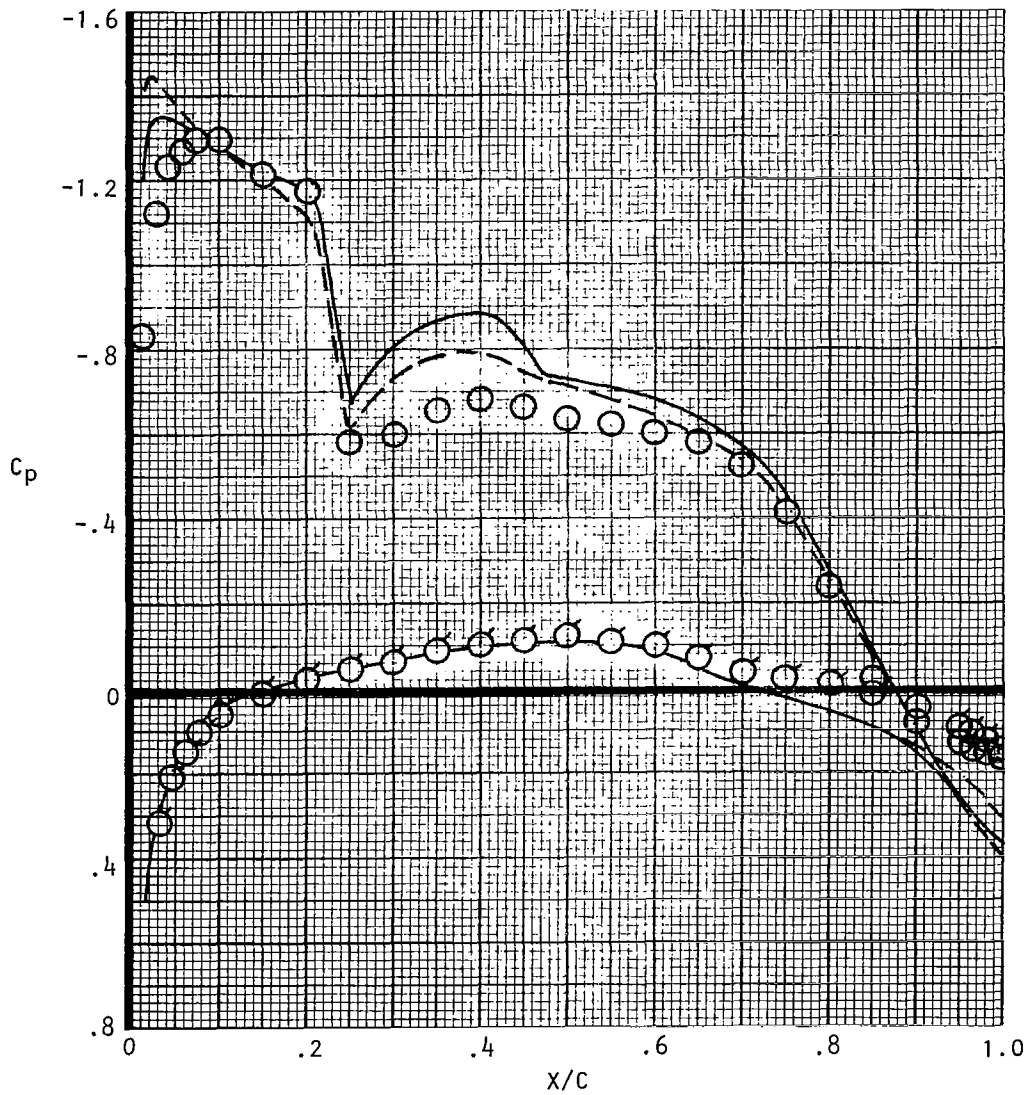

Figure 20. Airfoil C141H7472 theoretical and experimental pressure match.

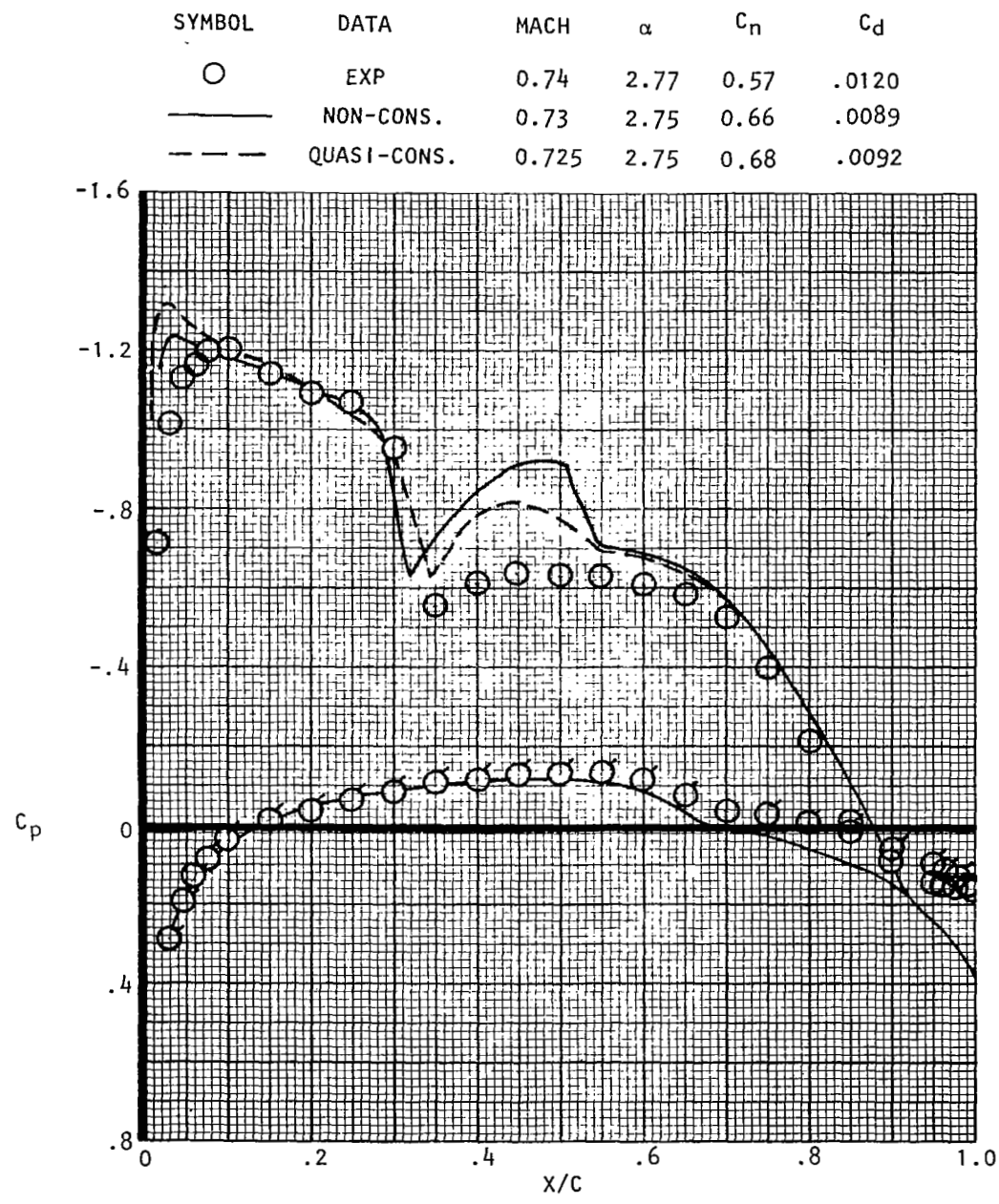

Figure 20. Continued.

SYMBOL	DATA	MACH	α	C_n	C_d
O	EXP	.78	2.5	0.58	.0160
———	NON-CONS.	.75	2.4	0.65	.0089
— — —	QUASI-CONS.	.76	2.5	0.60	.0138

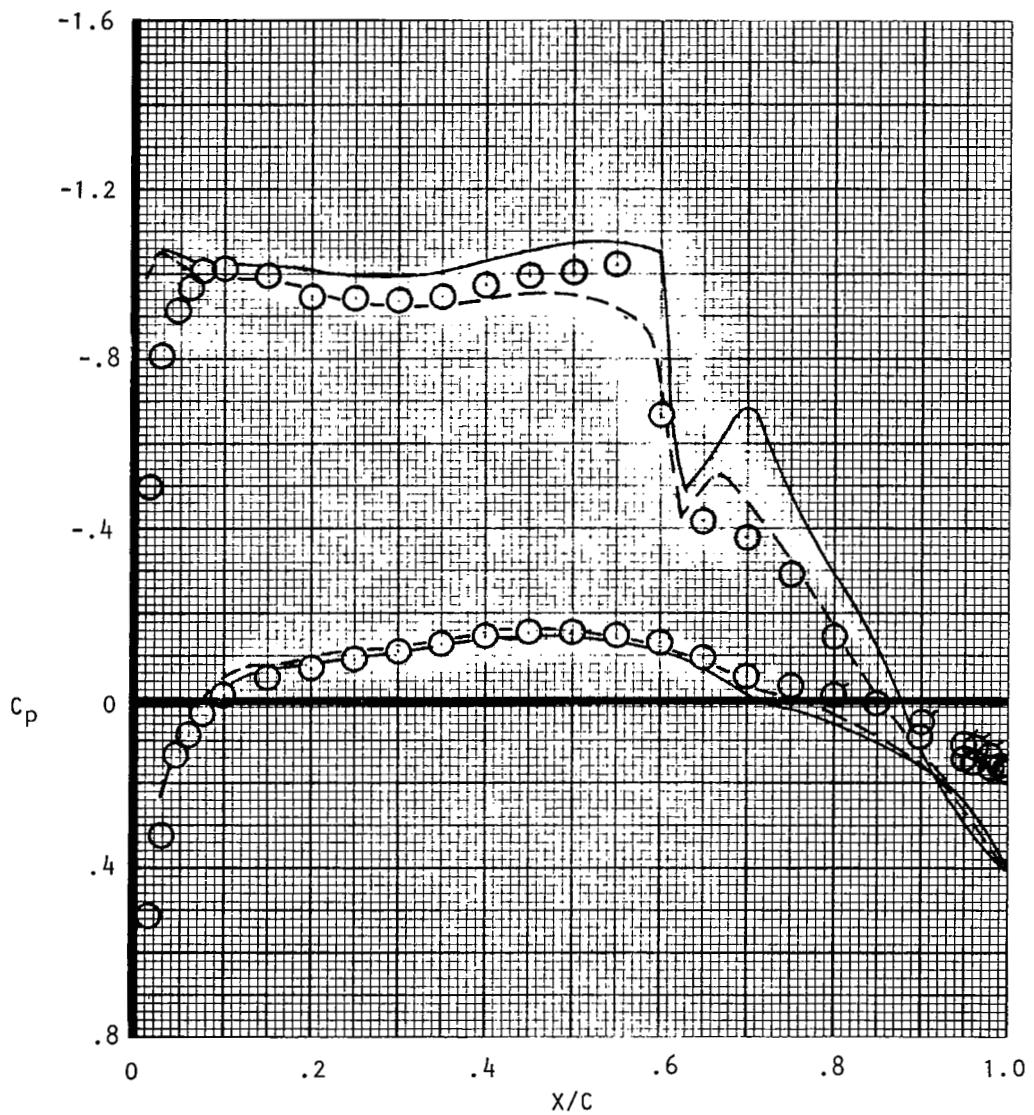

Figure 20. Concluded.

APPENDIX A: PLOTTED TEST DATA

Results from Lockheed-Georgia Comressible Flow Wind Tunnel Test 029 are detailed in plotted form in this appendix. The aerodynamic force coefficients for airfoil C141H7472 are shown in figures A1 through A9 for the basic test conditions of $R_N = 11 \times 10^6$, $\tau = 4\%$, and free transition. Figures A10 through A13 contain the aerodynamic coefficients for $R_N = 4 \times 10^6$, $\tau = 4\%$, and transition fixed at 5% chord.

The chordwise pressure distributions are shown for the basic test conditions in figures A14 through A29, and for $R_N = 4 \times 10^6$ in figures A30 through A36. Figures A37 and A38 contain the chordwise pressure distributions for wall porosities of 2%, 3%, 4%, 5%, and 6%.

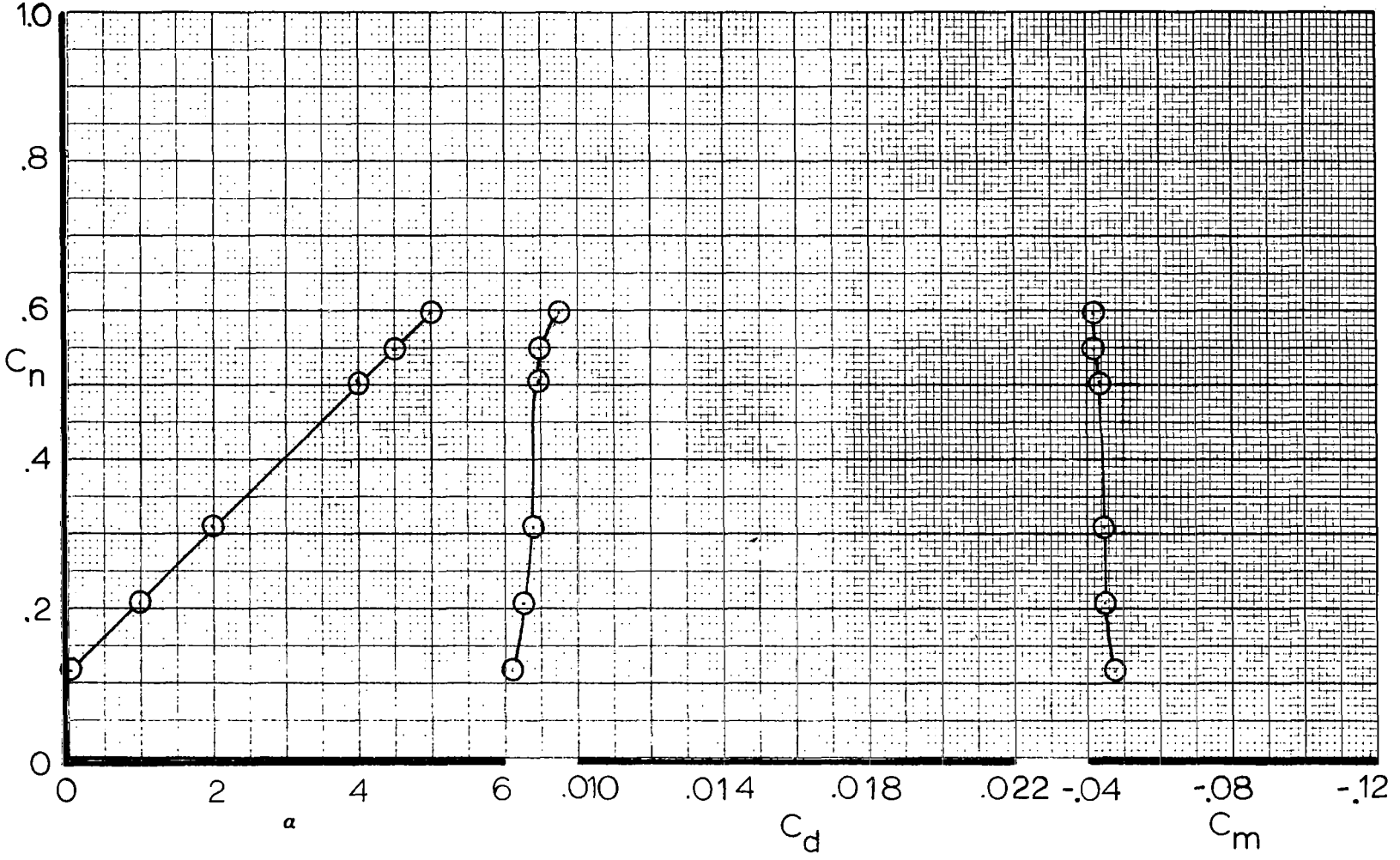

Figure A1. - Airfoil force data for $M = 0.45$, $R_N = 11 \times 10^6$, X/C_T = Free

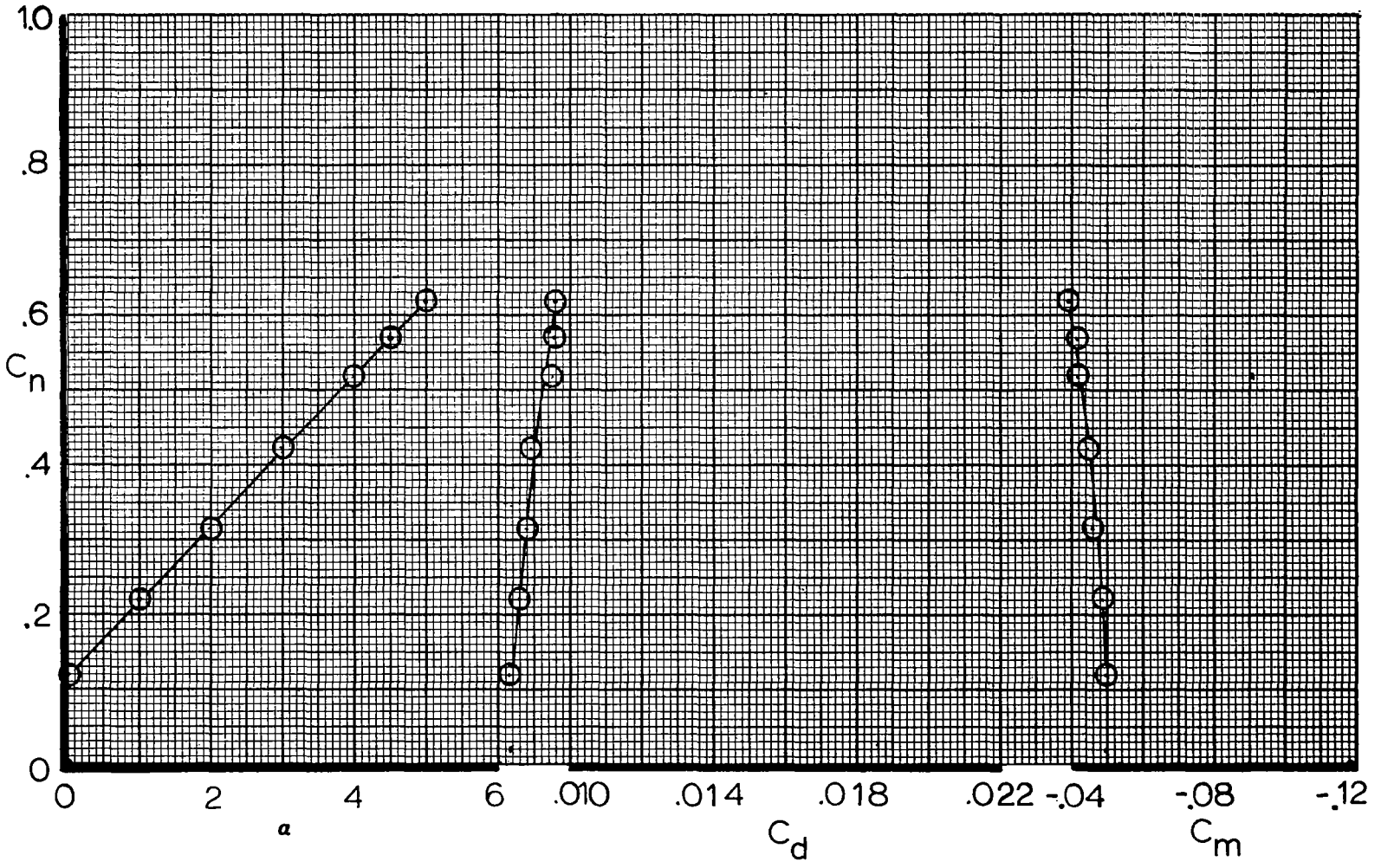

Figure A2 . - Airfoil force data for $M = 0.55$, $R_N = 11 \times 10^6$, X/C_T = Free

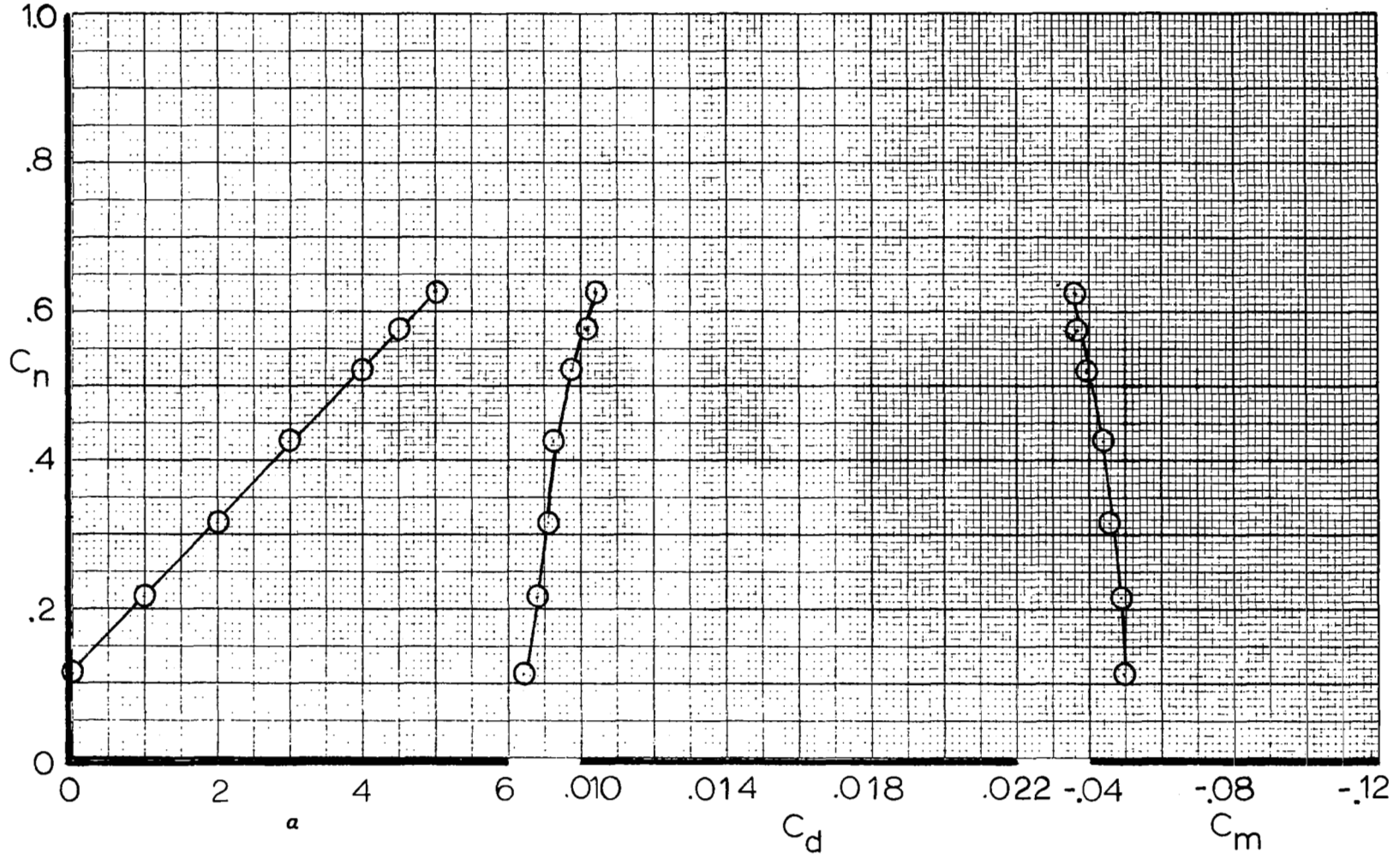

Figure A3. - Airfoil force data for $M = 0.60$, $R_N = 11 \times 10^6$, X/C_T = Free

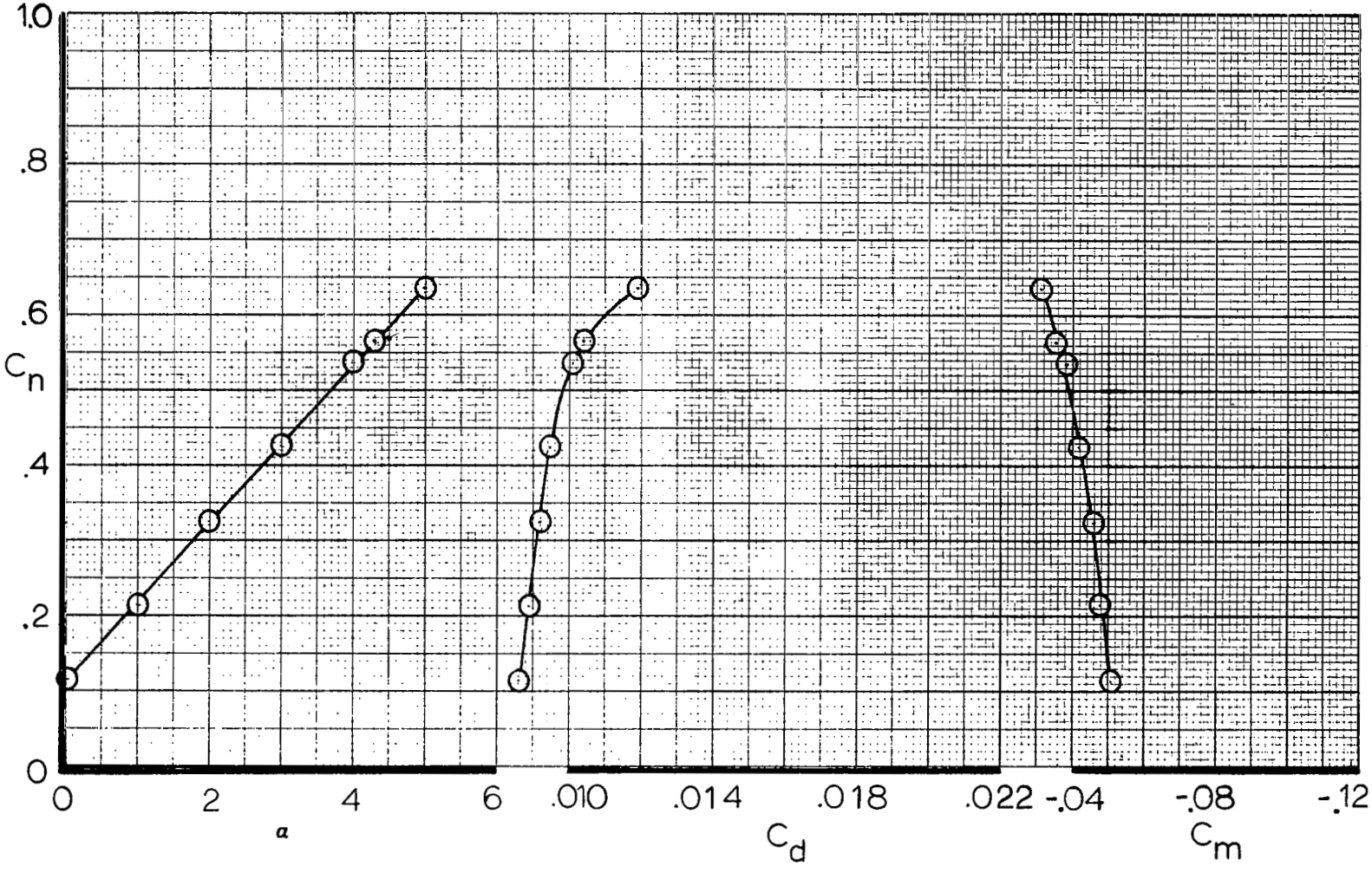

Figure A4. - Airfoil force data for $M = 0.64$, $R_N = 11 \times 10^6$, X/C_T = Free

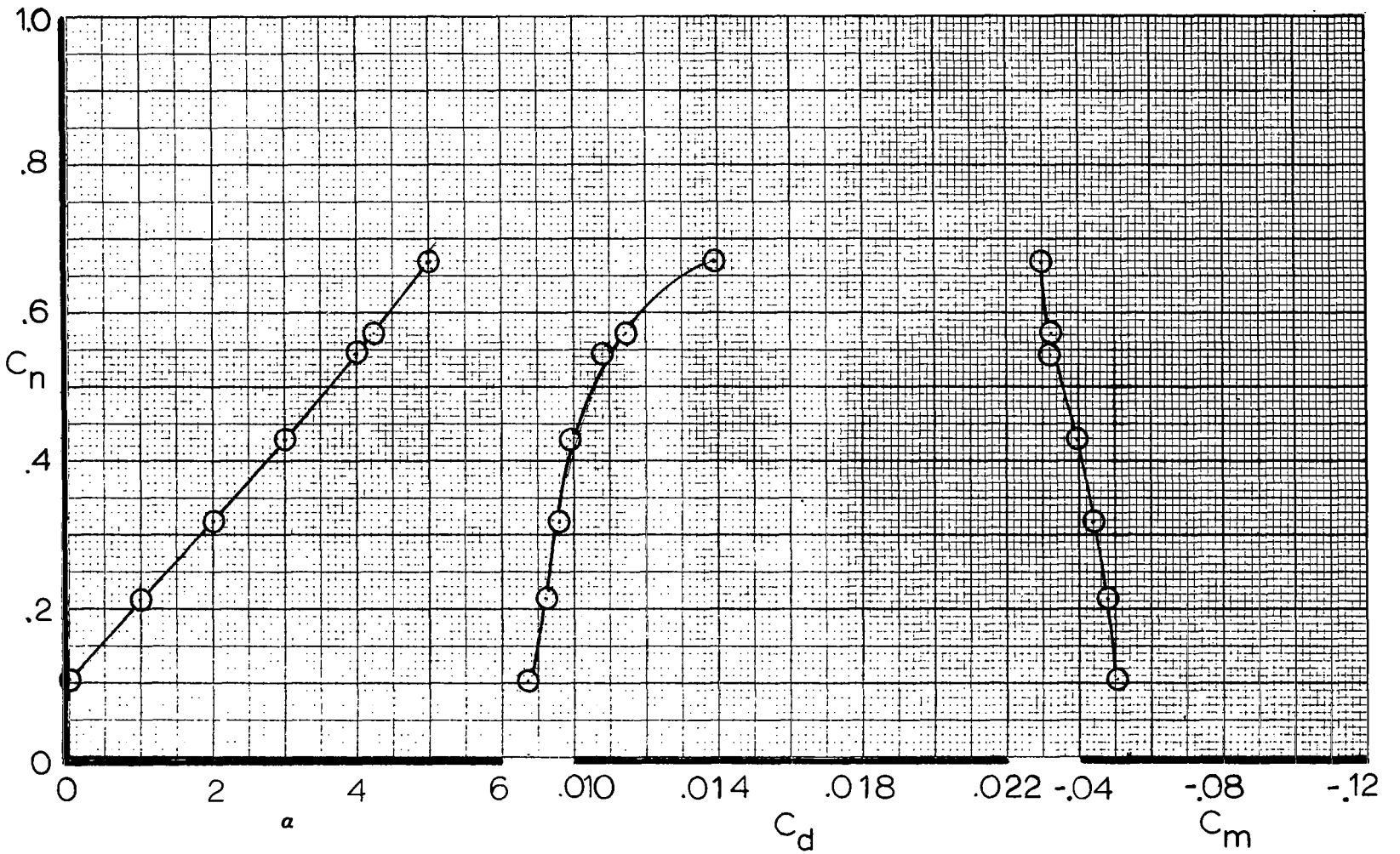

Figure A5. - Airfoil force data for M = 0.68, $R_N = 11 \times 10^6$, X/C_T = Free

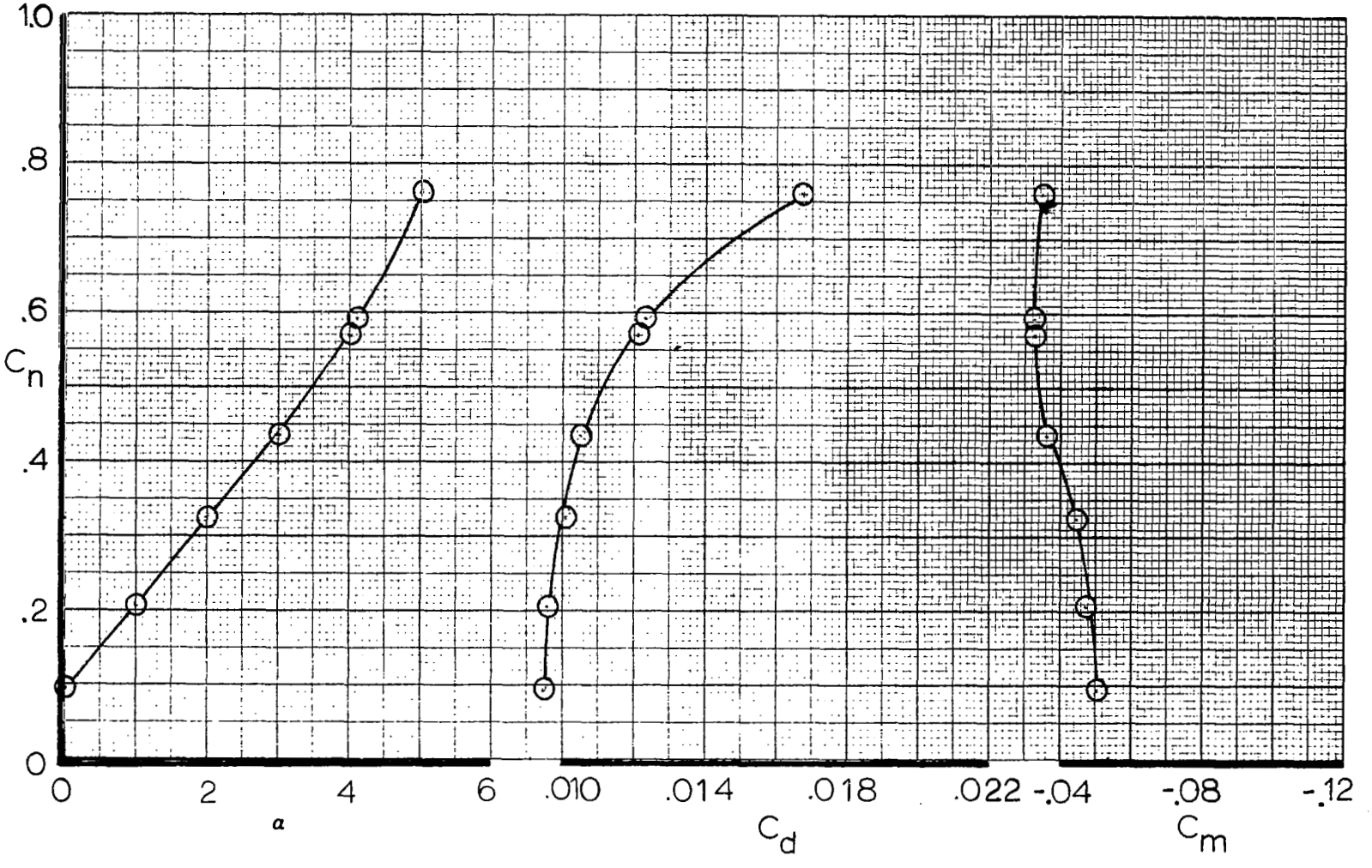

Figure A6 . - Airfoil force data for M = 0.72, $R_N = 11 \times 10^6$, X/C_T = Free

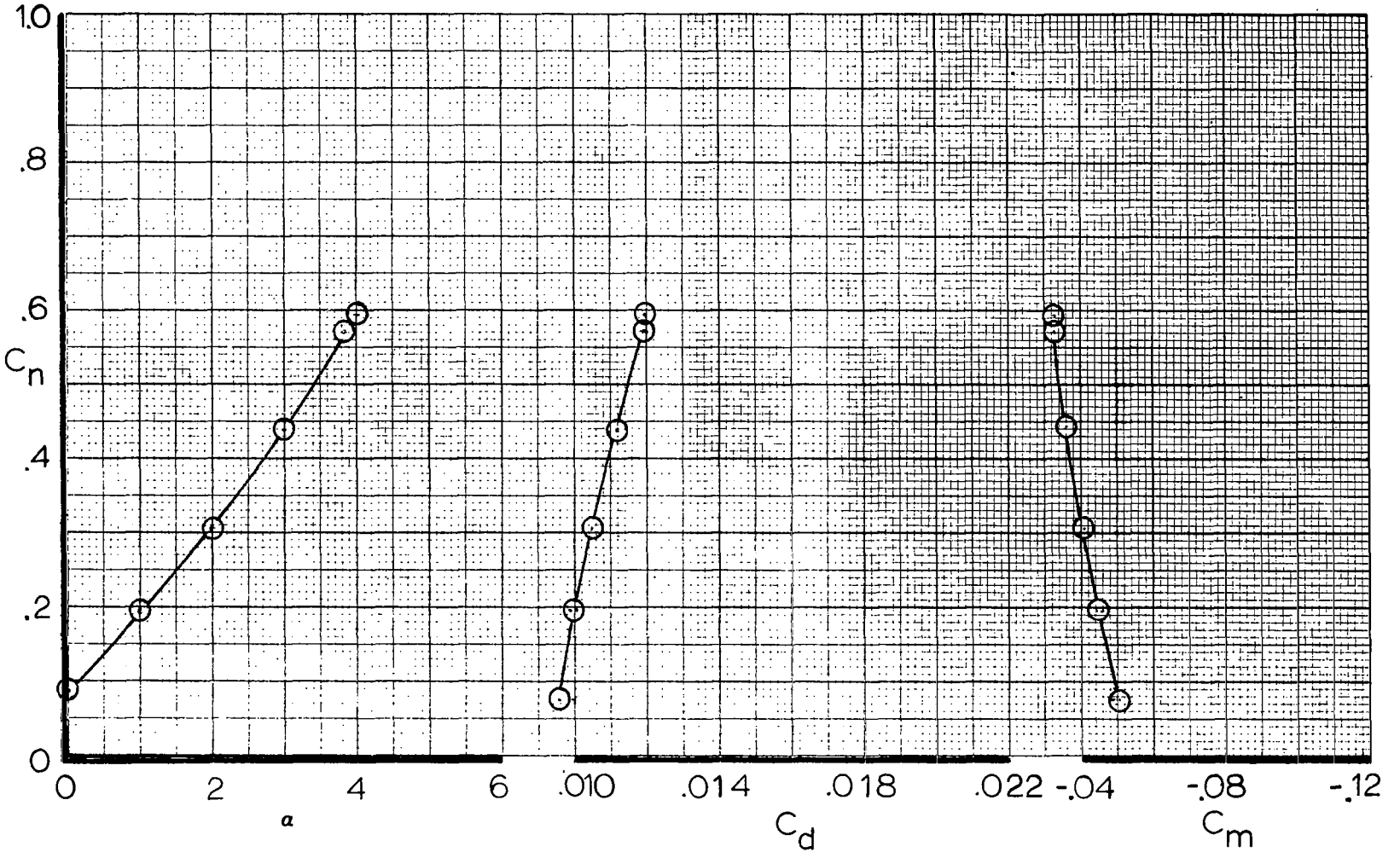

Figure A7 . - Airfoil force data for $M = 0.74$, $R_N = 11 \times 10^6$, X/C_T = Free

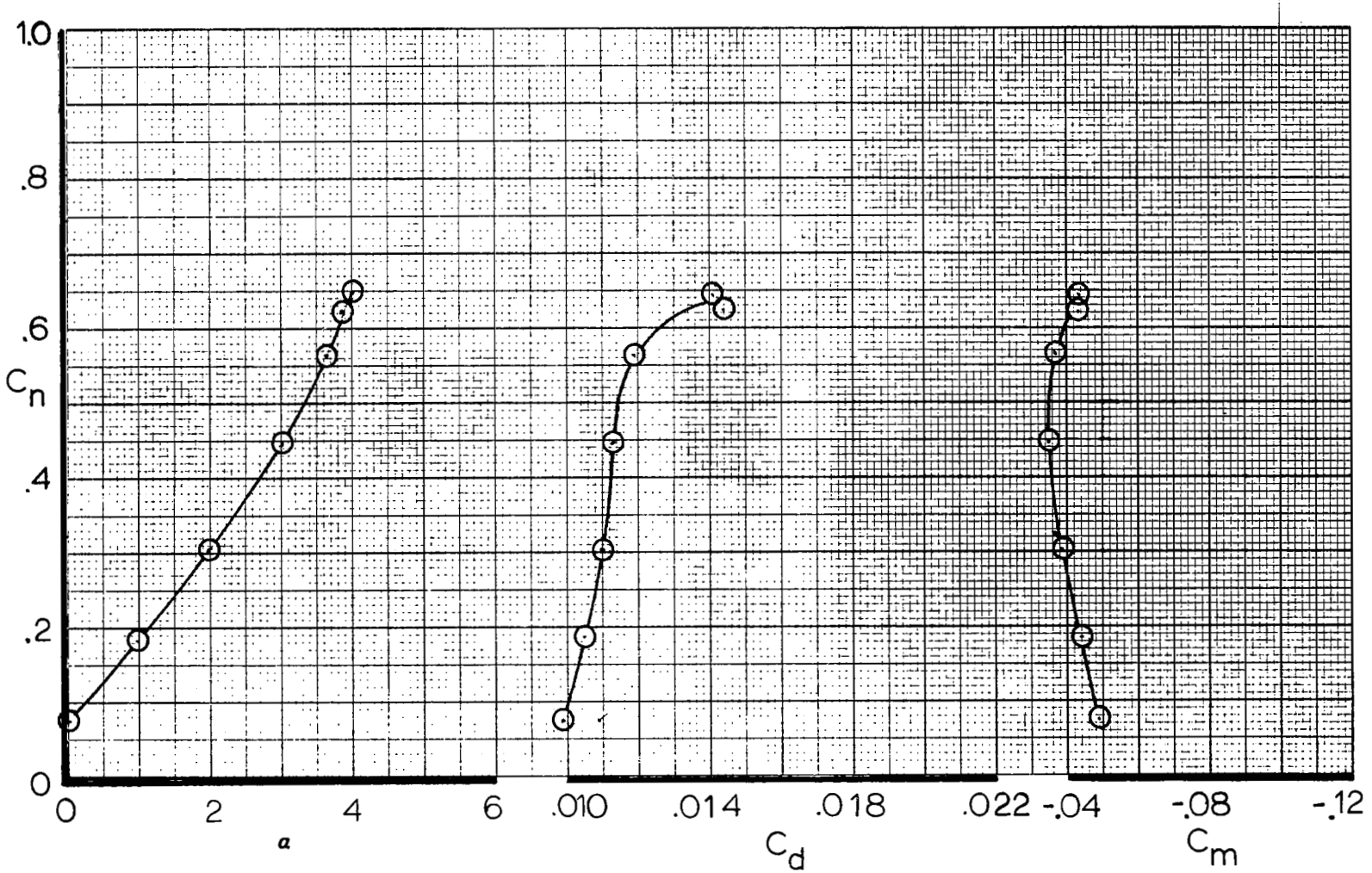

Figure A8 . - Airfoil force data for M = 0.76, $R_N = 11 \times 10^6$, X/C_T = Free

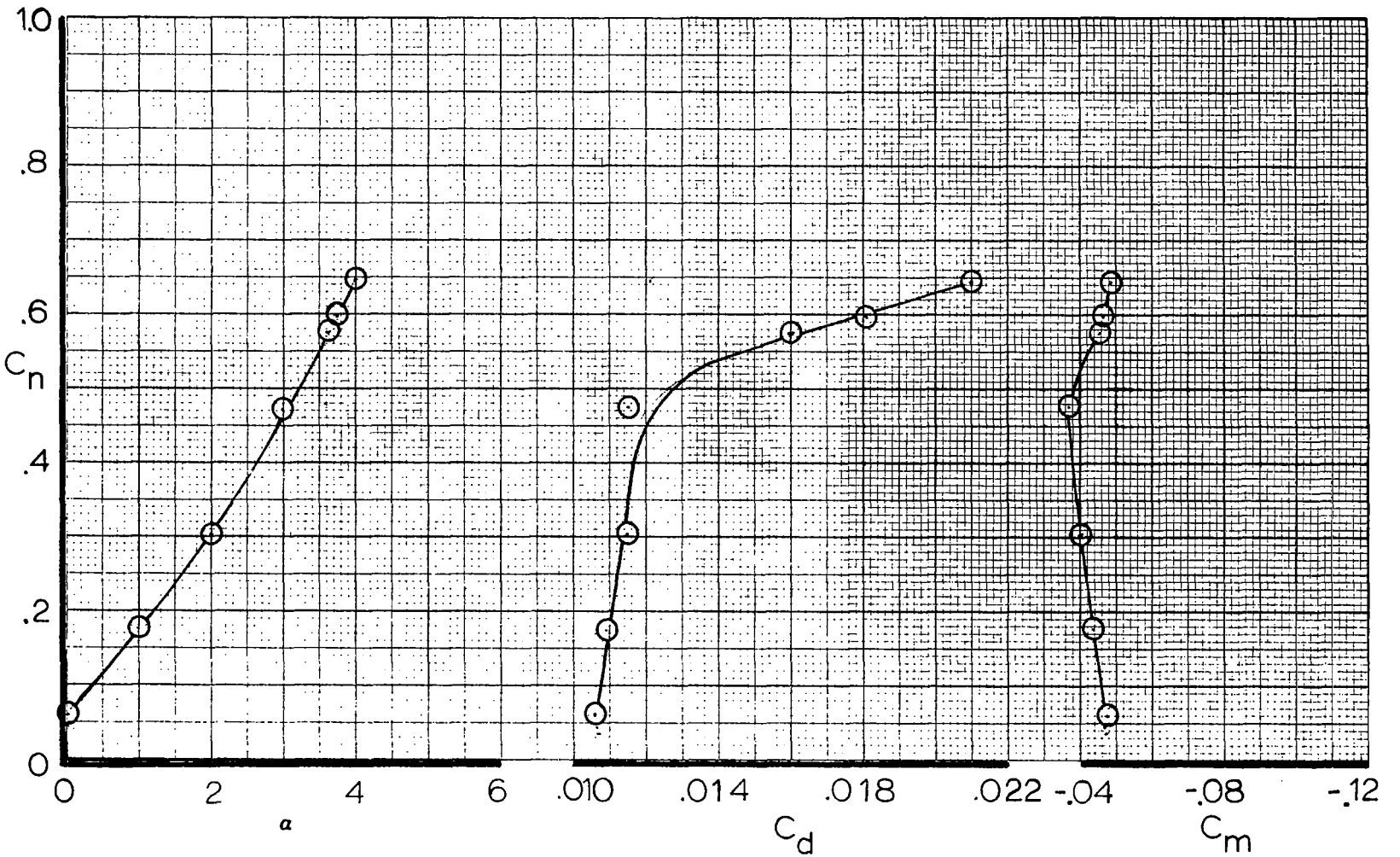

Figure A9 . - Airfoil force data for M = 0.78, $R_N = 11 \times 10^6$, X/C_T = Free

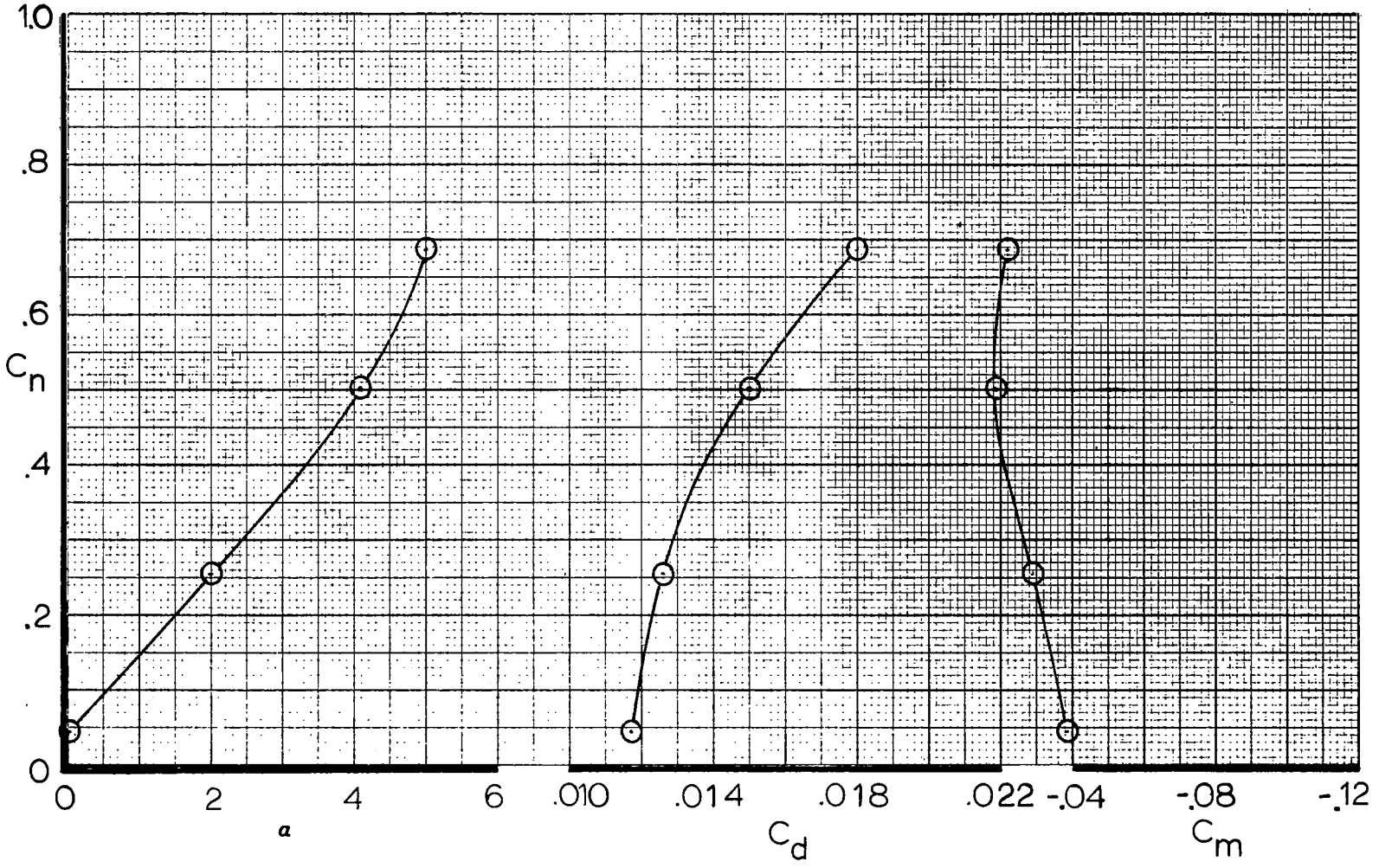

Figure A10. - Airfoil force data for $M = 0.72$, $R_N = 4 \times 10^6$, $X/C_T = .05$

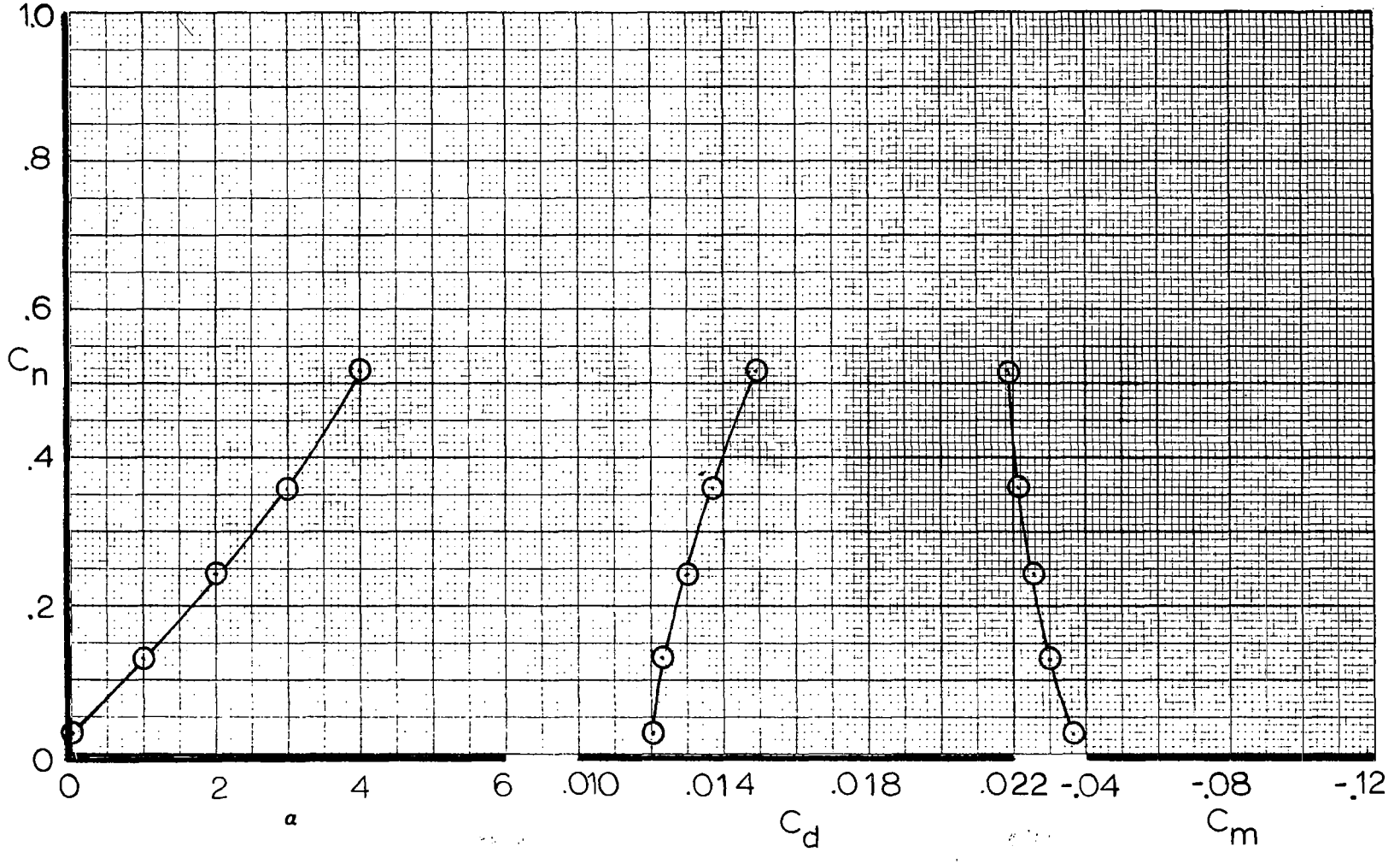

Figure A11. - Airfoil force data for $M = 0.74$, $R_N = 4 \times 10^6$, $X/C_T = .05$

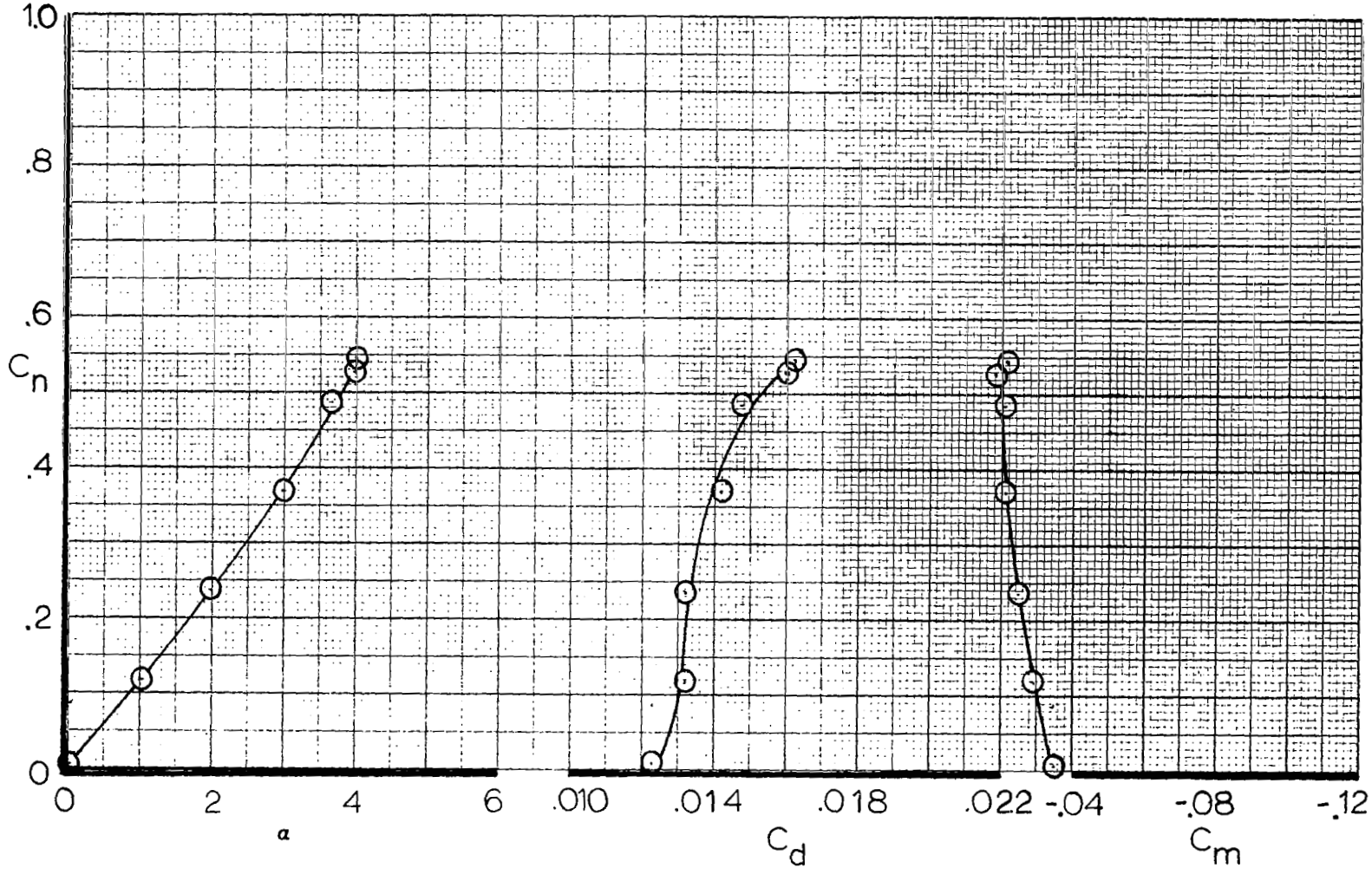

Figure A12 . - Airfoil force data for M = 0.76, $R_N = 4 \times 10^6$, $X/C_T = .05$

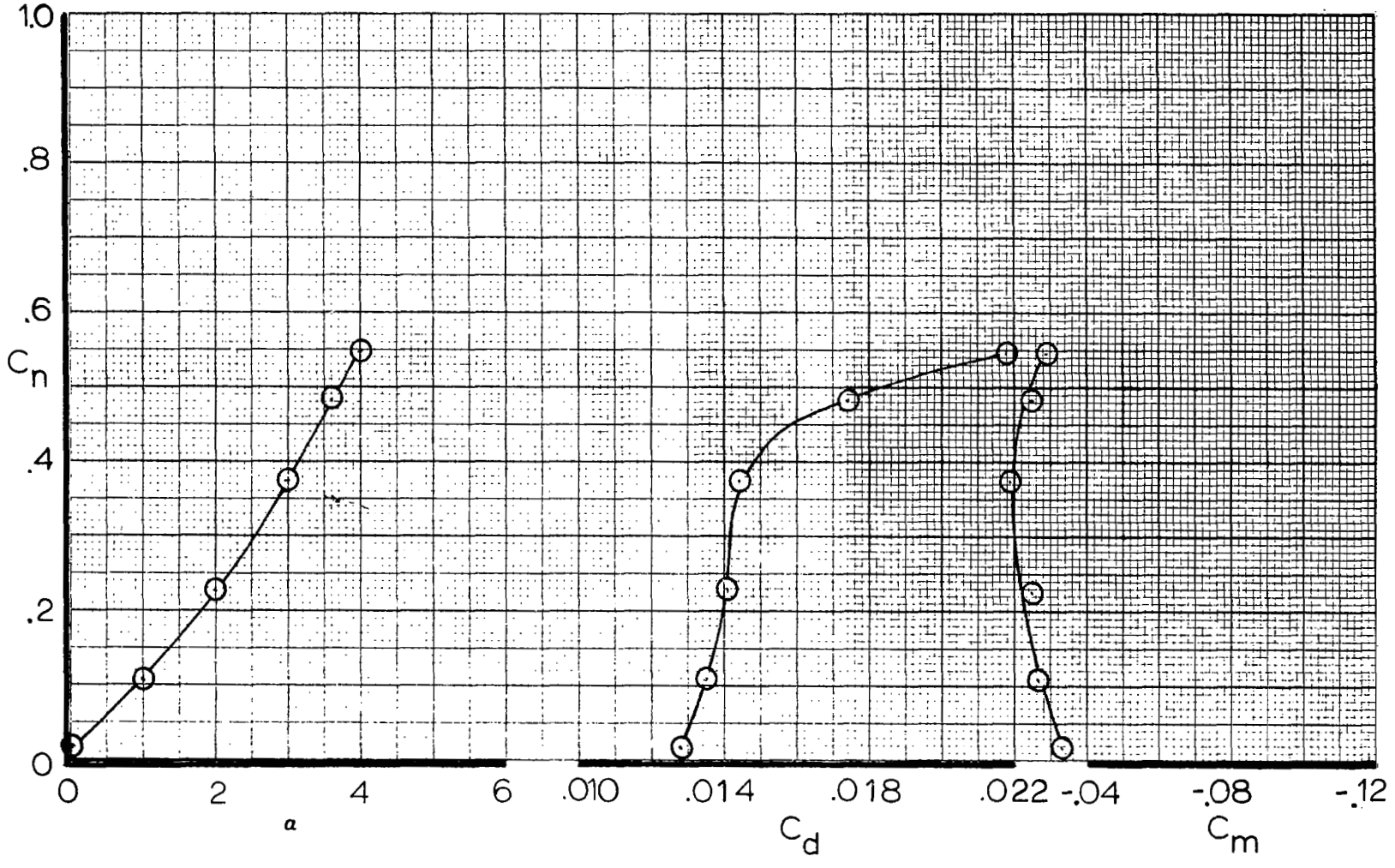

Figure A13. - Airfoil force data for $M = 0.78$, $R_N = 4 \times 10^6$, $X/C_T = .05$

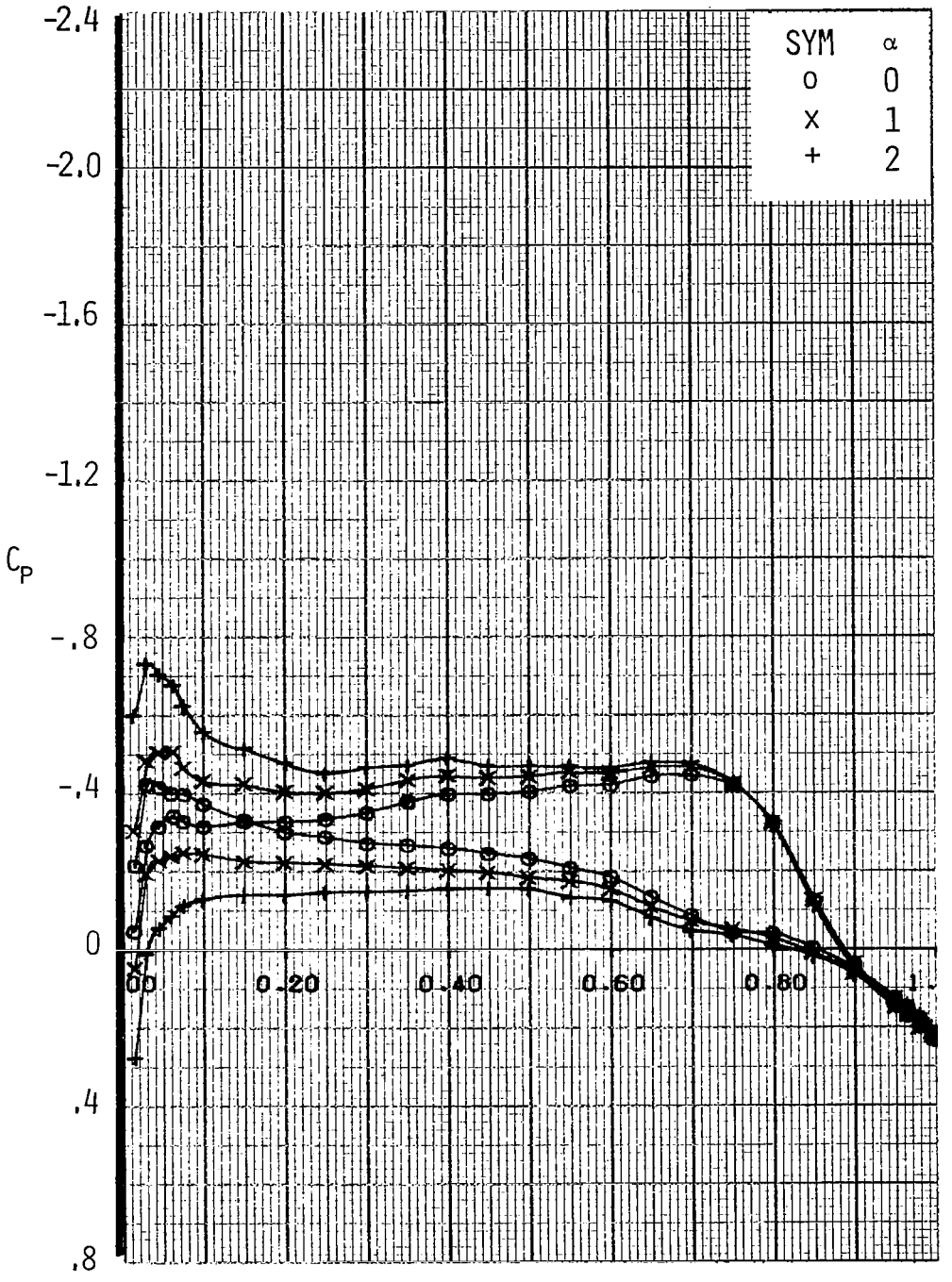

Figure A14.- Airfoil Pressure Distribution for M = 0.55, $R_N = 11 \times 10^6$, X/C_T = Free.

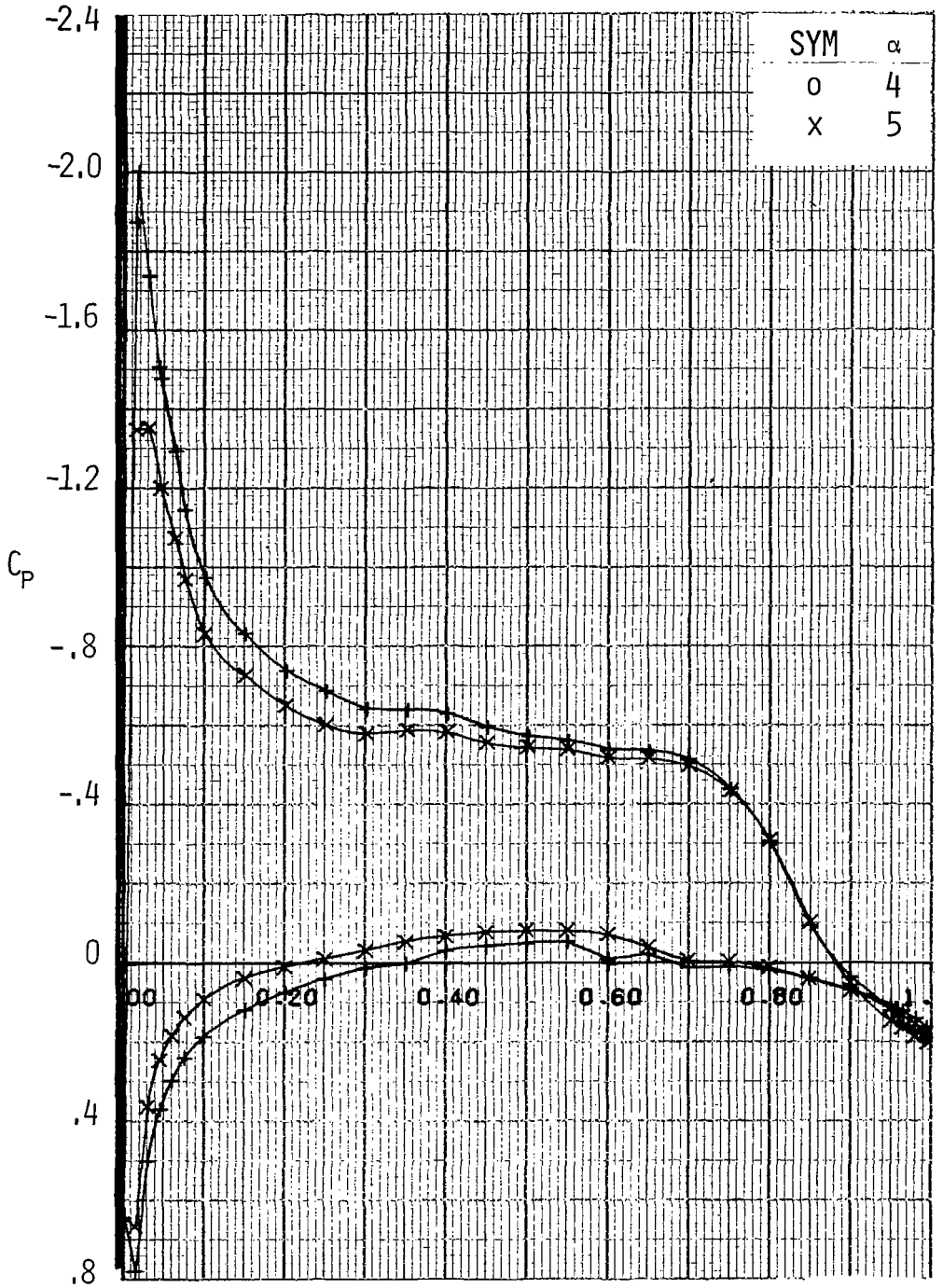

Figure A15.- Airfoil Pressure Distribution for M = 0.55, R_N = 11 x 10^6, X/C_T = Free

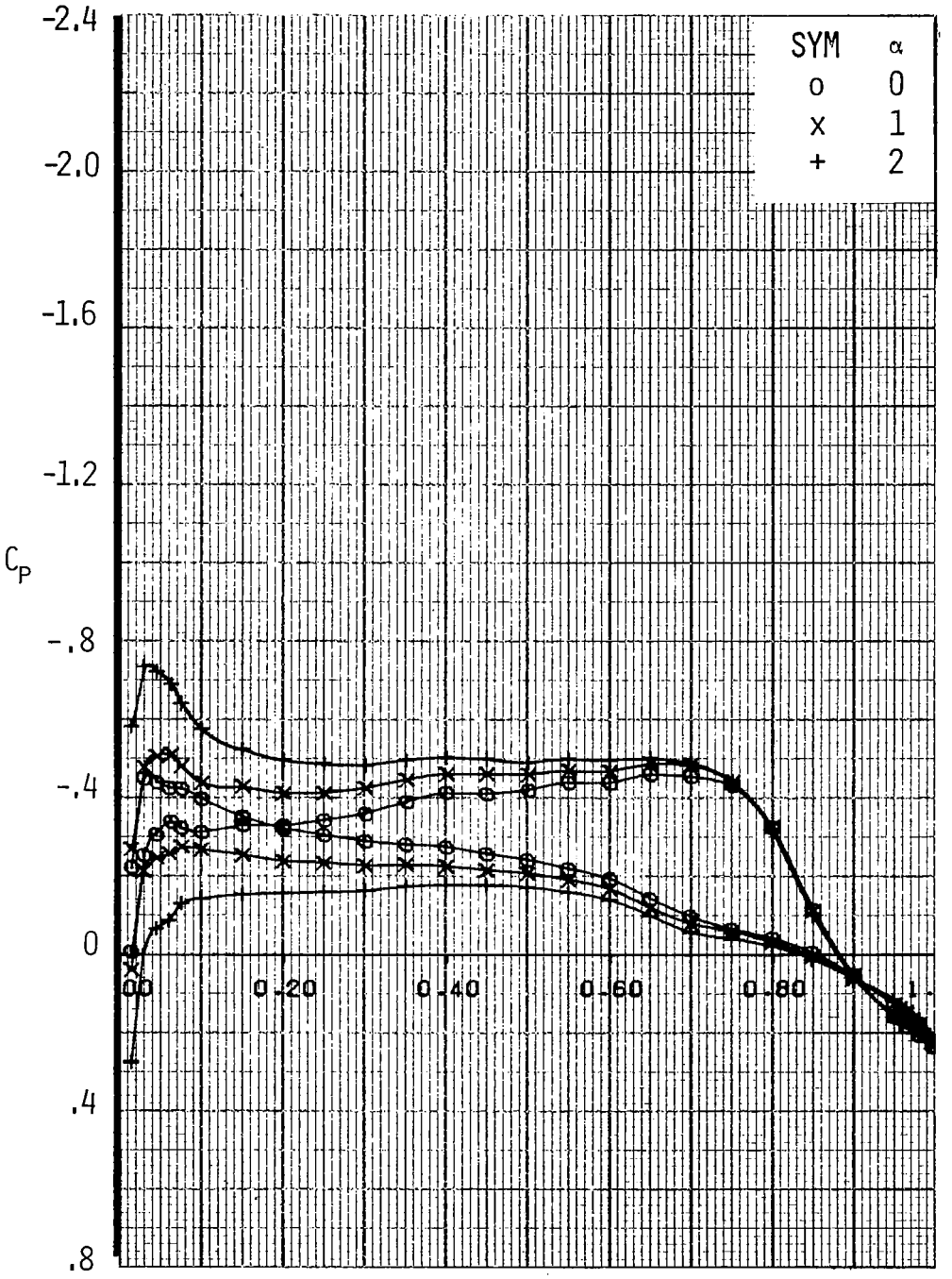

Figure A16.- Airfoil Pressure Distribution for M = 0.60, $R_N = 11 \times 10^6$, X/C_T = Free

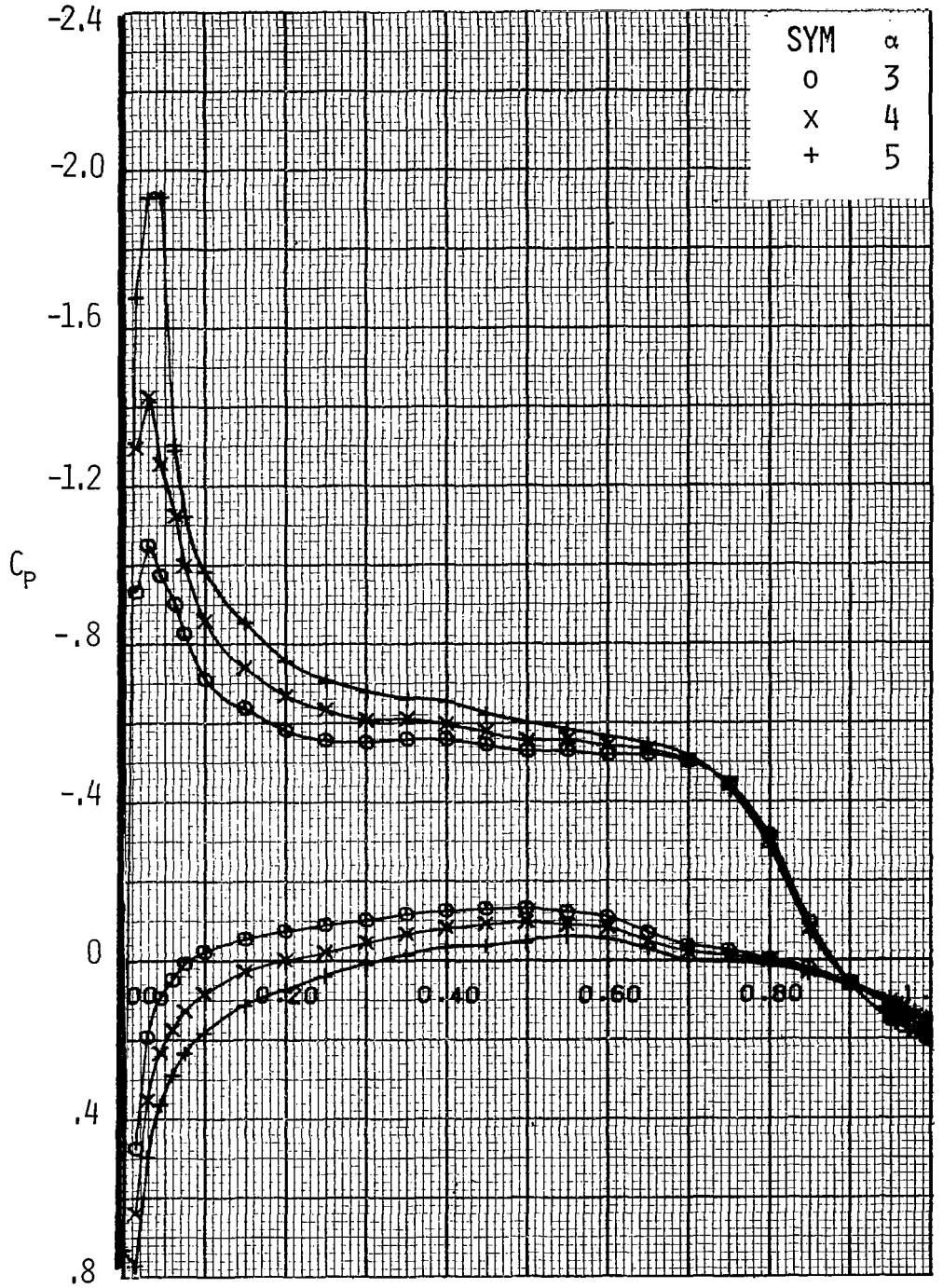

Figure A17.- Airfoil Pressure Distribution for M = 0.60, R_N = 11 x 10^6, X/C_T = Free

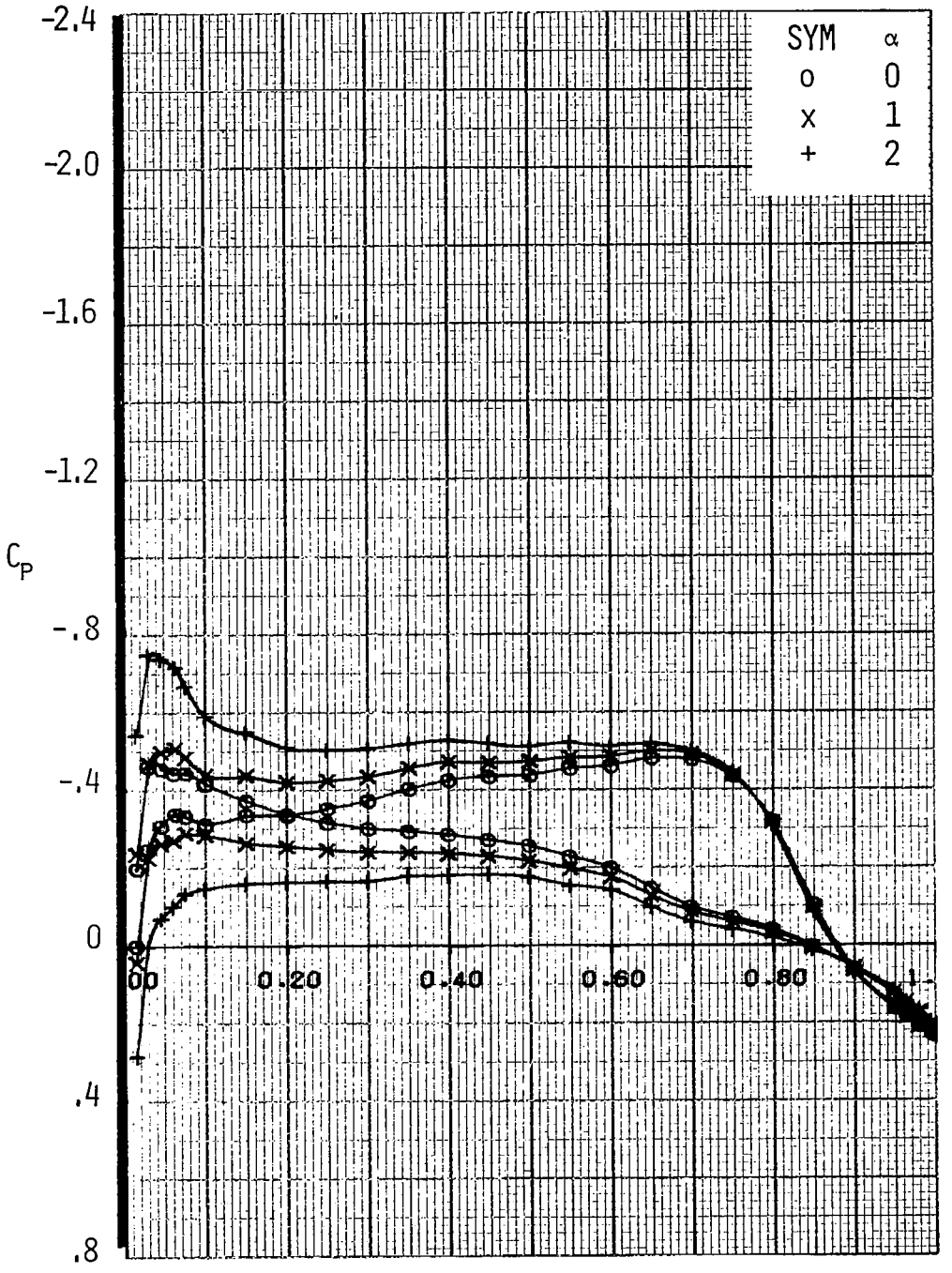

Figure A18.- Airfoil Pressure Distribution for M = 0.64, $R_N = 11 \times 10^6$, X/C_T = Free

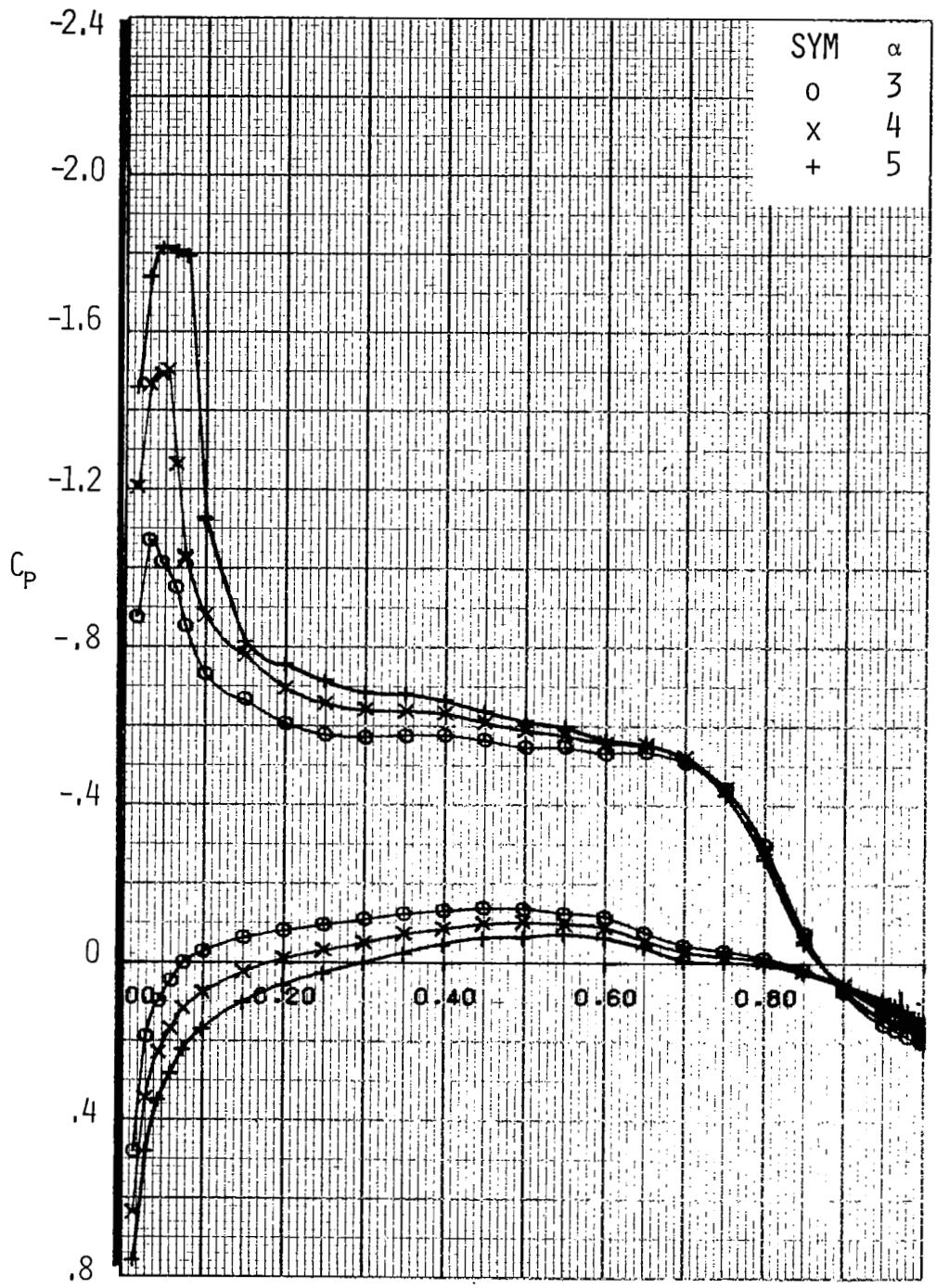

Figure A19.- Airfoil Pressure Distribution for M = 0.64, R_N = 11 x 10^6, X/C_T = Free

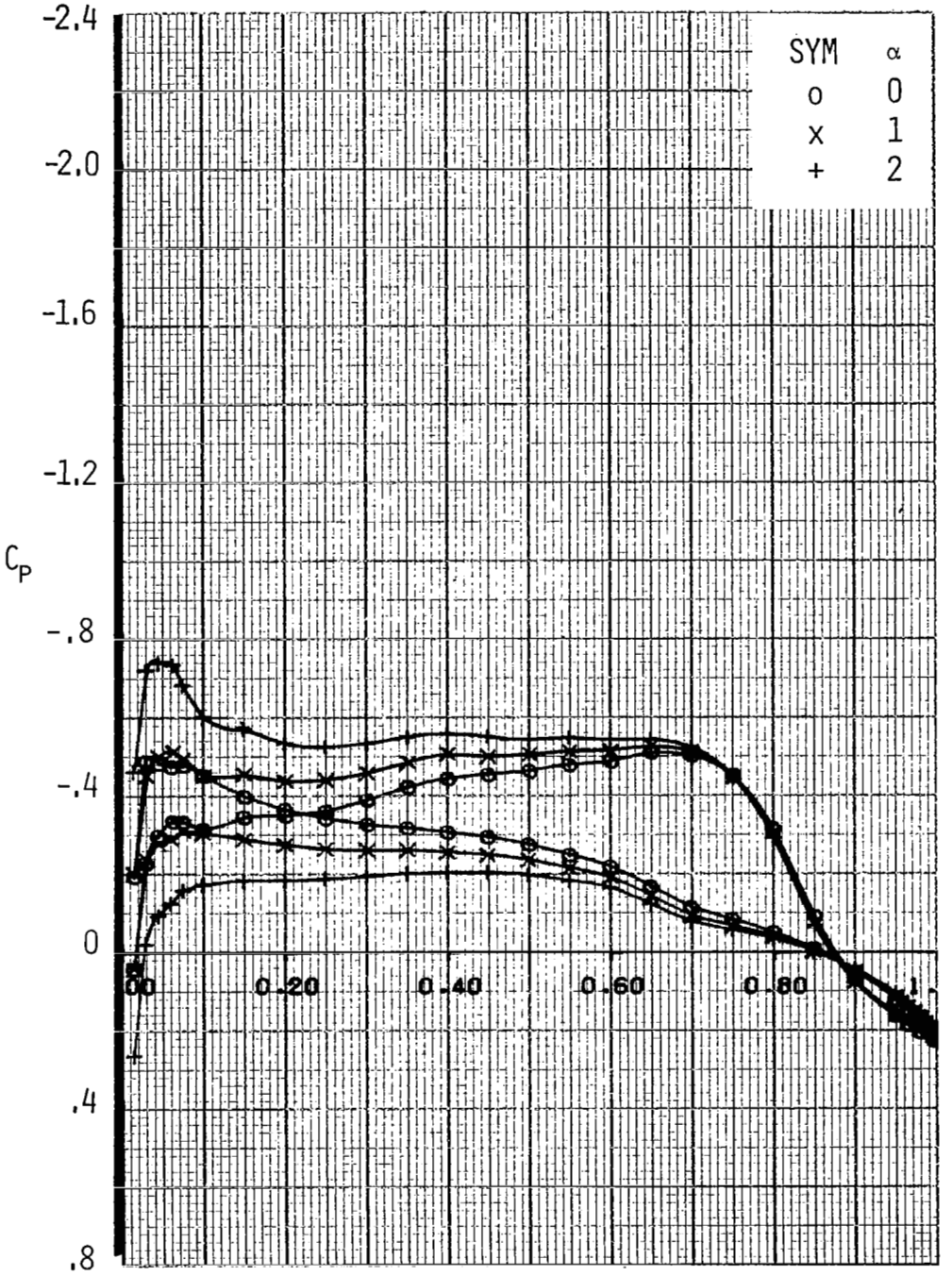

Figure A20.- Airfoil Pressure Distribution for M = 0.68, $R_N = 11 \times 10^6$, X/C_T = Free

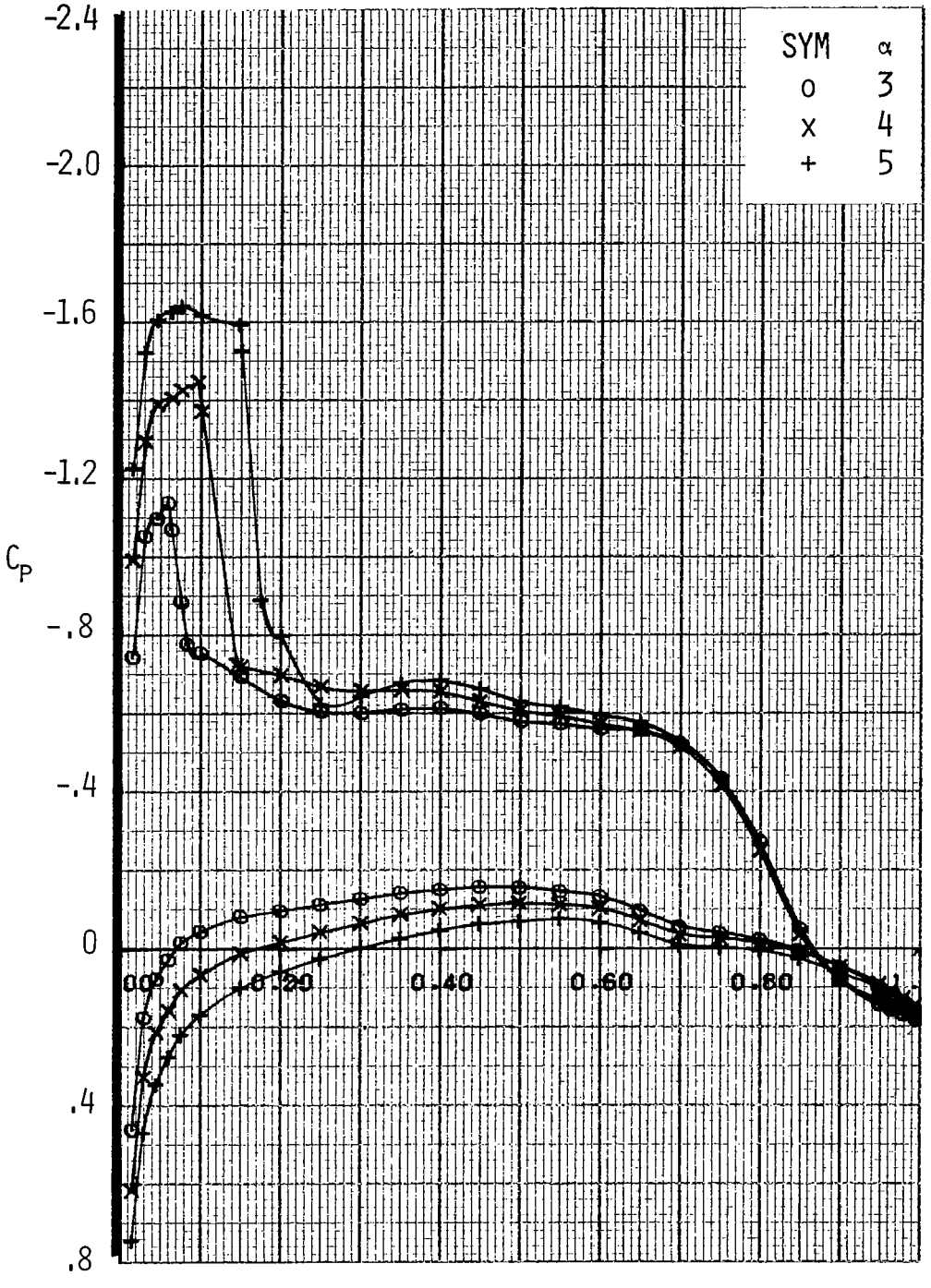

Figure A21.- Airfoil Pressure Distribution for M = 0.68, R_N = 11 x 10^6, X/C_T = Free

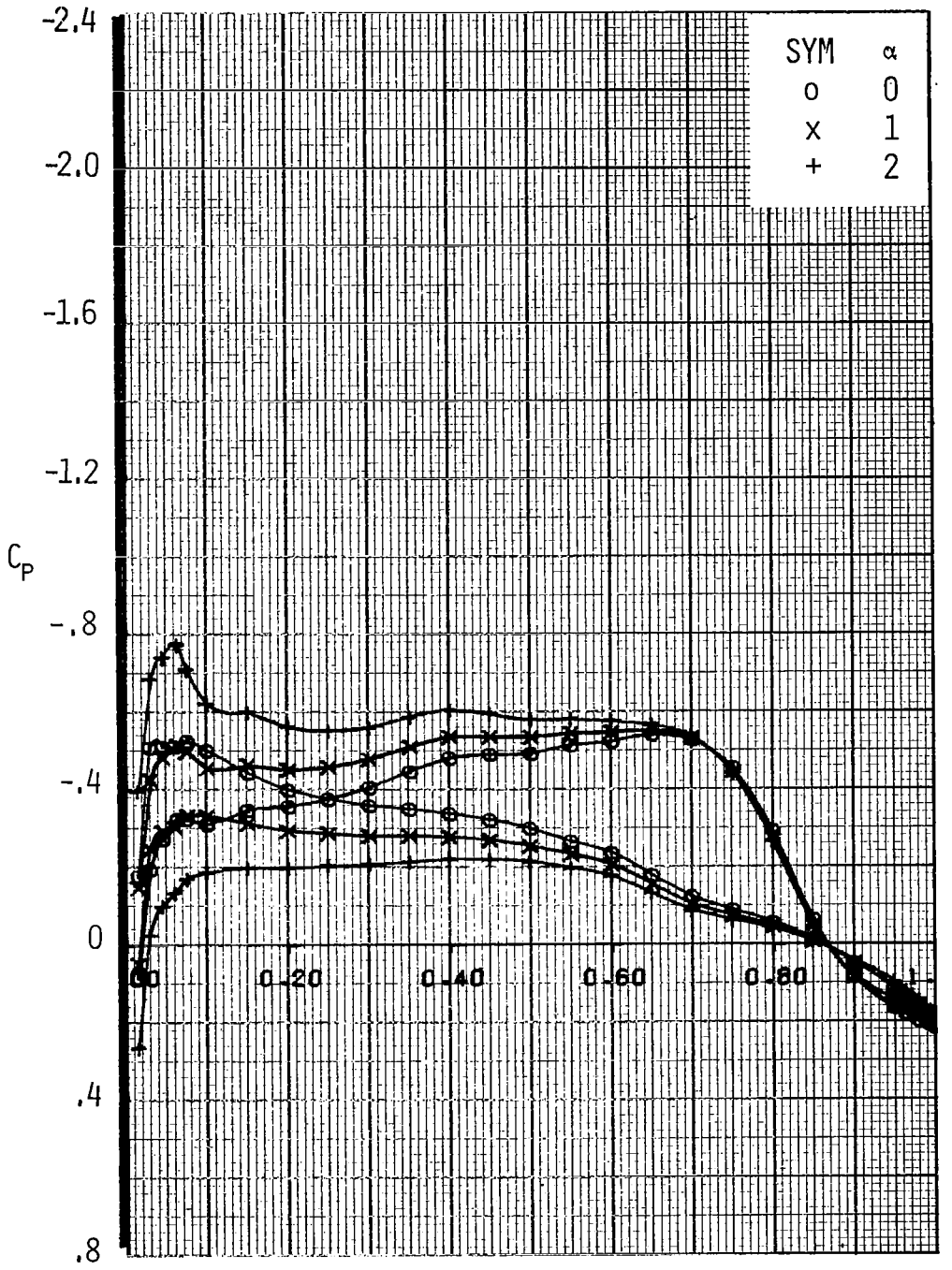

Figure A22.- Airfoil Pressure Distribution for M = 0.72, $R_N = 11 \times 10^6$, X/C_T = Free

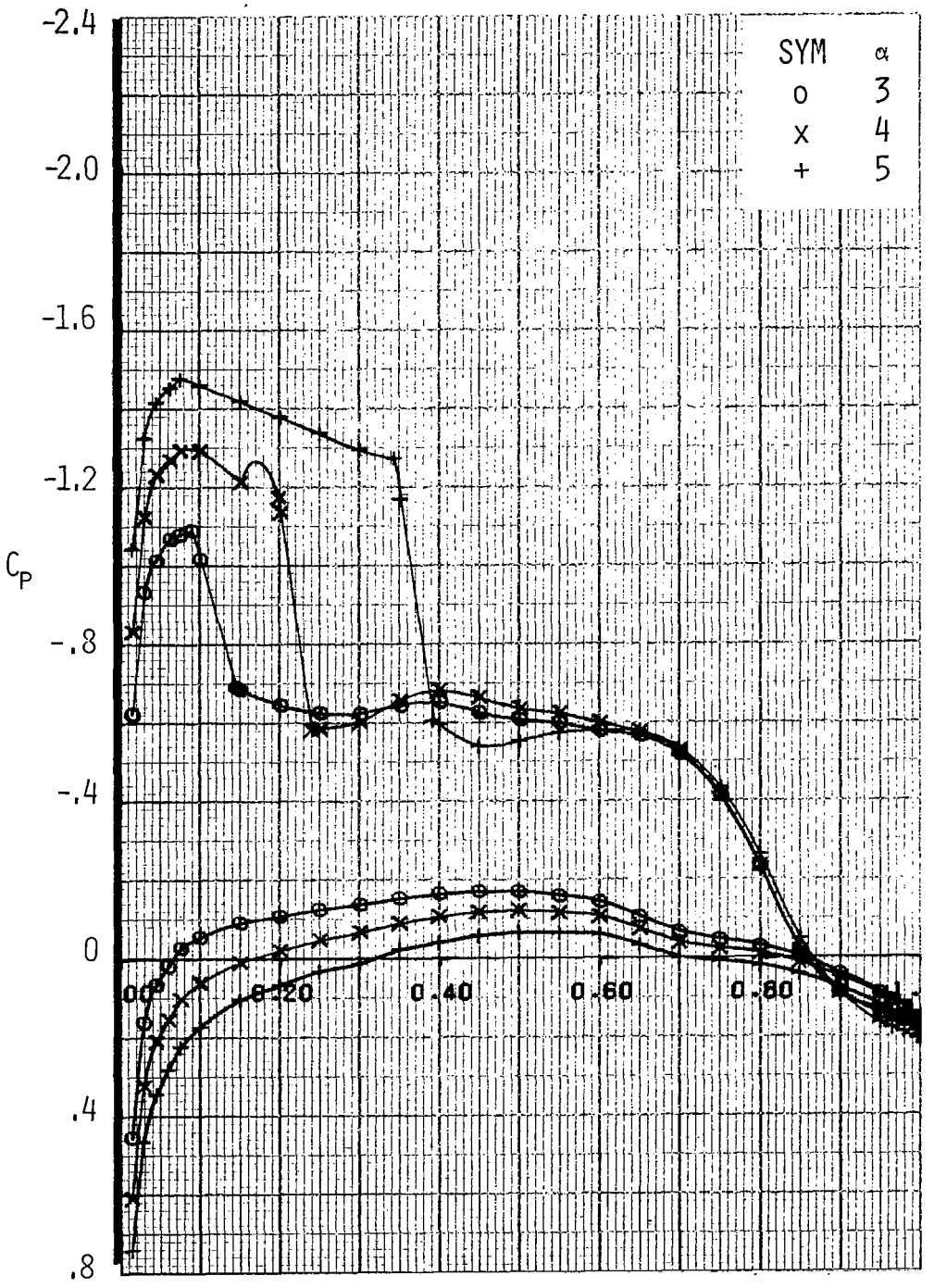

Figure A23.- Airfoil Pressure Distribution for M = 0.72, R_N = 11 x 10^6, X/C_T = Free

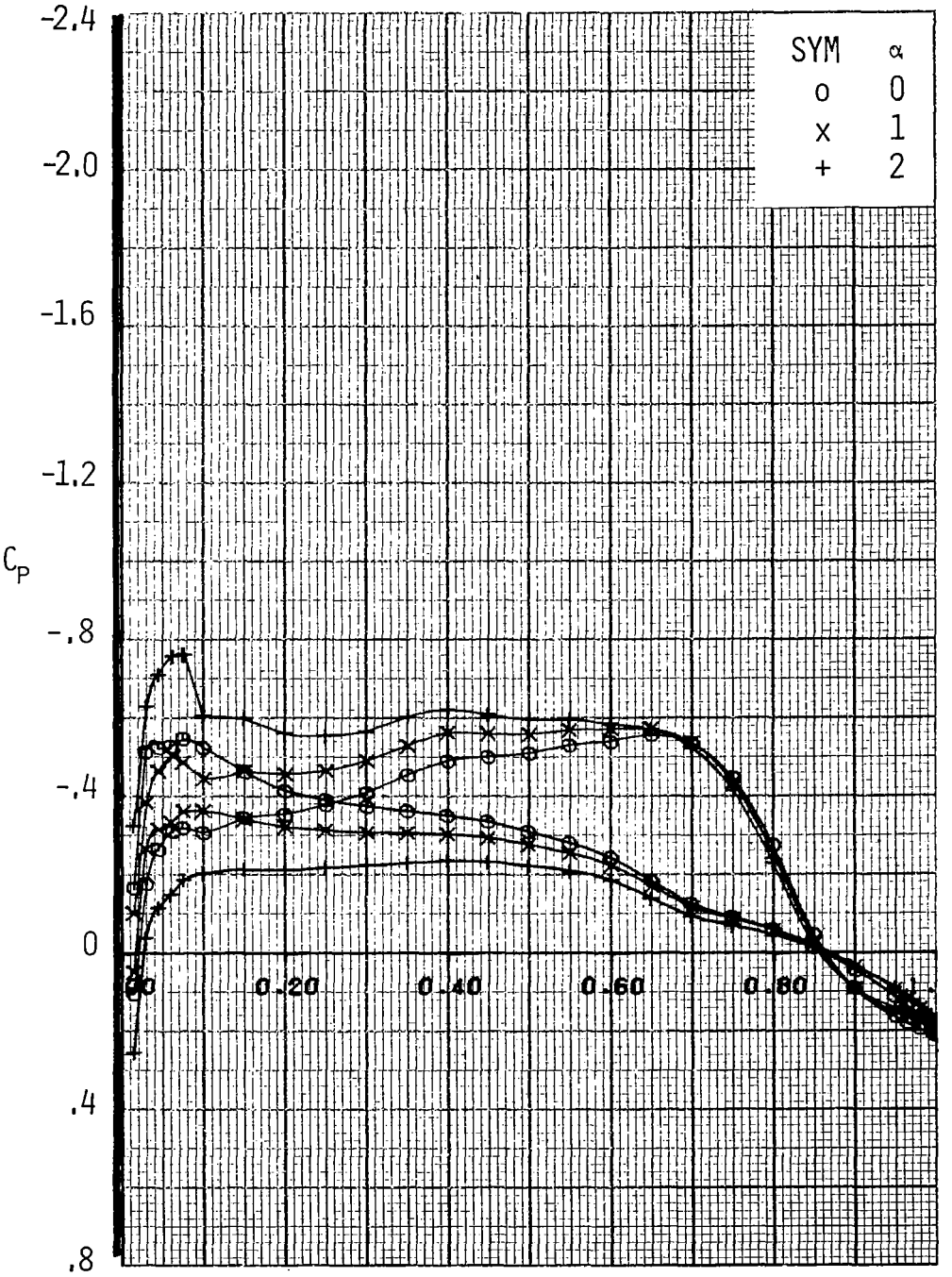

Figure A24.- Airfoil Pressure Distribution for M = 0.74, $R_N = 11 \times 10^6$, X/C_T = Free

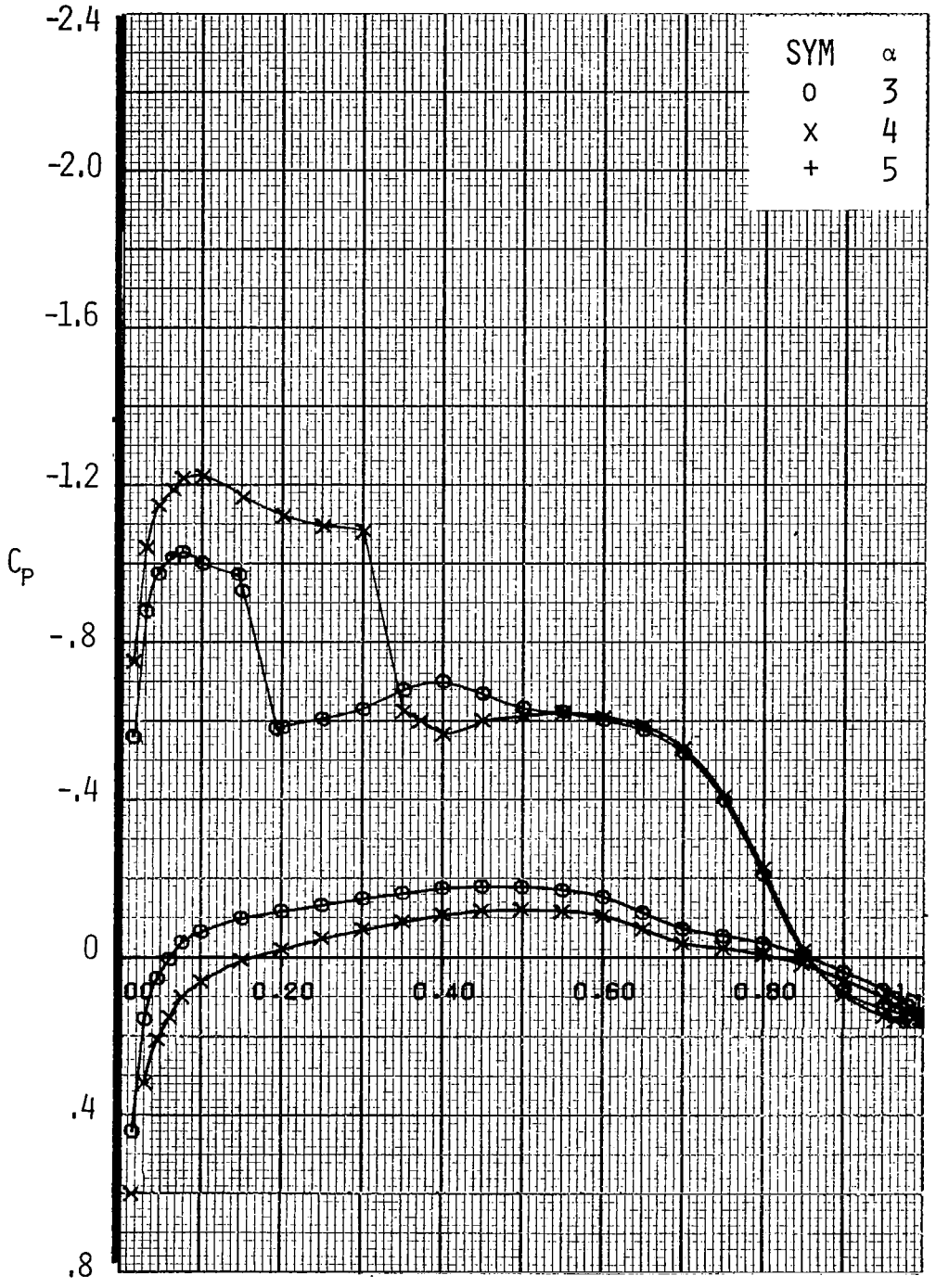

Figure A25 .- Airfoil Pressure Distribution for M = 0.74, R_N = 11 x 10^6, X/C_T = Free

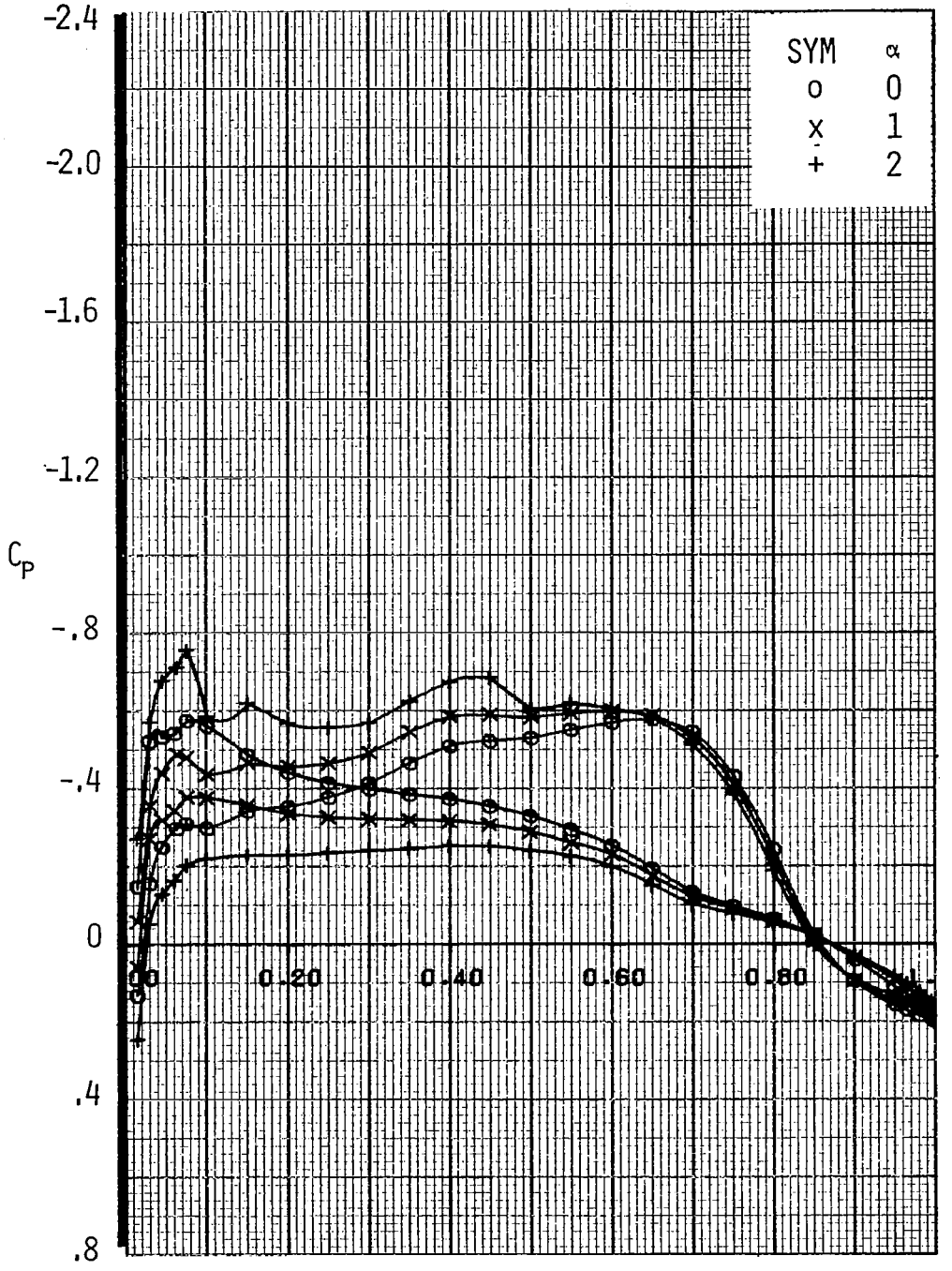

Figure A26.- Airfoil Pressure Distribution for M = 0.76, $R_N = 11 \times 10^6$, X/C_T = Free

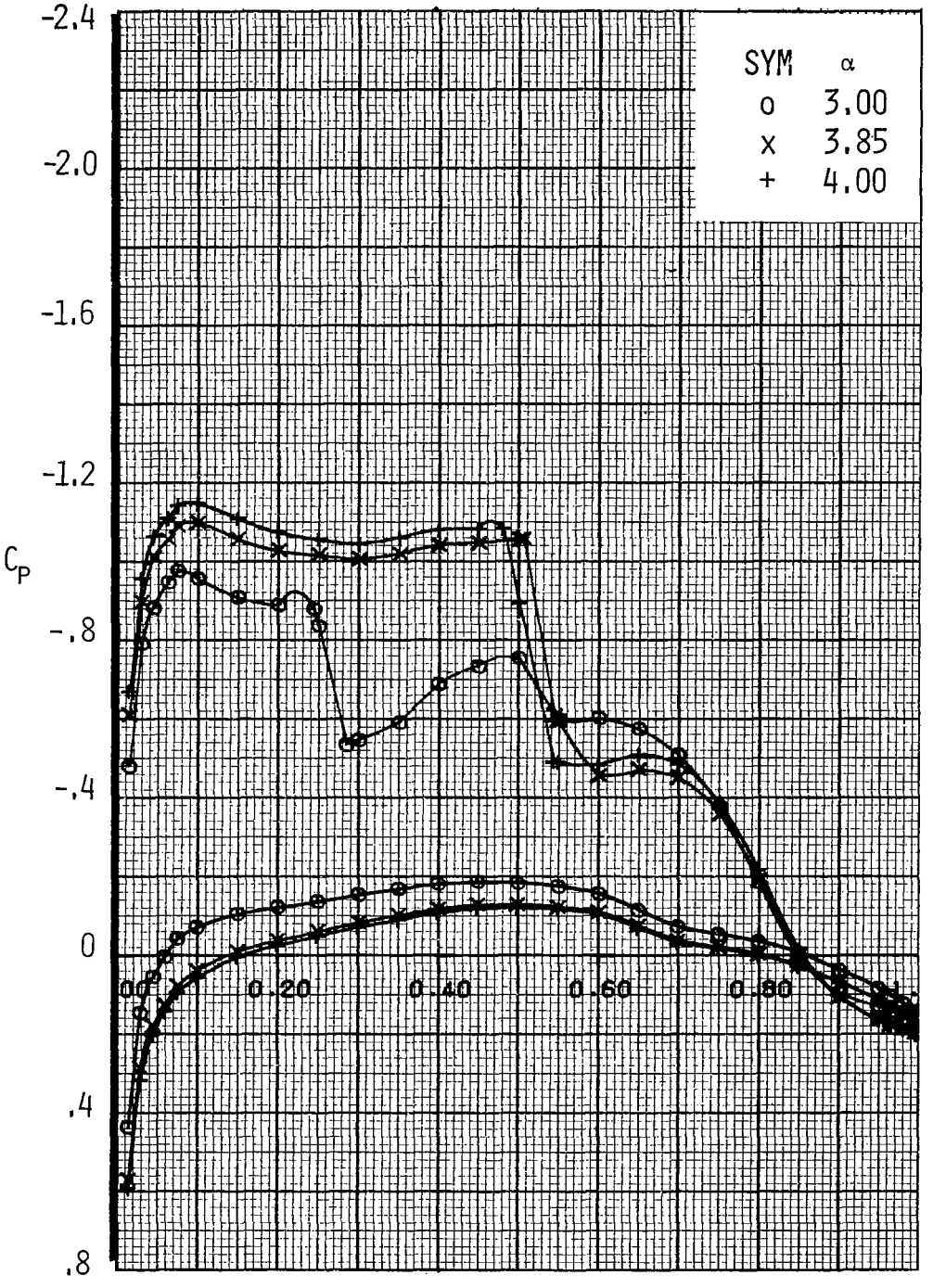

Figure A27.- Airfoil Pressure Distribution for M = 0.76, R_N = 11 x 10^6, X/C_T = Free

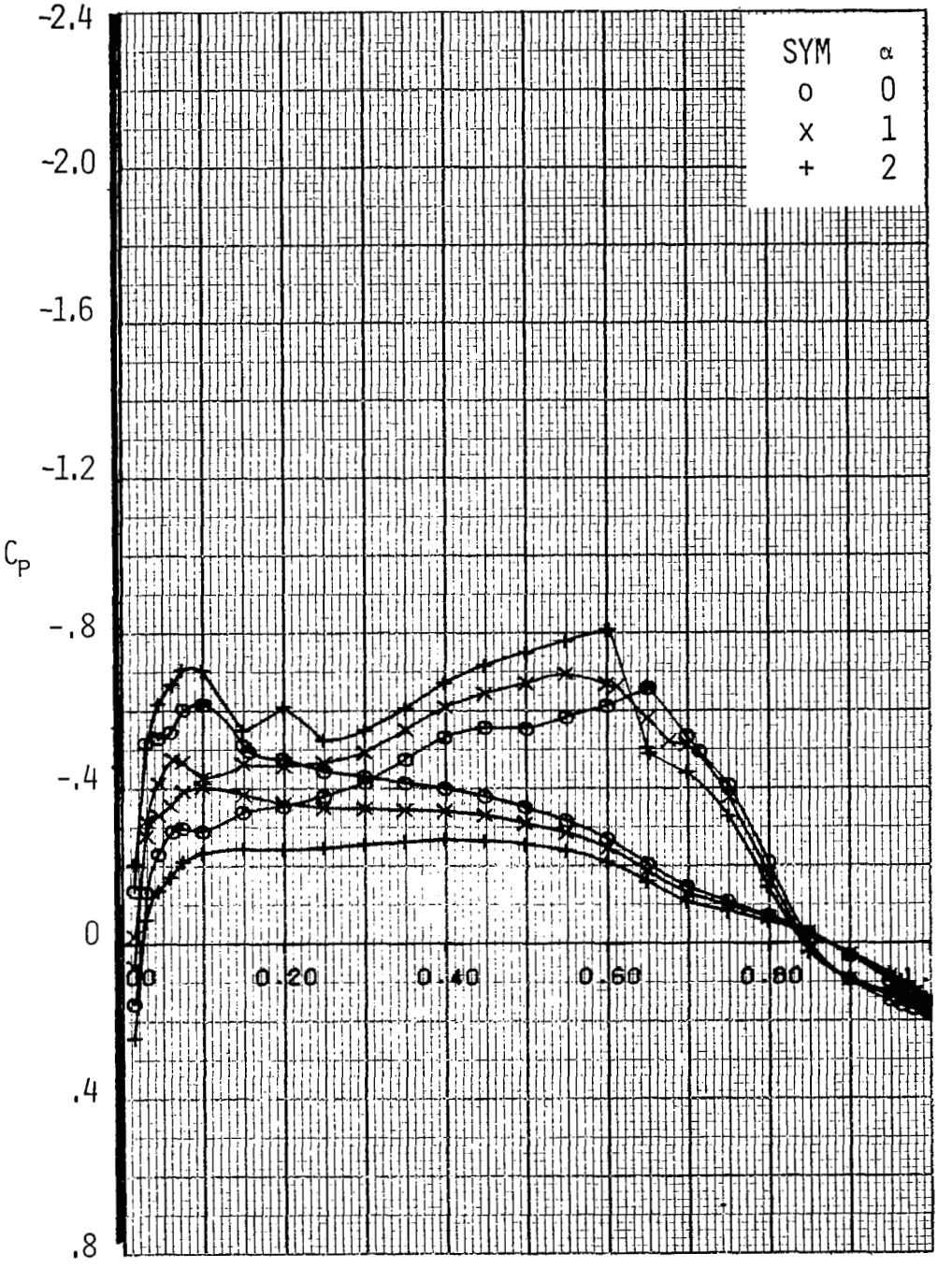

Figure A28.- Airfoil Pressure Distribution for M = 0.78, $R_N = 11 \times 10^6$, X/C_T = Free

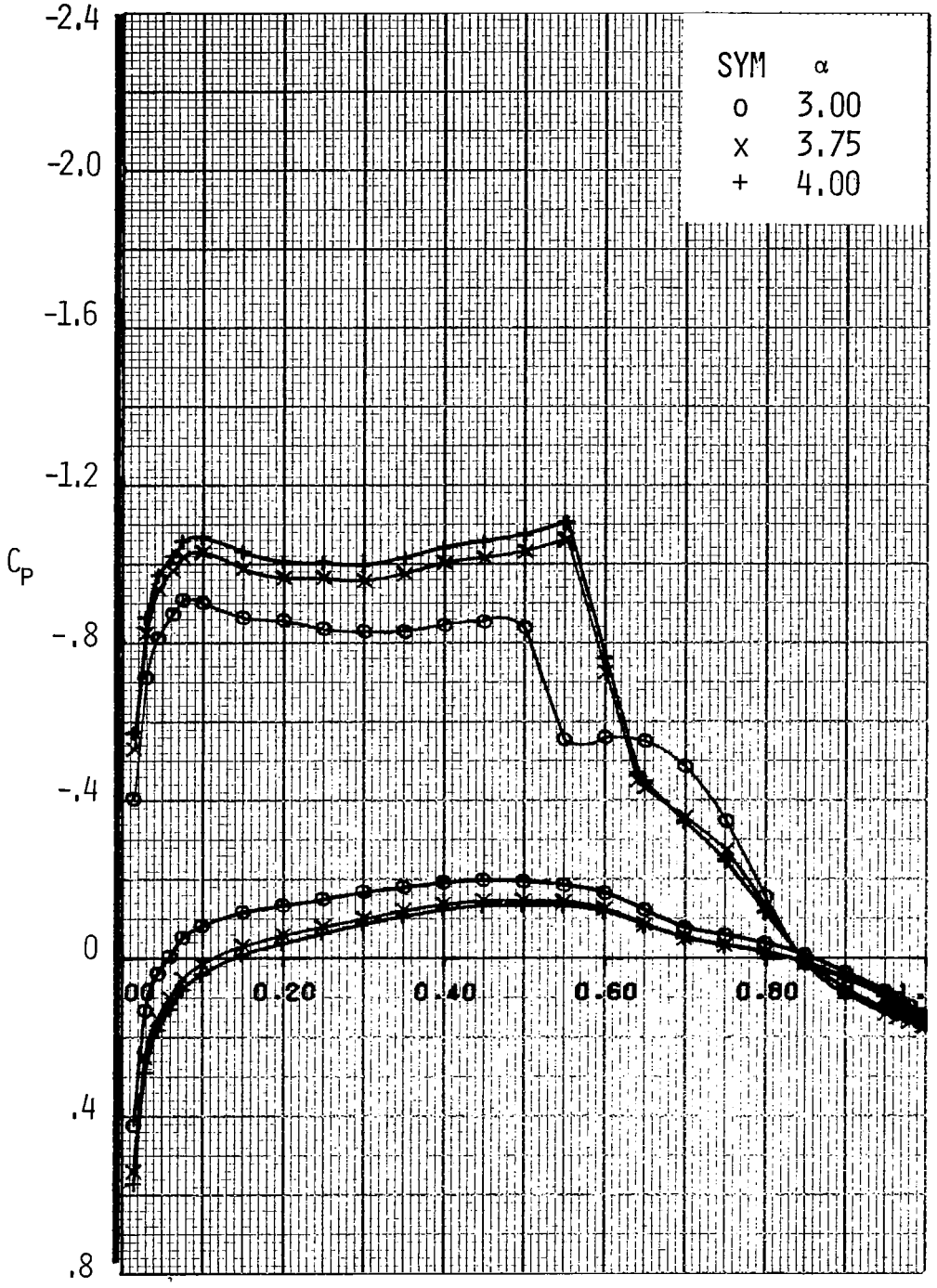

Figure A29.- Airfoil Pressure Distribution for M = 0.78, R_N = 11 x 10^6, X/C_T = Free

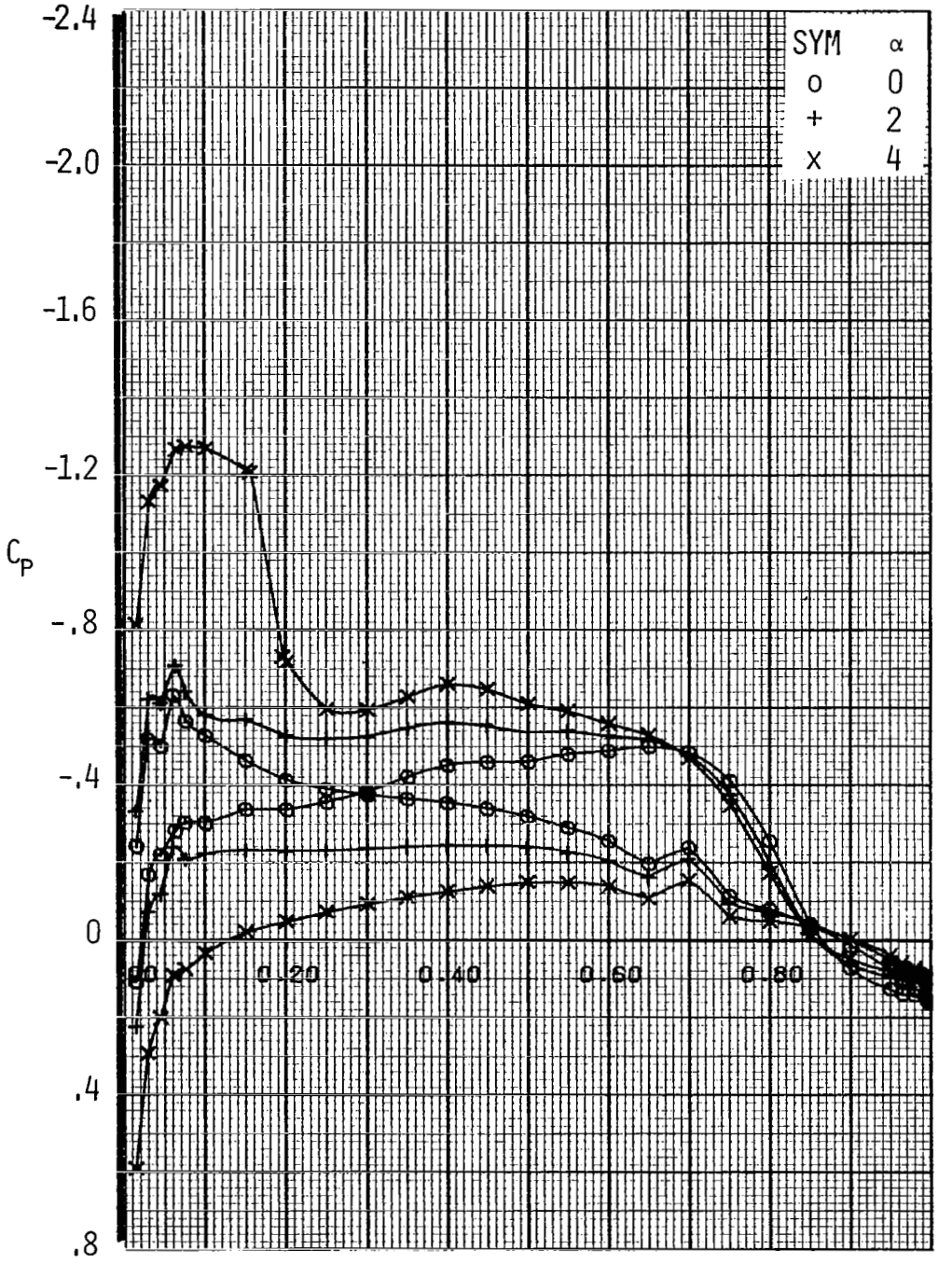

Figure A30.- Airfoil Pressure Distribution for $M = 0.72$, $R_N = 4 \times 10^6$, $X/C_T = .05$

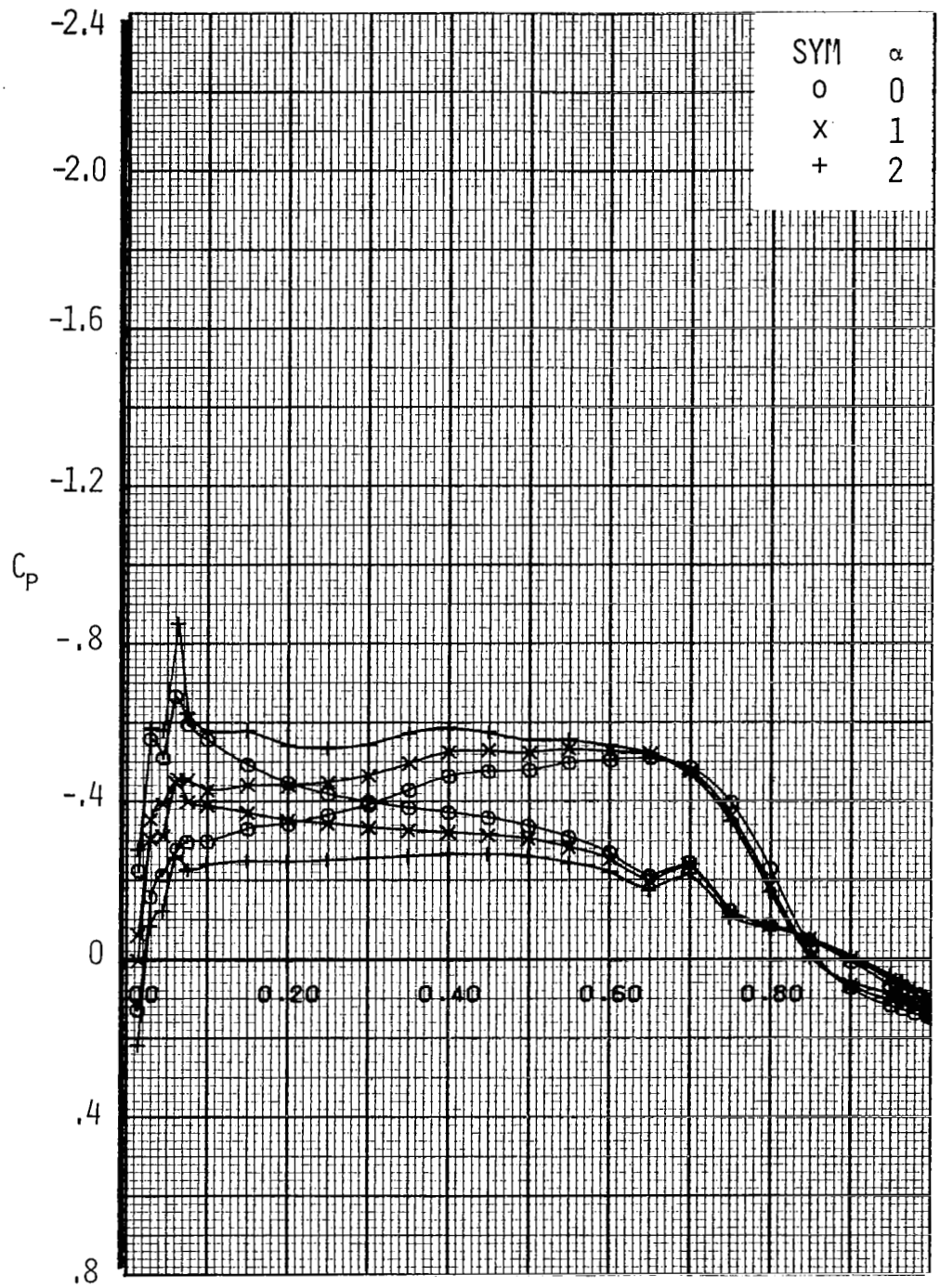

Figure A31 .- Airfoil Pressure Distribution for $M = 0.74$, $R_N = 4 \times 10^6$, $X/C_T = .05$

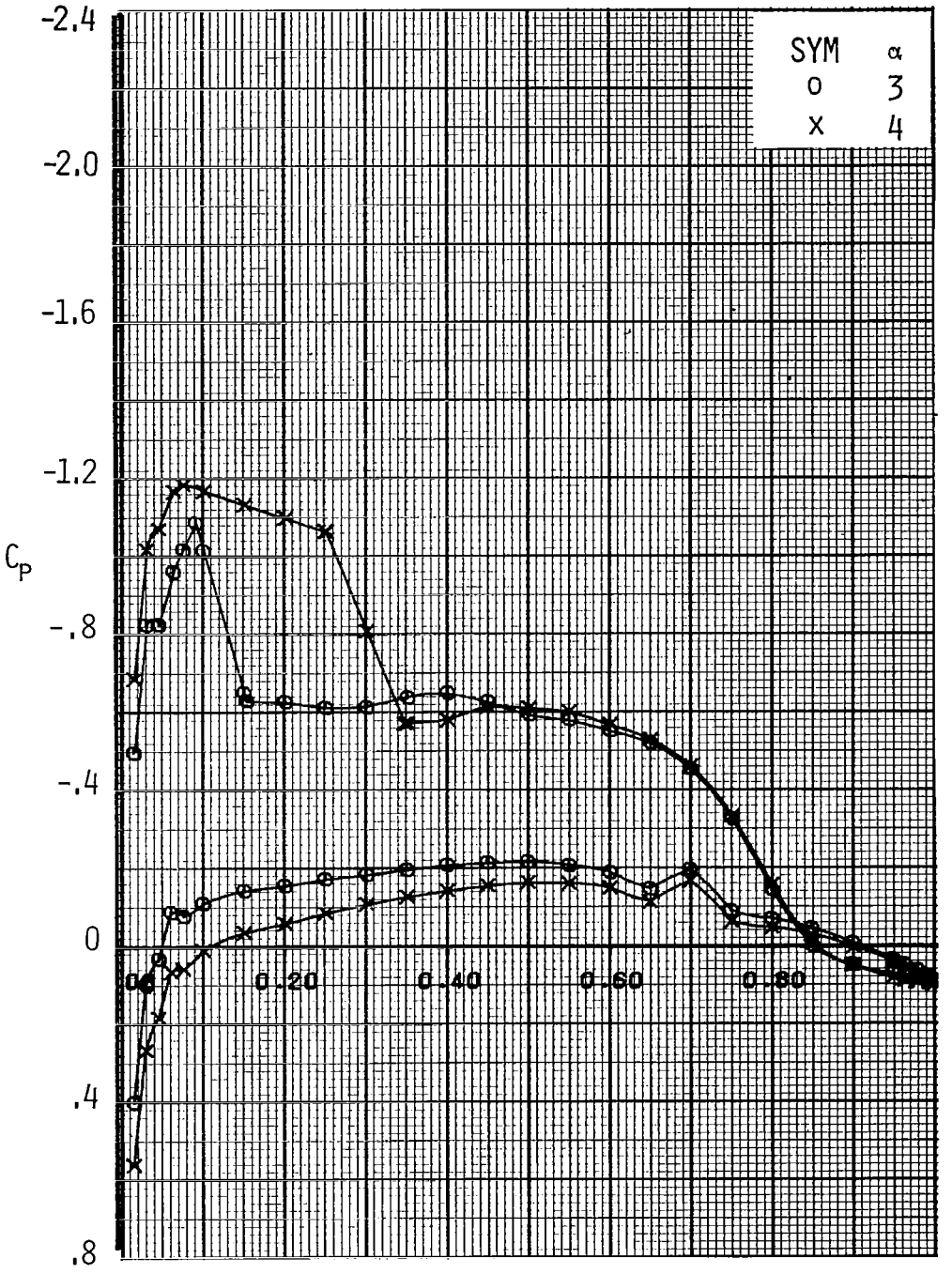

Figure A32.- Airfoil Pressure Distribution for M = 0.74, $R_N = 4 \times 10^6$, $X/C_T = .05$

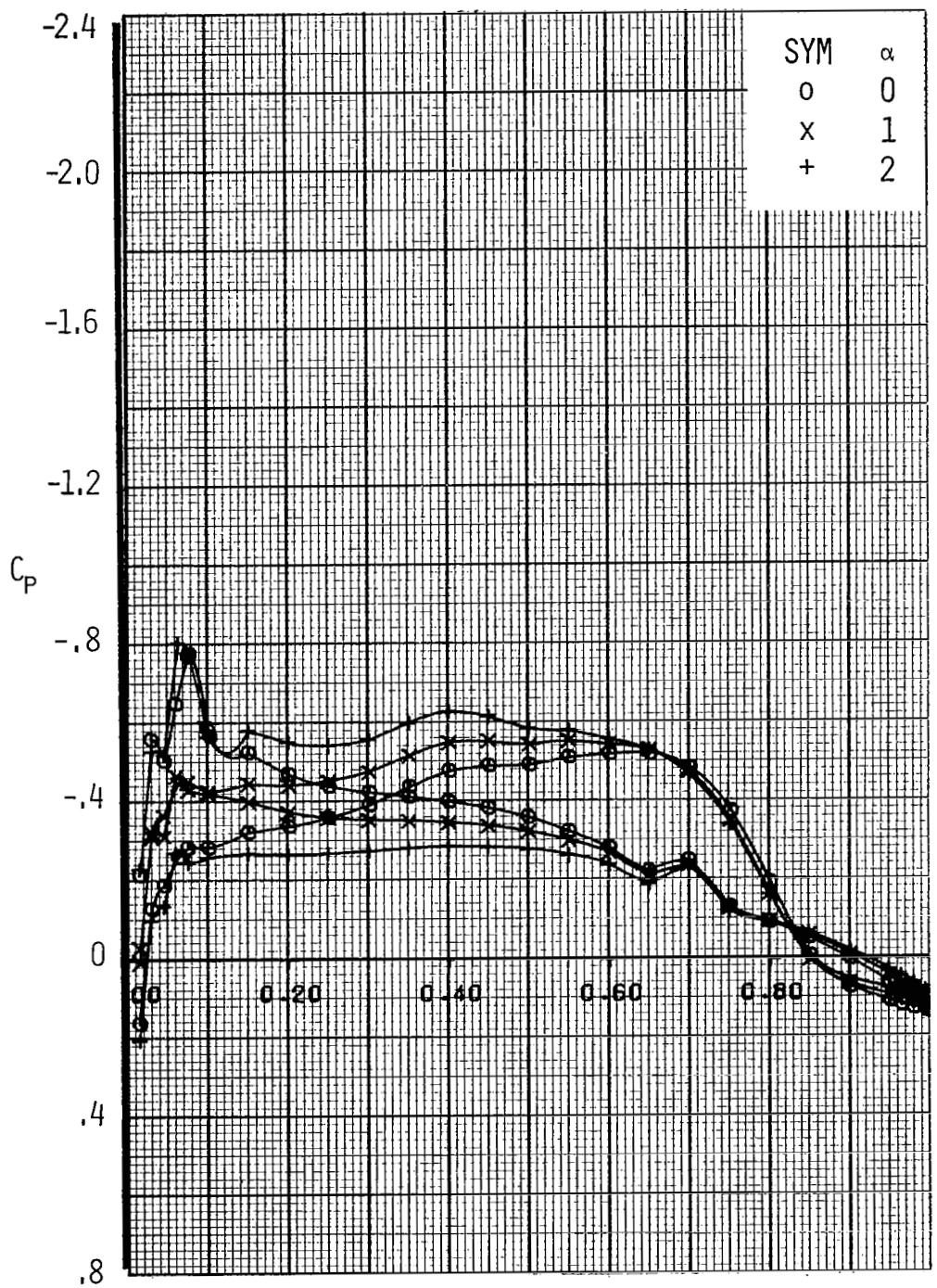

Figure A33.- Airfoil Pressure Distribution for M = 0.76, $R_N = 4 \times 10^6$, $X/C_T = .05$

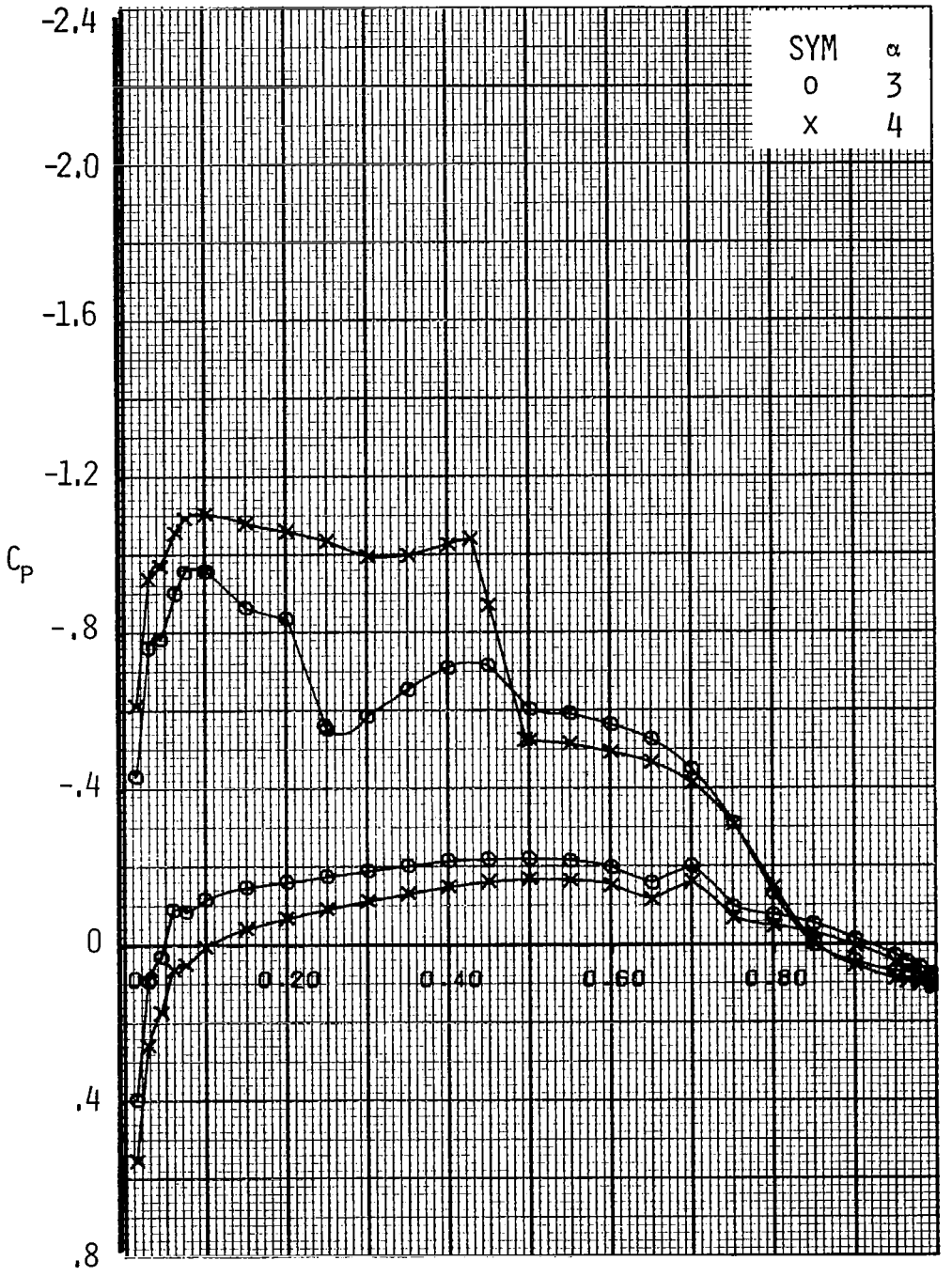

Figure A34 .- Airfoil Pressure Distribution for M = 0.76, $R_N = 4 \times 10^6$, $X/C_T = .05$

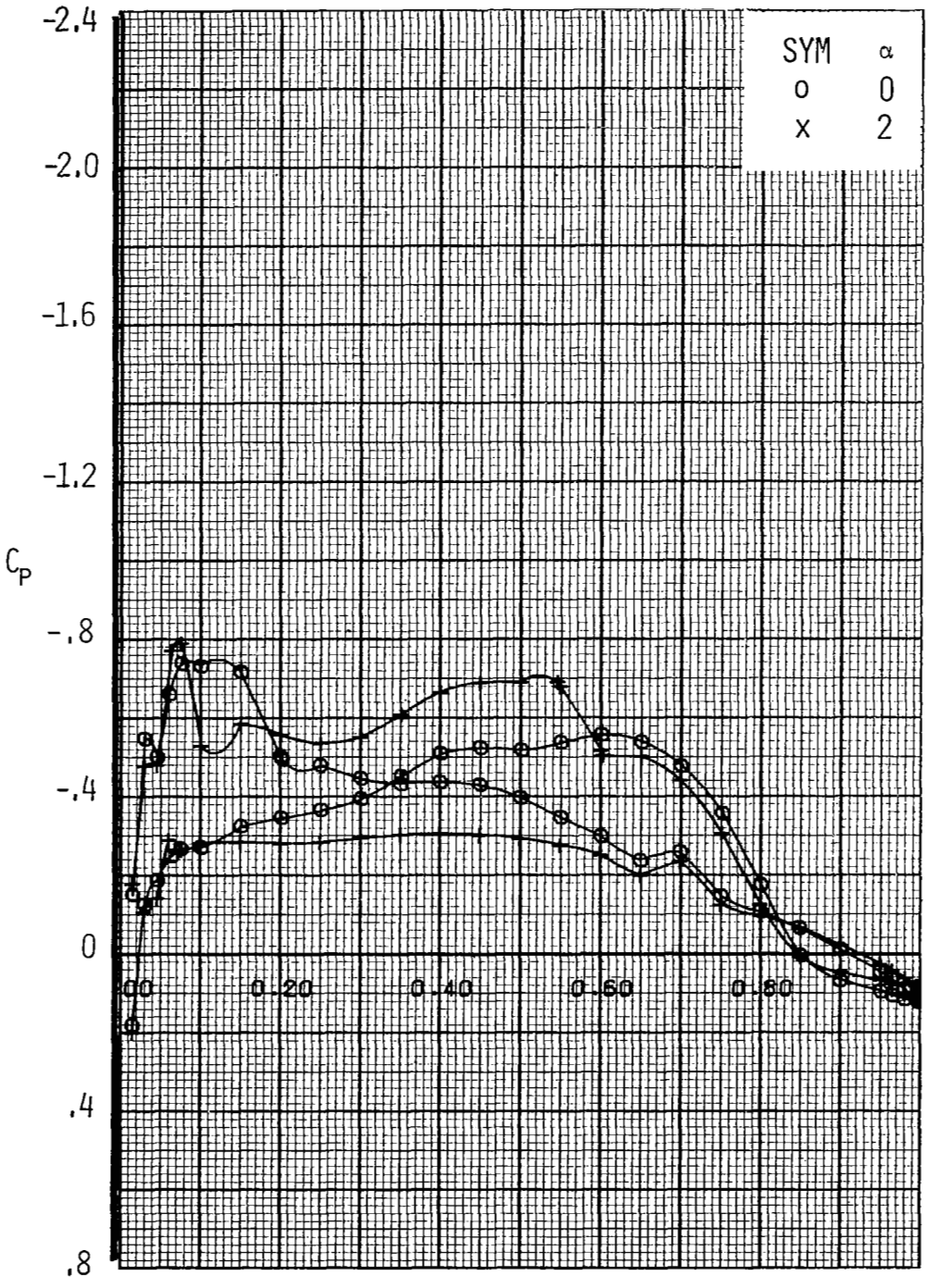

Figure A35.- Airfoil Pressure Distribution for M = 0.78, $R_N = 4 \times 10^6$, $X/C_T = .05$

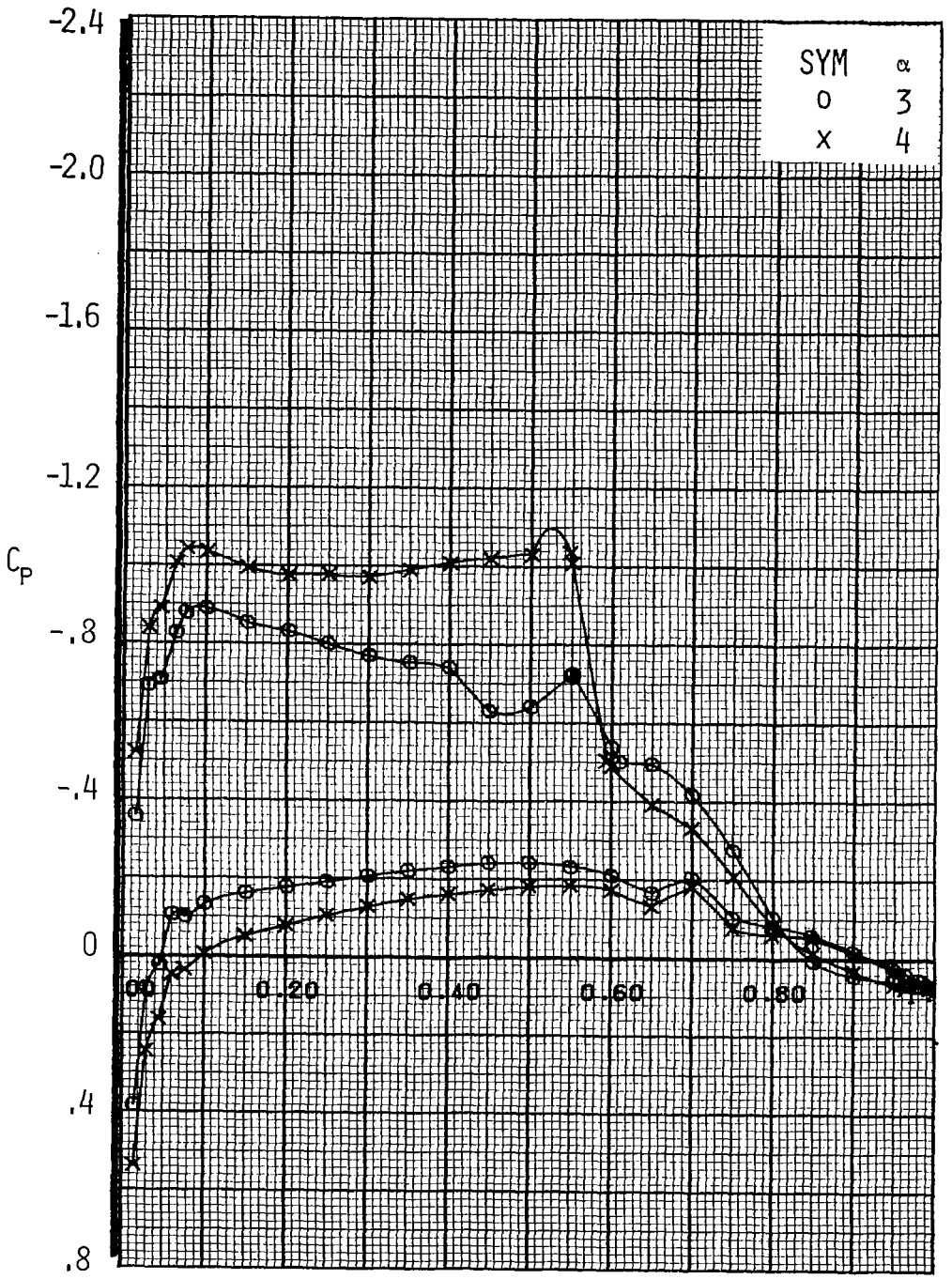

Figure A36.- Airfoil Pressure Distribution for M = 0.78, $R_N = 4 \times 10^6$, $X/C_T = .05$

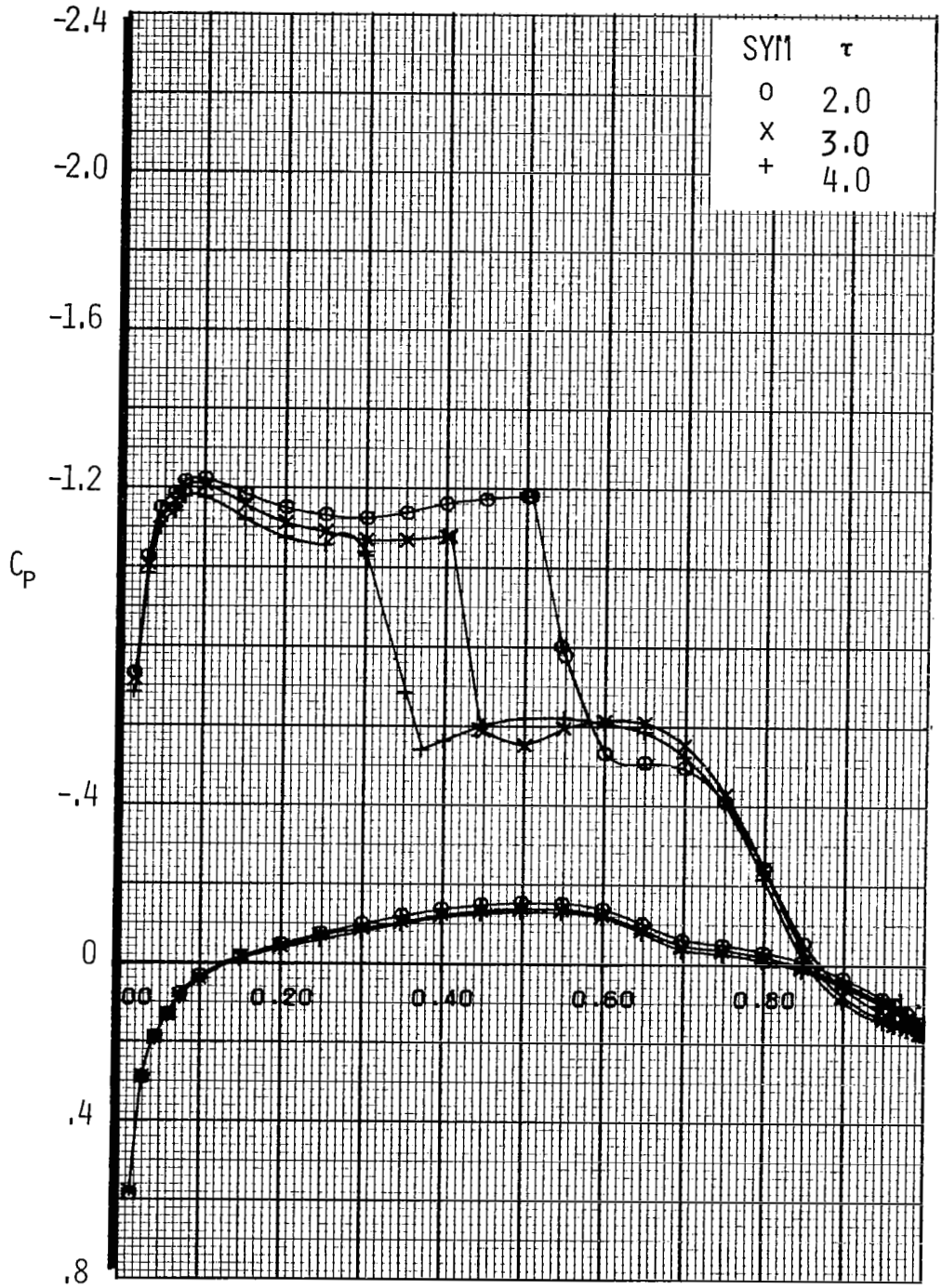

Figure A37.- Effect of Wind Tunnel Wall Porosity on Airfoil Pressure Distribution, $M = .74$, $R_N = 11 \times 10^6$, $\alpha = 3.85$.

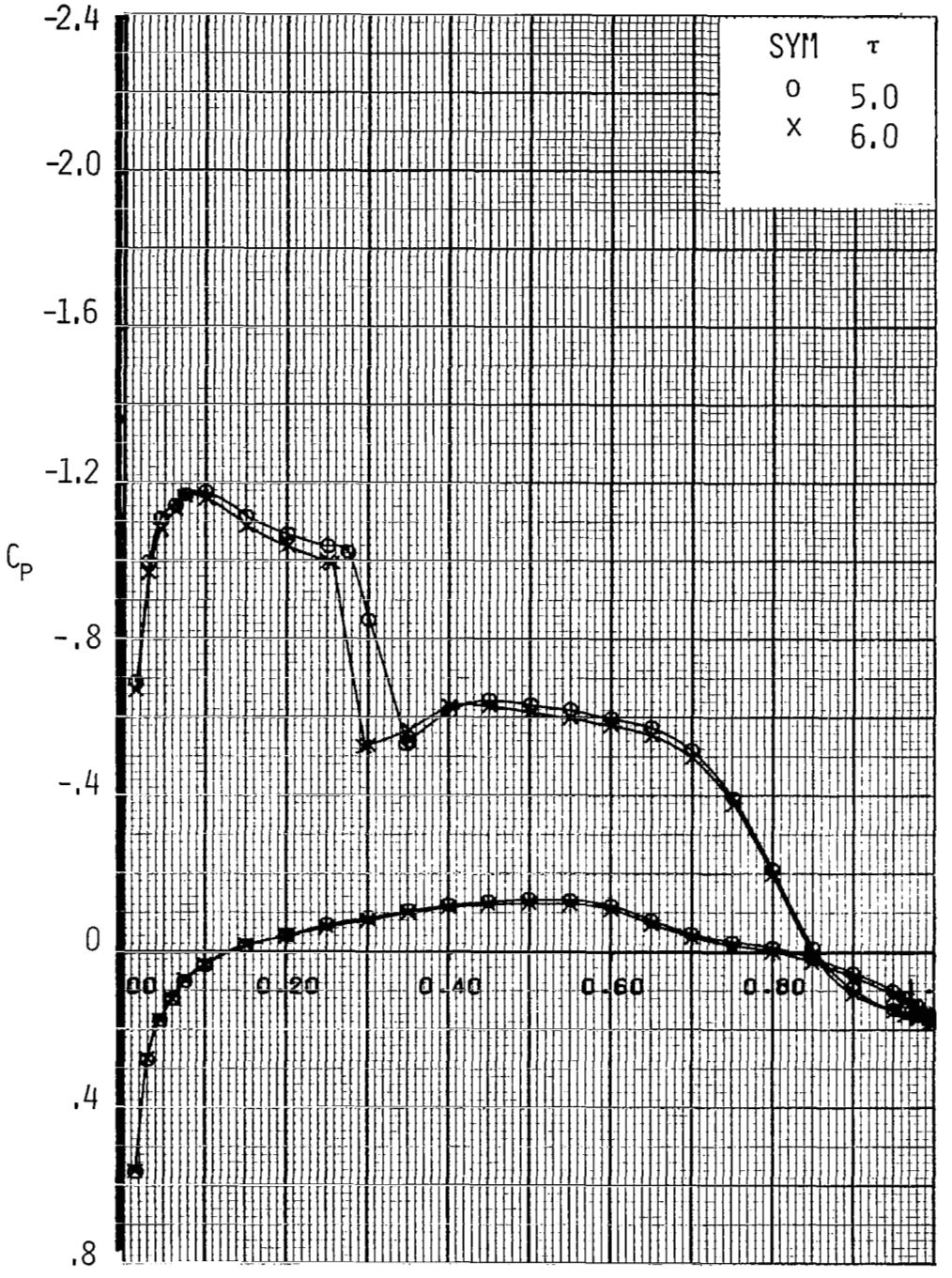

Figure A38.- Effect of Wind Tunnel Wall Porosity on Airfoil Pressure Distribution, M = .74 R_N = 11 x 10^6, α = 3.85.

1. Report No.	2. Government Accession No.	3. Recipient's Catalog No.
NASA CR-3065		

4. Title and Subtitle	5. Report Date
ANALYSIS OF A THEORETICALLY OPTIMIZED TRANSONIC AIRFOIL	November 1978
	6. Performing Organization Code
7. Author(s)	8. Performing Organization Report No.
M. E. LORES, K. P. BURDGES, G. D. SHREWSBURY	LG78ER0212
	10. Work Unit No.
9. Performing Organization Name and Address	
LOCKHEED-GEORGIA COMPANY MARIETTA, GEORGIA	11. Contract or Grant No. NAS2-8697
	13. Type of Report and Period Covered
12. Sponsoring Agency Name and Address	CONTRACTOR REPORT
NATIONAL AERONAUTICS AND SPACE ADMINISTRATION WASHINGTON, D. C. 20546	14. Sponsoring Agency Code

15. Supplementary Notes

AMES RESEARCH CENTER, NASA, TECHNICAL MONITOR — RAYMOND M. HICKS

16. Abstract

Numerical optimization was used in conjunction with an inviscid, full potential equation, transonic flow analysis computer code to design an upper surface contour for a conventional airfoil to improve its supercritical performance. The modified airfoil was tested in the Lockheed-Georgia Compressible Flow Wind Tunnel. The modified airfoil's performance was evaluated by comparison with test data for the baseline airfoil and for an airfoil developed by optimization of leading edge of the baseline airfoil. While the leading edge modification performed as expected, the upper surface re-design did not produce all of the expected performance improvements. Although the drag divergence Mach number was increased, the modified airfoil exhibited more drag creep than the baseline section. This larger drag creep is attributable to the early formulation (at approximately $M_\infty = .68$) of a relatively strong leading edge shock wave.

Theoretical solutions computed using a full potential, transonic airfoil code corrected for viscosity were compared to experimental data for the baseline airfoil and the upper surface modification. These correlations showed that the theory predicted the aerodynamics of the baseline airfoil fairly well, but failed to accurately compute drag characteristics for the upper surface modification. This failure is shown to be attributable to the inability of the theory to properly treat the thick trailing edge boundary layer associated with the upper surface modification.

17. Key Words (Suggested by Author(s))	18. Distribution Statement
airfoils, supercritical	Unlimited

19. Security Classif. (of this report)	20. Security Classif. (of this page)	21. No. of Pages	22. Price*
Unclassified	Unclassified	99	$6.00

* For sale by the National Technical Information Service, Springfield, Virginia 22161

NASA-Langley, 1978